An Investigation Of Bed Armoring Process And Its Implications For Channel Bed Stability

A Dissertation

Presented to

the faculty of the School of Engineering and Applied Science

University of Virginia

in partial fulfillment

of the requirements for the degree

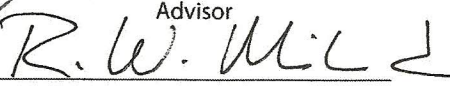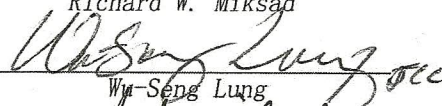Doctor of Philosophy

by

Lu Tan

August

2012

APPROVAL SHEET

The dissertation

is submitted in partial fulfillment of the requirements

for the degree of

Doctor of Philosophy

by

_____

Lu Tan
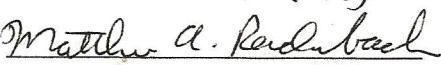
The dissertation has been read and approved by the examining committee:

_____

Joanna C. Curran

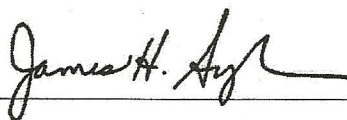Advisor

_____

Richard W. Miksad

_____

Wu-Seng Lung

_____

Patricia L. Wiberg

_____

Matthew A. Reidenbach

_____

Accepted for the School of Engineering and Applied Science:

_____

Dean, School of Engineering and Applied Science

August

2012

ABSTRACT

Interaction of river bed surface and near bed flow determines bed topographic variability and bed stability. Flume experiments have been conducted to simulate and correlate the effects of flow rate and sand proportion in bulk sediment on the hydrodynamics associated with submerged clusters formed in gravel-bed rivers during the armoring process, and subsequently, on bed stability of armored gravel-bed rivers.

Sediment mixtures with 1, 9, 24, and 38% sand content were used to create four unique sediment beds. Three different levels of flow rate were conducted against different sediment mixtures to test their effects on the development of armored bed surfaces and variables describing the cluster bedforms spatial distribution. The detail of the High-resolution Digital Elevation Models (DEMs) combined with panoramic photography documented bed surface topographies in each experiment and allowed us to identify individual clusters, measure their geometries and their spatial distributions. Three-dimensional flow velocities around individual, coupled and grouped clusters, as well as isolated clusters formed in different experiments with different sand content were measured using an Acoustic Doppler Velocimeter. Where high frequency, detailed, three-dimensional velocity measurements were taken around clusters of different spatial arrangements, turbulence was characterized through turbulence statistics including Reynolds Stress, and Turbulence Kinetic Energy (TKE) to quantify any change in shear stress necessary to mobilize the armored bed. To evaluate the resistance to transport created by the different armored beds, the Shields stresses of the bed were calculated both in localized areas around clusters and for the bed as a whole. Shields stresses for

sediment of size D_{s50} on armored surface is highly correlated with drag coefficient and total shear stress. Bed stability was more affected by sand content in bulk sediment than flow rate magnitude. It decreased with increasing sand content in bulk sediment and decreasing flow rate. The clusters density and median spacing for each run are positively correlated to hydraulic boundary condition variation and exhibits strong correlation with bed stability.

ACKNOWLEDGEMENTS

It would not have been possible to finish this doctoral dissertation, without the tremendous help and supports I constantly received from all the people around me, to only some of whom it is possible to give particular mention here.

Above all, most thanks and appreciation goes to Dr. Joanna Crowe Curran for preserving with me as my adviser throughout time it took me to complete this research and write this dissertation. She is a wonderful stories-teller with a broad spectrum of knowledge in almost every aspect in water resources engineering related topics. Aside from inspirations and keeping me on the right track throughout the entire process of my Ph.D research under her earnest instructions, her positive attitude, patience and tolerance rendered a newcomer young graduate student like me parachuting in this field more confidently with a clear sense of purpose.

I would also like to thank my committee members, Dr. Richard Miksad, Dr. Winston Lung, Dr. Patricia Wiberg and Dr. Matthew Reidenbach for their time and expertise. Dr. Miksad and Dr. Lung's insight on fluid mechanics and its influences on sediment transport were quite helpful. Dr. Wiberg's vast knowledge in sediment transport process and her advice and comments on my dissertation proposal were top-notch. Dr. Reidenbach provided invaluable advices and helps on the experimental design of my research and technical supports for the feasibility of PIV measurements of flow field for my future work.

I am grateful to all the members in Curran's group who generously shared their professional experiences and provided their assistance, comments and encouragements, in particular, Kristen Cannatelli, Kevin Waters, James Danberg, Celine Heckel-Jones, Benjamin Popovich and many others. Without these people, the experiments and results would have never happened. Their hard work, dedication and desire to help supported every step of the way. Many thanks to Dr. André Zimmermann and Dr. Daniel Wren, who have generously offered me technical assistance in LabVIEW programming and data analysis.

My wife Bo was always standing behind me as the origin of my happiness and strength in the past five years stay in University of Virginia and she was a crucial factor in my accomplishments. We met the first day of school in 2007 when she was also a new graduate student in Statistics Department and I was captured by her intelligent and charismatic personality immediately. She eventually became my date, my fiancée, and my wife who encouraged me to be steadfast and overcome all the difficulties through every step of the way. She has also witnessed me grown from a young man to a young father. On that token, I would also like to thank to my son Alex, who has "devoted" to make laughter and "shouts of joy" while this dissertation being produced.

Last but never be the least, I thank my parents, in-laws and many other friends. Without these wonderful, inspiring, and considerate people, I would not be who I am today, nor would I have accomplished as much as I have through the years. Their unlimited support, comfort, encouragement, and zest of life are greatly appreciated.

TABLE OF CONTENTS

List of Tables

List of Figures

List of Symbols

The following list includes abbreviations and symbols that are frequently used in this work. Units are expressed in terms of length (L), time (T), and mass (M).

a	Shape factor in Hey's flow resistance eqaution
A_{bed}	Bed area [L^2]
A_r, A_s	Constants in log law equations
B	Flume width [L]
B_{xz}	Body force term in longitudinal Reynolds Navier-Stokes Equation
C_d	Drag coefficient
d_s	Maximum particle (keyclast) size in cluster [L]
d_{sm}	Mean of key clast size of all clusters for each experiment [L]
D	Particle size [L]
D_{cbf}	Critical transported grain size at bankfull flows
D_i	Mean particle size of ith size fraction [L]
D_{s50}	Median particle size for sediment on bed surface [L]
e	Elevation function of the location (x_i, y_i) for bed surface
ff	Darcy-Weisbach coefficient (flow resistance coefficient)
f_i	Proportion of ith size fraction in bulk sediment
F_i	Proportion of ith size fraction on bed surface
Fr	Froude Number
F_s	Sand fraction on bed surface
g	Acceleration due to gravity [LT^{-2}]
h	Flow depth above lowest bed elevation around cluster [L]
h_o	Mean flow depth above mean bed elevation [L]
h_s	Cluster height above mean bed elevation [L]
H	Hole size in quadrant analysis
$I_{i,H}(t)$	Threshold indicator function for quadrant analysis
K_s	Equivalent roughness length [L]

K_i	Arbitrary coefficients in Yen's flow resistance equation
K_f	Effective bedform scale roughness length [L]
K_g	Effective grain scale roughness length [L]
L_s	Cluster length [L]
n_c	Total clusters quantity on armored bed surface
N_c	Quantity of measured clusters on armored bed surface
p_i	Proportion of ith size fraction in the bedload
q_b	Unit total bedload transport rate [$ML^{-1}T^{-1}$]
q_i	Unit bedload transport rate of the ith size fraction [$ML^{-1}T^{-1}$]
q^*	Non-Dimensional bedload transport rate
Q	Flow rate in flume for equilibrium transport condition[L^3T^{-1}]
Qi	Four quadrants for a u'-w' plane plot (i = 1,2,3, and 4)
Q_a	Flow rate in flume during bed armored[L^3T^{-1}]
Q_{pipe}	Discharge in water inlet pipe [L^3T^{-1}]
r	Water inlet pipe radius [L]
R	Hydraulic Radius [L]
R_{adv}	ADV signal correlation
RBSI	Relative Bed Stability Index
Re	Flow Reynolds number
S	Bed slope
S_f	Friction slope
TI	Turbulence Intensity in x, y, z directions
TKE	Turbulence Kinetic Energy [L^2T^{-2}]
u_i, v_i, w_i	Instantaneous 3-D velocities at z [LT^{-1}]
$\bar{u}, \bar{v}, \bar{w}$	Mean 3-D velocities at z [LT^{-1}]
u', v', w'	Fluctuations of 3-D velocities [LT^{-1}]
$u_{rms}, v_{rms}, w_{rms}$	Root-mean-square 3-D velocities [LT^{-1}]
u_*	Shear velocity [LT^{-1}]
U	Cross-sectional time and space averaged longitudinal velocity [LT^{-1}]

U^+	Normalized longitudinal velocity
W^*	Non-Dimensional bedload transport rate
W_i^*	Non-Dimensional fractional transport rate for i^{th} size fraction
W_s	Cluster width [L]
x,y,z	Cartesian longitudinal, lateral, and vertical coordinates. [L]
x_i, y_i	Coordinates of bed surface plane location i
z_o	Characteristic roughness height at which $u = 0$ [L]
$z*$	Normalized local elevation by total flow depth
Z	Mean water depth [L]
β_i	Parameter estimators in multiple linear regression model
γ	Specific gravity of sediment particles [ML^{2}T^2]
$\gamma(\Delta s)$	Semivariance of bed elevation data when lag distance $= \Delta s$ [L^2]
δ	Boundary layer thickness [L]
δ_{xz}	Isotropic tensor component in x-z plane
η	Vertical bed elevation from an arbitrary datum [L]
κ	von Karmann constant
ϕ	Grain size in logarithm scale
λ	Clusters spacing [L]
λ_c	Threshold clusters spacing [L]
λ_{cm}	Mean Clusters spacing [L]
λ_{median}	Median Clusters spacing [L]
λ_p	Porosity of the bed deposit
λ_x	Downstream cluster-to-cluster spacing [L]
λ_y	Transverse clusters-to-cluster spacing [L]
μ	Fluid absolute viscosity [ML^{-1}T^{-1}]
ρ	Fluid density [ML^{-3}]
ρ_c	Total cluster density [L^{-2}]
$\rho_{Ic}, \rho_{Cc}, \rho_{Gc}$	Isolated, coupled and grouped cluster density [L^{-2}]
ρ_s	Sediment material density [ML^{-3}]

$\sigma_{\lambda c}$	Standard deviation of cluster spacing [L]
τ_b	Average bed shear stress [ML^{-1}T^{-2}]
τ_{cr}	Critical bed shear stress [ML^{-1}T^{-2}]
τ_{ci}, τ_{ri}	Critical and reference bed shear stress for i^{th} size fraction [ML^{-1}T^{-2}]
τ_b^*	Non-Dimensional average bed shear stress
τ_{cr}^*	Non-Dimensional critical bed shear stress
τ_{xy}, τ_{xz} or τ_{Re}	Reynolds stress components [ML^{-1}T^{-2}]
$\tau^*_{r50}a$	Non-Dimensional reference shear stress yield from WCSBTM
$\tau^*_{r50}b$	Non-Dimensional reference shear stress yield from F_s
υ	Fluid kinematic viscosity. [L^{2}T^{-1}]
Δs	Lag distance in semivariogram [L]
Δss	The break of slope lag distance in semivariogram [L]
Δs_{max}	Range of the process in semivariogram [L]

Chapter 1.

INTRODUCTION

1.1 Purpose of the Research

The geomorphology of gravel-bed rivers has long been a topic of interest to earth scientists and water resources engineers. The river bed surface mediates interaction between the flow and the bed sediments. The interface also defines the habitat for aquatic insects, salmonid spawning, and juvenile fish; and it determines the sediment available for transport (Wilcock and DeTemple, 2005). Topographic diversity of the channel bed has been linked to biological diversity in stream systems and has been applied as an indicator of stream health (Bartley and Rutherford, 2005).

In gravel-bed rivers, there exists a feedback mechanism between the resistance of grains to entrainment and the bed topographic variability. The roughness of the bed is generally defined only in terms of a single, characteristic grain size regardless of the distribution of sediment grain sizes, and the size, shape and spatial distribution of any bed structures. Thus, bed structures are assumed to have a consistent effect at all sites and at all flows (Bathurst, 1982). However, recent studies on sediment transport have shown that sediment gradation within the channel bed, the spatial distribution of grains on the bed surface, and the inherent arrangement of grains to create grain scale bed roughness all play important roles in sediment transport and bed stability (Church and Hassan, 1998; Strom and Papanicolaou, 2007, 2008, 2009; Gran et al. 2006). When a gravel bed surface

incorporates a structure on the bed surface, the stability of the overall bed increases (Iseya and Ikeda, 1987; Hassan and Reid, 1990; De Jong, 1991; Strom et al., 2004; Lamarre and Roy, 2005). The formation of large roughness elements (LREs) (Figure 1.1.1) on the bed surface creates localized areas of variable flow with the regions directly downstream of large clasts acting as refuge for aquatic biota (Cardinale et al., 2002). A cluster arrangement of gravels is the most common type of LRE found on an armored bed. I use the definition of clusters put forward by Strom and Papanicolaou (2004; 2007; 2010) that clusters are "discrete, organized groupings of particles that sit above the average elevation of the surrounding bed surface." Clusters increase overall bed resistance (Brayshaw, 1984; Canovaro et al., 2007) which has been documented as an increased time to entrainment of any grains from the clusters (Iseya and Ikeda, 1987; De Jong, 1991). Topographic structures formed from LREs, such as clusters, act to increase the roughness of the overall bed surface.
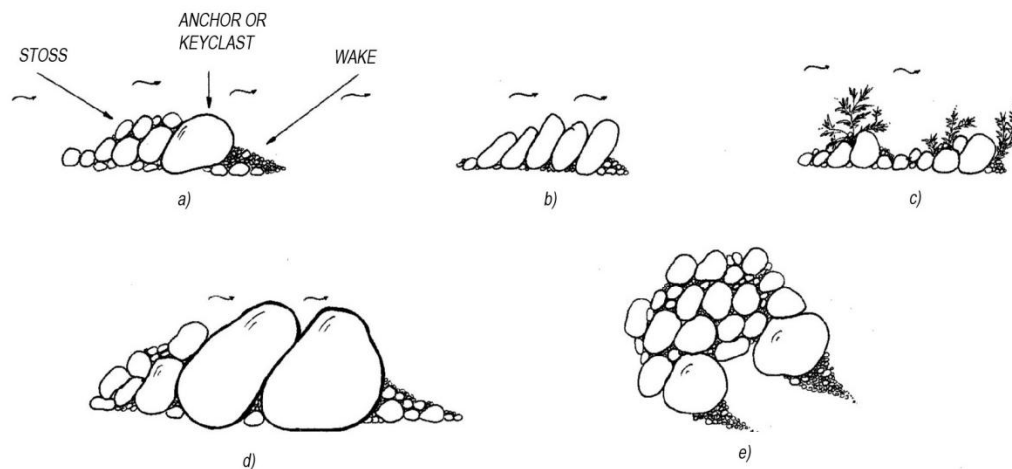
Figure 1.1.1 Schematics of Large Roughness Elements (LREs): a) Cluster; b) imbrication; c) vegetation bar; d) cobble cluster; e) complex cluster; (Wittenberg, 2002)

Predicting sediment movement in river channels requires a fundamental understanding of the interaction between the channel flow and channel boundary. Research into grain and form roughness in alluvial channels has a long history, such that skin friction is known to be relatively insignificant when alluvial bedforms are present while grain and bedform roughness are significant. Moreover, the number and arrangement of clusters on the bed surface are hypothesized to be part of a feedback system with the flow rate in the channel through which the density and arrangement of clusters adjusts to local flow conditions to maintain a maximum flow resistance over the channel bed and maintain a subcritical flow regime (Hassan and Reid, 1990; Brayshaw, 1984).

Estimates of the percent cover of a gravel bed river by clusters range from 5% (Brayshaw, 1984; Clifford, 1996) to 75% (De Jong, 1991) of the bed area. Flow resistance increases around clusters due to alteration of the immediate flow field. Consistent turbulent flow patterns develop that include vortex shedding downstream of clusters (Buffin-Belanger and Roy, 1998; Hassan and Church, 2000; Lamarre and Roy, 2005). Two-dimensional field measurements of the turbulence around clusters have shown that there is a 10-fold increase in turbulence in the wake area immediately downstream of the cluster (Buffin-Belanger and Roy, 1998). The formation of counter rotating vertical vortices around the roughness element is indicated by large amounts of horizontal turbulent momentum exchange (Lacey and Roy, 2008a, b). These findings point to a strong three-dimensional component to turbulence around clusters, which has not been fully elucidated.

The population of grains on the surface of a gravel bed river is often coarser than those in the subsurface. When this occurs, the river is considered armored, with the armor layer being the coarse surface layer. An improved understanding of armored channel bed stability is necessary to predict the effect of controlled flow releases on the downstream channel morphology. During a controlled flow release, break-up of the armor layer may or may not be a goal. Often a flushing flow is designed to remove only fines from the channel bed but leave the armor layer intact (Kondolf and Wilcock, 1996; Batalla and Vericat, 2009). When the armor layer breaks, the channel bed often erodes and incision may occur. This may negatively impact aquatic life in the channel that is dependent on stability of the larger grains on the bed surface. In some cases, gravel augmentation is pursued to replace the gravel lost following removal of the armor layer. However, the effect of specific boundary configurations on flow resistance is largely unknown, which prevents advances in modeling sediment transport that would improve predictions related to flow releases. This research is motivated by the need to connect bed stability and cluster occurrence with channel boundary conditions of discharge and bed grain size distribution. By linking boundary conditions, bed surface structures and critical shear stress (bed stability) together, the result of this research will help engineers and scientists with a better understanding of how to regulate flow release magnitudes and adjust the grain size distribution of added sediment to achieve a desired bed stability which will help lead to an optimal riverine environment based on both sustainable and efficient goals and principles.

1.2 Hypotheses

Disparate studies have focused on defining the role of microforms in bed stability and have recognized their presence in armored beds. The presence of microforms on the bed surface has been well documented in the field (Wittenberg, et al., 2007; Brayshaw 1983; Hassan and Reid, 1990; Strom and Papanicolaou, 2008, 2009) where studies indicate the dominant independent variables controlling cluster formation and topography are the flow rate during cluster formation and the sediment as described by the D_{50} and D_{84} grain sizes, for which the subscripts denote percentage of the particles that are finer by weight (Strom and Papanicolaou, 2009). Based on the results of both field and flume investigations of the contribution of microforms to bed stability, three main hypotheses are defined for this dissertation.

The first hypothesis is that the density of clusters on the armored bed increases as the sand fraction in the bed sediment increases and the spacing between clusters decreases. Cluster density is measured as both the total number and local number of clusters per square-meter of flume area. The spatial distributions of clusters that form under each distinct combination of boundary conditions tested are measured using a spacing parameter, which is defined as a correlation function for two adjacent clusters on the bed (see Chapter 3). Sands are expected to increase the mobility of the coarse fraction during armoring, enabling a greater number of large sediment grains to arrange into clusters. The clusters spacing parameter and cluster density will be measured to test this hypothesis that spatial coordination between clusters increases as the sand fraction increases.

The second hypothesis is that the density and the spatial coordination of clusters on the armored bed increases as the flow rate during armor formation increases. Previous research indicates a correlation between cluster formation and the flow rate under which the bed armor develops.

The third hypothesis is that the stability of the bed surface increases with the density and the number of spatially coordinated clusters on the bed. Clusters are expected to affect bed stability by altering local turbulent flow patterns. Thus, as the number of clusters on the bed surface increases, a greater amount of the flow in the near bed region is expected to be affected in a manner that increases overall bed stability.

The roughness of the bed surface will also increase with an increasing proportion of bed coverage by clusters. By increasing the overall bed roughness, cluster bedforms will help dissipate flow energy and shelter the uncluttered bed areas. Thus, as the flow patterns in the near bed region are affected and the overall bed roughness increased, the stability of the unclustered portion of the bed surface will also increase.

To test these hypotheses and to gain a better understanding of the processes associated with bed armoring and cluster formation, a physical model was used to gather data under a range of sediment and flow boundary conditions. Eight experiments on gravel-bed channel armoring were carried out in a recirculating flume to test the overarching theory of an increase in armored bed stability with cluster presence as well as the individual hypotheses listed above. This dissertation details the results of this research. The dissertation is organized into 7 chapters of which Chapter 4-6 represent peer-review journal articles. This introductory chapter is followed by a literature review and a chapter

detailing experimental methods. The final chapter is a summary of the full dissertation and the conclusions drawn from this research.

Chapter 2.

LITERATURE REVIEW

2.1   Boundary Layer Theory

As water flows over a gravel bed surface, a pair of resisting and shearing forces is generated at the sediment-water interface. The magnitude of the shear and resistance forces is determined by the fluid viscosity and velocity. A flow velocity gradient develops throughout the flow depth from the bed surface up to the flow surface. For flow in relatively smooth open channels, a boundary layer forms in the immediate vicinity of the bounding bed surface. Figure 2.1.1 illustrates the semi-log plot of boundary layer comprising four flow regions that are characterized by different velocity gradients: viscous sub-layer (linear region), buffer layer, logarithmic region, and outer region, where $U^+=\bar{u}/u_*$ and $z^+=zu_*/v$; $\bar{u}$ is the mean longitudinal velocity at height z, and u_* is the friction velocity or shear velocity; v is the fluid kinematic viscosity.
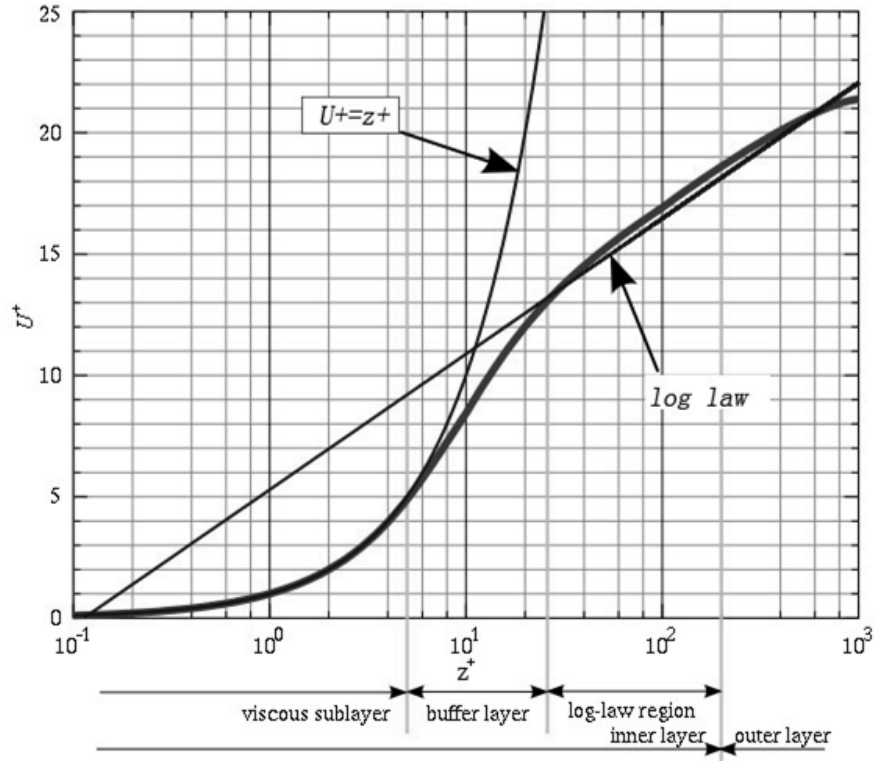
Figure 2.1.1 Schematic of dissection of boundary layer

The inner layer or wall region is composed of the viscous sub-layer and logarithmic overlap layer and limited to $z/Z < 0.2$ (Chow, 1959), where z is the vertical height above the solid surface and Z is the water depth. The flow profile in the overlap layer follows the "logarithm law of the wall" established using Prandtl's turbulent mixing length concept and von Karman's similarity hypothesis for turbulence.

$$\frac{\bar{u}}{u^*} = \frac{1}{\kappa} \ln \frac{z}{z_0}$$

2.1.1

in which u is the time-averaged longitudinal velocity at height z from the wall, u^* is the shear velocity $= (\tau_b/\rho)^{1/2}$; κ = von Karman's constant = 0.40; z_o = the characteristic roughness length at which $u = 0$. Upon a dimensional analysis, z_o is found to be a function only of u^* and the kinematic viscosity v, showing that $u^* z_o/v$ is a constant; therefore, Equation 2.1.1 can be written as

$$\frac{\overline{u}}{u^*} = \frac{1}{\kappa} ln \frac{u^* z}{\upsilon} + A_s \qquad\qquad 2.1.2$$

in which A_s is a constant of 5.5 for the hydraulically smooth flow created during Nikuradse's experiment. This equation is strictly applied in the logarithm layer or overlap layer, in which both turbulent shear stress and viscosity are important. In the viscous sub-layer, the friction stresses are dominated by viscosity. The flow is considered to be in the laminar condition, where the streamlines are linear and parallel. Equation 2.1.2 simplifies to

$$\frac{\overline{u}}{u^*} = \frac{u^* z}{\upsilon} \qquad\qquad 2.1.3$$

In the outer region, far from the viscous influence near the wall, the water surface velocity becomes significant, and viscosity values are small in comparison. A velocity defect law is applicable

$$\frac{\overline{u_s} - \overline{u}}{u^*} = \frac{1}{\kappa} \ln \frac{z}{\delta} + A_1 \qquad\qquad 2.1.4$$

in which $\overline{u_s}$ is the maximum time-averaged point velocity at the outer edge of the boundary layer and δ is the boundary layer thickness. The boundary layer thickness in shallow, wide, smooth channels is generally the same as the water depth Z (i.e. $\delta=Z$).

Flows in gravel-bed rivers are almost always turbulent. In rivers with a coarse bed surface the roughness elements protrude through the thickness of a viscous sub-layer into the main part of the flow (Nezu and Nakagawa, 1993a). This creates a hydraulic condition of fully rough turbulent flow. In this case, the viscosity is no longer important but the height of the roughness elements K_s becomes very influential in determining the velocity profile which is dependent only on Z/K_s; and the flow resistance is almost

entirely due to the form drag on the projection of the protrusion. The logarithmic law of the wall for rough-walled open channel becomes:

$$\frac{\bar{u}}{u^*} = \frac{1}{\kappa}\ln\frac{z}{k_s} + A_r \qquad\qquad 2.1.5$$

in which A_r is determined to be a constant of 8.5 by Nikuradese for sand-grain roughened pipes in fully rough-turbulent flow and K_s is the equivalent roughness, which can be assumed to be equal to the median grain diameter, D_{50} for closely graded sand bed rivers. However, in poorly sorted gravel-bed rivers, the mean grain size is often too small to be a good representative of the bed roughness, and a range of values have been proposed. Researchers suggested the equivalent roughness height, K_s, to be some factor multiplied by a characteristic particle size D_i for which i represents the percentage of the particles are finer by weight. (Hey, 1979; Bray, 1979; Van Rijn, 1982; Gomez, 1993). Many researchers consider that K_s cannot be estimated using a single grain size (Hey and Thorne, 1983, 1986; Bray, 1985; Kirchner et al., 1990; Robert, 1990; Wiberg, 1991; Carling et al., 1992) because the distribution of grain sizes and the arrangement, size, and shape of clusters or other bed forms are not the same across different sites or under the variable flow conditions in a river. In Chapter 6, this factor is further evaluated as the dimensionless effective roughness length K_f/D_{50} for form scale and K_g/D_{50} for grain scale.

2.2   Sediment Transport

The sediment transport rate, which is determined by hydraulic and sediment boundary conditions, regulates the bed aggradation and degradation via the sediment continuity equation (Equation 2.2.1).

$$\left(1 - \lambda_p\right)\frac{\partial \eta}{\partial t} = -\frac{\partial q}{\partial x} \qquad\qquad 2.2.1$$

In the above relation λ_p denotes the porosity of the bed deposit, η denotes the vertical bed elevation from an arbitrary datum, and $\frac{\partial q}{\partial x}$ denotes the sediment transport flux in longitudinal direction. The variation in bed surface topography creates a feedback between hydraulic parameters and boundary layer hydrodynamics, influencing the momentum and energy transfer regime, and ultimately influencing sediment transport rate (Figure 2.2.1).
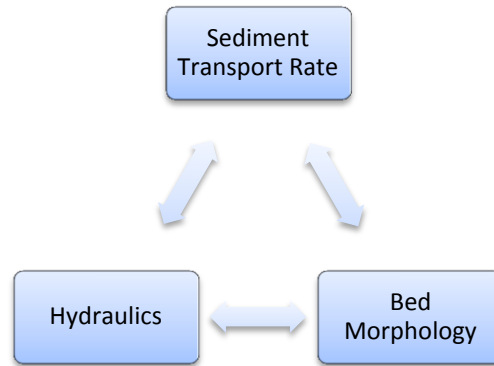
Figure 2.2.1 Schematic of feedback system for sediment transport, bed morphology and Hydraulics condition

Flow forces acting to mobilize sediment particles on the bed surface are often expressed in terms of a boundary shear stress τ_b . Boundary shear stress τ_b can be calculated using the cross-sectional averaged flow depth Z and friction slope S_f, with the DuBoy's equation:

$$\tau_b = \rho g Z S_f \qquad\qquad 2.2.2$$

The threshold for sediment incipient motion is defined by a critical shear stress τ_{cr}. The critical shear stress is calculated using the DuBoy's equation with the flow depth and slope at the value for which a grain begins to move. The critical shear stress is commonly non-dimensionalized as:

$$\tau_{cr}^* = \frac{\tau_{cr}}{(\rho_s - \rho)gD} = \frac{h_c S_f}{(\gamma - 1)D} \qquad \text{2.2.3}$$

where γ is the specific gravity of sediment particles, typically $2.65g$ for quartz dominated bed sediment, and D is the particle diameter of interest. Most methods for calculating sediment transport rate consider the shear stress acting on the boundary that is in excess of the critical stress to be the shear stress responsible for transporting the sediment as bedload. The relation between excess shear stress and sediment transport rate has been defined empirically by the Meyer-Peter and Muller bed load transport rate relation equation (Equation 2.2.4a), which was recently updated by Wong and Parker (2005) (Equation 2.2.4b).

$$q^* = 8(\tau_b^* - \tau_{cr}^*)^{1.5} \qquad \text{2.2.4a}$$

$$q^* = 3.97(\tau_b^* - \tau_{cr}^*)^{1.5} \qquad \text{2.2.4b}$$

where $q^* = \frac{q_b}{\sqrt{(\gamma-1)gDD}}$ is the dimensionless bedload transport rate; $\tau^* = \frac{\tau_b}{\rho(\gamma-1)gD}$ is the dimensionless shear stress.

As a rule of thumb, river bed stability is evaluated by the ratio of averaged boundary shear stress to critical shear stress $\frac{\tau_b^*}{\tau_{cr}^*}$ (Johnson et al. 1999). If $\frac{\tau_b^*}{\tau_{cr}^*} > 1$ for the representative particle size, the particle will be mobilized. If, once the sediment is mobilized, it is maintained in the water column through the turbulent forces in the flow, it will be transported as suspended load. For uni-size sediment, the non-dimensional critical shear stress τ_{cr}^* is plotted against non-dimensional particle Reynolds number. This curve is termed the Shields Curve and depicts the relation between critical shear stress and

particle size (Figure 2.2.2). The curve is often used to estimate the non-dimensionalized

critical shear stress, or Shields stress, required to mobilize a particle or bed surface.
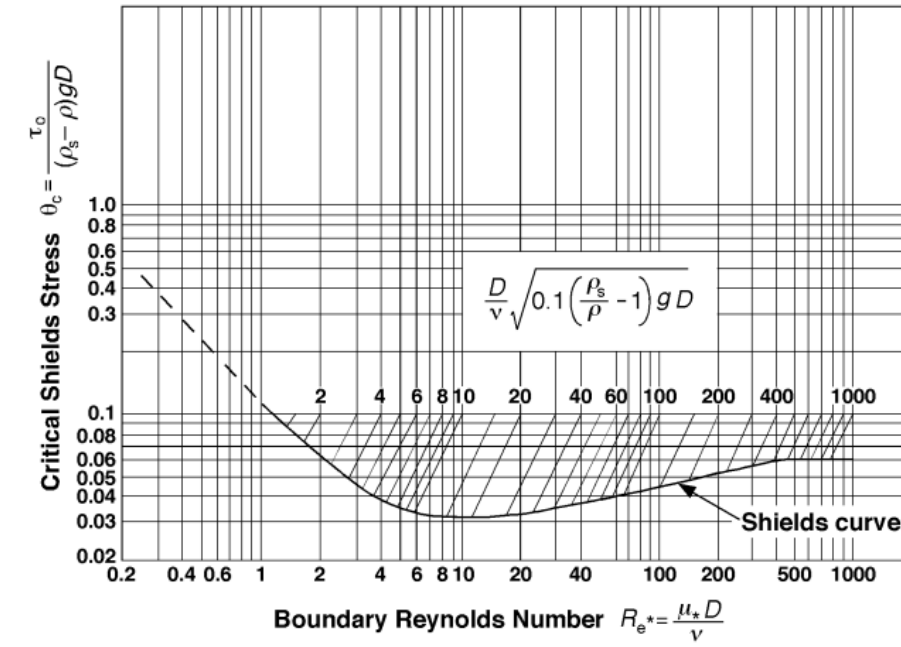
Figure 2.2.2 Shields curve (Buffington, 1999)

2.3 Mixed-size Sediment and Fractional Transport Rates

The sediment in a natural, water worked bed is generally poorly sorted and

encompasses a wide range of size fractions. Individual grain size is determined by the

size of its second principle axis, or its b-axis. A size fraction refers to a specified range of

sizes within the size distribution of the sediment. Sand size sediments are those with b-

axis measurements between 0.063 mm – 2.0 mm. Gravels are those sediments larger than

2.0 mm. If the mean or median size of the bulk bed material is in the gravel range, the

river is termed a gravel-bed river, and similarly if it is in the sand size range, the channel

is considered a sand-bed river. Assumptions of an equal sediment density and spherical

sediment shape were made for many of the early sediment studies. Because silica is the

primary component of the majority of sediments, the assumption of a constant sediment density is valid for majority of natural sediment. While sediments are not explicitly assumed to be spherical in most studies, the effect of grain shape is rarely considered as it has been shown to be less important to sediment transport than the range of grain sizes in the sediment.

Sediment transport rate is an indicator of bed stability. The distribution of surface roughness and the critical shear stress associated with the incipient motion of individual grain size fractions are two crucial factors of central importance in river engineering. Critical shear stress represents the threshold shear stress in sediment transport functions. Incipient motion for each size fraction in a sediment mixture is of great importance when considering the entrainment of individual grains, or more generally, the proportion of grains on the bed surface that may be entrained.

Fractional transport rates q_i are defined as unit transport rate (in mass per unit time, per unit cross-stream width of the flow) of the ith size fraction in the total transportable sediment. The total unit transport rate q_b can be obtained by dividing the mass of the sediment transport by the time interval and the width of the channel, where the subscript b signifies bed load. A sample of the transported sediment is collected, dried, and sieved to find the proportion p_i of each size fraction in the sample. Fractional transport rates are then calculated by multiplying q_b and p_i, ie. $q_i = q_b \times p_i$.

Under the theory of equal mobility, for a given value of bed shear stress, the normalized fractional sediment transport rate, expressed as the ratio of the fractional transport rate of a given size range q_i (ability to transport) to the proportion of the given

size range in the bulk sediment mixture f_i (availability), should be identical for all of the sediment size fractions. Under high flows, the critical shear stress for each fractions τ_{ci} becomes approximately equal despite different sizes in the mixture.

Mixed-size sediment transport usually deviates from perfect equal mobility and exhibits gradation independence. The experimental results of Wilcock and Southard (1989) showed that the coarsest and finest size fractions in a sediment mixture are more difficult to transport. The finest sediment fraction has low mobility as a result of the winnowing process and hiding effect that act to shelter the smaller grains from the flow. However, the combined effects of hiding-sheltering and rollability are insufficient to counteract fully the effect of a low particle weight. In contrast to equal mobility for all size fractions, the concept of partial transport was raised by Wilcock and McArdell in 1997. It is defined as the condition in which only a portion of the grains on the bed surface move over the duration of a transport event (Wilcock and McArdell,1997;). The Surface-Based Transport Model (Wilcock and Crowe, 2003) applied the sand fraction on the bed surface to the hiding function to explain and adjust the departure from equal mobility. It showed that the amount of sand on the bed surface directly impacts the overall transport rate and incorporated this into a fractional transport model.

It is difficult to directly measure or calculate the critical shear stress for each size fraction of a sediment mixture. For the purpose of estimating sediment transport rates, the reference shear stress, τ_r, is defined as the "shear stress that produces a small constant and agreed-upon reference transport rate" (Wilcock et al., 2009). The reference shear stress is close to but slightly larger than the critical shear stress. A dimensionless fractional

transport rate parameter W_i^* is defined as $W_i^* = \frac{(s-1)gq_i}{F_i u_*^3}$, where F_i is proportion of ith size fraction on bed surface. W_i^* is independent of sediment size, D, which facilities the development of a transport function that holds for all sizes. The reference shear stress is taken as the shear stress when W^* =0.0002 (Parker et al, 1982). The equal mobility, partial transport, and surface based transport model all apply W^* in their calculations of bedload transport rate. The Surface-based sediment transport model developed by Wilcock and Crowe (2003) is used reversely in Chapter 6 to calculate the bed stability in terms of the non-dimensional reference shear stress through the sediment transport rate for grain size Ds_{50} on surface.

2.4   Armoring Process

Church et al. (1998) identified two fundamental processes associated with channel bed development in self-formed gravel-bed rivers: bed surface coarsening and armoring; and large roughness elements and bedform development. Coupled measurements of river bed surfaces and sub-surfaces verified that in many gravel-bed rivers, the bed is vertically stratified (Frostick, 1984; Hassan et al. 2006). Instead of a uniform distribution of grain size throughout the bed, gravel-bed rivers are typically composed by a frame of coarse particles overlying a matrix of finer sediment in the substrate due to the processes associated with bed surface armoring (Figure 2.4.1).

Figure 2.4.1 Armored bed with a frame of coarse particles on the surface

The development of the armor layer, that is, a surface layer coarser than the subsurface material, was detected by Wolman (1954) and then observed and discussed by many others (Little and Mayer, 1976; Proffitt, 1980; Parker et al., 1982; Parker and Klingeman, 1982; Day and Egginton, 1983; Leopold, 1992; Mao et al., 2009). These contributions revealed that armor layers develop in two different types: static armoring and mobile armoring.

Two theories describe the process of bed armoring. The first is that armoring is a result of selective entrainment depending on particle weights (Sutherland 1987). If channel flow is strong enough and sustained, it mobilizes some of the finer sediment while the remaining sediments are left immobile, or static. In this situation, the flows generate shear stresses less than that needed to entrain the coarser and heavier gravels but large enough to transport the finer and lighter particles downstream. During equilibrium transport, the input and output grain size distributions are the same whereas the transport

rate for each size fraction is subject to change corresponding to the flow and the sediment available to transport from the bed surface. This process occurs during a period of sustained low flow in a river and is simulated by a recirculating flume where the sediment input is essentially the bed material itself. If the sediment is coarse enough, vertical sorting may occur during which the fine particles sift downward into the substrate. The sediment transport rate becomes zero upon armoring (Wilcock and Southard, 1989). This is called a static armor because the surface particles remain in place during low flows. Weight selective transport is offset by the countervailing effects of hiding. The hiding effect occurs when the flow forces exerting on the more exposed, coarser, heavier particles are greater than the forces acting on the finer particles, which tend to be hidden and sheltered from the mobilizing forces in the flow by the larger particles. Hiding effects reduce the intrinsic difference in mobility between coarser and finer surface grains (Parker and Klingeman, 1982).

The second theory of armor formation relies on the winnowing of fine sediment from the bed surface. A vertical winnowing effect (Figure 2.4.2) occurs when the armor layer creates a pavement that acts as a thin buffer zone between the flow and the channel subsurface.

Figure 2.4.2 Schematic of fine particles winnowing and armored surface (Parker and Klingeman, 1982)

The surface pavement regulates the availability of substrate grains to the bedload as the channel to approaches equilibrium. The intrinsic high mobility of finer particles is counteracted by decreased availability on the bed surface whereas the coarse portion with an intrinsic low mobility is enhanced by an increased stock on the bed surface. With over-representation of coarse sediment on the bed surface, the slopes of both bed and water surfaces increase so that the hydraulic conditions adjust to increase the mobility of the coarser fractions (Wilcock and Southard, 1989). The bed adjusts to create equal mobility (Parker et al, 1982; Parker and Kingeman, 1982; Parker and Toro-Escobar, 2002). The coarse surface layer formed under a flow that is transporting all size fractions in the sediment is called a mobile armor (Parker and Klingeman, 1982; Andrews and Parker, 1987). Equal mobility is a requirement for equilibrium sediment transport in the feed flume system only where the feeding sediment composition is a constraint.

An armor layer increases the resistance to entrainment of the bed surface. Coarsening creates a rougher surface with greater intergranular friction angles which increase the stresses necessary to entrain the bed surface and decrease bed transport rates (Parker et al., 1982; Buffington and Montgomery, 1999; Vericat et al., 2006). Armor layers break-up with large catastrophic events and are re-formed during the falling limb of the flood hydrograph (Carling and Reader, 1982; Parker and Klingeman, 1982; Vericat et al., 2006). When the mobility of a gravel bed is estimated from the grain size distribution of the bed surface without consideration of the surface structure, the results often over-predict transport rates (Measures and Tait, 2008).

2.5   Clusters

Coarsening and structural modification of the bed surface generate interlocked imbrications of LREs which increase the stability of the armored layer (Brayshaw 1984). LREs and bedforms are observed to develop during armoring with low to zero sediment input from upstream. Clusters are one of the most common bedforms in a gravel-bed river, and are the essential research objectives in this study. Clusters form when particles deposit around a larger, key clast on the bed surface. Keystones generally have grain sizes of D_{90} or greater (Brayshaw, 1984; Wittenberg and Newson, 2005). Smaller stones and gravels accumulated against these keystones create an imbricated cluster. The shape of a cluster is often a streamlined stripe with a stoss and a wake. The keystone is preceded by smaller particles deposited in the "stoss" segment of the cluster, and followed by a deposition of fine particles in the sheltered "wake" area (Figure 1.1.1; Brayshaw 1984). Wittenberg and Newson (2005) observed all clusters to be composed by

stoss-side deposits while only 50% had wake-side fines and attributed this to either a lack of available fines or a low height of the keystone.

Clusters are more stable than individual particles and able to capture and retain incoming particles and then release them in pulses, thus exerting a considerable influence on sediment transport rates and bed stability (Strom et al. 2004). Fractional sediment transport models that do not incorporate the cluster effect on bed stability may incorrectly estimate the sediment transport rate for entire bed and particular size fractions (Tait et al. 1992; Church et al. 1998). Hassan and Reid (1990) studied the spatial distribution of clusters in two river reaches in British Columbia, Canada, and found that clusters were positioned immediately downstream from each other. They suggested that this spatial arrangement maintained maximum flow resistance. Similar to the correlation function developed by Strom and Papanicolaou (2008) to define cluster spacing, λ (Equation 2.5.1) was defined in this case as the distance from individual cluster to the nearest cluster along a downstream diagonal direction:

$$\lambda = \sqrt{\lambda_x{}^2 + \lambda_y{}^2} \qquad\qquad 2.5.1$$

where λ_x is the downstream cluster-to-cluster spacing for which $\Delta y = 0$ and λ_y is the transverse cluster-to-cluster spacing for which $\Delta x = 0$. For natural clustered beds, x and y are taken to be the streamwise and cross-stream directions respectively.

Isolated clusters on bed surfaces influence particle movement within the cluster while also influencing the surrounding flow field (Best 1996, Buffin-Belanger and Roy 1998; Lacey and Roy 2008). However, the spatial interactions among closely spaced clusters and their coactions on local flow fields have not been fully described. Clusters

may be sorted into three categories corresponding to the density of keystones within a cluster group: 1) Isolated Cluster. An Isolated Cluster is a single cluster composed of one keystone with at least 2 smaller gravels around it. The cluster influences the local hydrodynamics and bed particle availability. 2) Coupled Clusters. A pair of coupled clusters are composed by two Isolated Clusters, for which the distance between the clusters is less than a threshold spacing λ_c, where λ_c is defined as a length of $7d_s$ and d_s is the maximum gravel size for the coupled clusters. The arrangement of coupled clusters can be in any direction, including streamlined or transverse. 3) Grouped Clusters. Grouped clusters are defined as groups of more than two Isolated Clusters which are spaced such that the largest distance between any two of the grouped clusters is less than the threshold spacing λ_c.

2.6   Turbulent Flow in Open Channels

Chow (1959) defines the flow as turbulent if the viscous forces are weak relative to the inertial forces. The effect of viscosity relative to inertia can be represented by the Reynolds number, defined as

$$\boldsymbol{Re} = \frac{UR}{v} \qquad\qquad 2.6.1$$

in which U (m/s) is the cross-sectional time and space averaged longitudinal velocity of flow; R (m) is the hydraulic radius; and v (m^2/s) is the kinematic viscosity of water. The flow Reynolds number is used to classify the flow as follows

- laminar flow $\boldsymbol{Re} < 500$

- transitional flow $500 < \boldsymbol{Re} < 12{,}500$.

- turbulent flow $\boldsymbol{Re} > 12{,}500$.

In laminar flow, the water particles appear to move in definite smooth paths, or streamlines, and infinitesimally thin layers of fluid seem to slide over adjacent layers. In turbulent flow, the water particles move in irregular paths, which are neither smooth nor fixed, but which in the aggregate still represent the forward motion of the entire stream. Between the laminar and turbulent states there is a transitional state (Chow, 1959).

Turbulence is a ubiquitous characteristic of flows in gravel-bed rivers, where flow Reynolds numbers fall in the fully turbulent range. When turbulence is present, it usually dominates flow patterns and results in increased energy dissipation, mixing, heat transfer, and drag forces. In gravel-bed rivers, the roughness layer is defined by the heterogeneous bed topography, which is defined by arrangements of particles into bedforms of different size, shape and orientation. Turbulent flows are three dimensional and are characterized by high frequency fluctuating velocities and areas of increased vorticities. Turbulent flow structures near the bed develop as a result of interaction between flow hydrodynamics and the bed topographic features as defined by the sediment grain size distribution. To address the hypotheses linking bed stability, armoring, and clusters, my laboratory studies are designed to detect and characterize the hydrodynamic processes and turbulence flow structures around clusters and over the armored bed. These efforts investigate the effects of flow hydraulics and bulk sediment grain size distribution on cluster densities, cluster geometries, and the local hydrodynamics around each cluster.

2.7   Velocity and Turbulence Statistics

Turbulent flow is characterized by rapid spatial and temporal variation of velocity, high momentum convection and energy dissipation. As a result of high irregularity, turbulent flows are statistically described in terms of component velocities

$$\bar{u} = \frac{1}{n}\sum u; \quad \bar{w} = \frac{1}{n}\sum w \qquad\qquad 2.7.1$$

in which $\bar{u}\ and\ \bar{w}$ are time-averaged mean velocity in longitudinal and vertical directions; n is the total number of measurement; and u and w are the instantaneous velocities. Longitudinal and vertical velocity fluctuations are defined as

$$u' = u - \bar{u}; \quad w' = w - \bar{w} \qquad\qquad 2.7.2$$

Two time series of velocity measurements can have an identical mean but be members of different ensembles since the amplitudes of their fluctuations may not be distributed the same. Statistical properties, such as standard deviation, and higher statistical moments are calculated to measure the differences in data records. The higher moments of the velocity time series, such as skewness and kurtosis, are often used to characterize the asymmetry of the probability density function (pdf) curve and to assist in quadrant analysis, which is discussed in Section 2.8.

A common approach to the study of turbulent fluid flow is through the application of the Reynolds-Averaged Navier-Stokes equations (RANS). These are the time-averaged Navier-Stokes equation using Reynolds decomposition, whereby an instantaneous value is divided into time-averaged mean value and fluctuating quantities. Change in flow momentum due to fluid motion and convection is equal to the sum of mean body force,

isotropic stress due to the mean pressure, viscous stress, and velocity fluctuation induced stress, which is referred as Reynolds stress. That is, in the longitudinal direction:

$$\rho \frac{\partial \bar{u}}{\partial t} + \rho \bar{u} \frac{\partial \bar{u}}{\partial z} = \rho \overline{B_x} + \frac{\partial}{\partial z}\left[-\bar{p}\delta_{xz} + \mu\left(\frac{\partial \bar{u}}{\partial z} + \frac{\partial \bar{w}}{\partial x}\right) - \rho\overline{u'w'}\right]$$

2.7.3

The direct measurement of the Reynolds stress in the longitudinal direction is a measure of the mean momentum flux due to turbulent fluctuations, and represents the stress generated by turbulent part of the flow. The Reynolds stress is calculated using the covariance of the instantaneous turbulent fluctuations of two of the three flow dimensions u_i' and u_j', where ρ is the water density. The Reynolds stress acting over the streamwise-vertical plane in the streamwise direction provides a measure of the anisotropic structure of the flow. This Reynolds stress is calculated as:

$$\tau_{xz} = \tau_{Re} = -\rho\overline{u'w'}$$

2.7.4

where ρ is the water density equal to 1000kg/m^3 and u' and w' are the longitudinal and vertical velocity fluctuations. Because the streamwise-vertical stress is the only component of the Reynolds stress tensor used in this manuscript, we refer to it here as the Reynolds stress.

Total shear stress has two components: stress produced by mean flow viscosity and stress contributed by turbulent momentum, the Reynolds stress.

$$\tau = -\rho\overline{u'w'} + \mu\frac{\partial \bar{u}}{\partial z} = \rho u_*^2\left(1 - \frac{z}{Z}\right)$$

2.7.5

In an open channel with fully rough flow, the total shear stress equals the Reynolds stress as the viscous stress is negligible. Shear velocity u_* can be obtained by extrapolating the linear stress profile to z/Z = 0. Theoretically, the Reynolds stress is zero

at the water surface and increases linearly towards the channel bed reaching a maximum value τ_b. With an acoustic Doppler velocimeter (ADV), 3D velocity tensors can be measured to yield the vertical Reynolds stress profile. In the wake region of LREs where there is a complex turbulent flow field, the vertical Reynolds stress profile may not be linear and the shear velocity u_* and total shear stress on bed are better estimated by single point Reynolds stress observations close to the bed (Lacey and Roy, 2008). The shear stress can also decrease substantially close to the bed if there are large protruding grains, bedforms or other LREs present on the bed, or if there are moving particles interrupting the flow (Biron et al, 1998; Voulgaris and Trowbridge, 1998; Nikora and Goring, 2000; Afzalimehr and Anctil, 2000, Martin et al., 2002). Considering all of the above, the Reynolds stress profiles calculated as part of this research were found by fitting least squares regression lines to the linear portion of the measured velocity profile. The line was then extrapolated to the bed to obtain the local bed shear stress.

The standard deviation of the velocity time series is physically interpreted using the Turbulence Intensity (TI) and the Turbulence Kinetic Energy (TKE). The normalized turbulence intensity is defined as

$$TI_x = \frac{u_{rms}}{u^*}; \;\; TI_y = \frac{v_{rms}}{u^*}; \;\; TI_z = \frac{w_{rms}}{u^*} \qquad\qquad\qquad \text{-} \qquad\qquad 2.7.6$$

in which u_{rms}, v_{rms}, w_{rms} are the root-mean-square velocities in longitudinal, lateral and vertical direction, respectively:

$$u_{rms} = \left[\frac{1}{n}\sum(u')^2\right]^{1/2}; \; u_{rms} = \left[\frac{1}{n}\sum(u')^2\right]^{1/2}; \; u_{rms} = \left[\frac{1}{n}\sum(u')^2\right]^{1/2} \qquad 2.7.7$$

In order to study turbulent energy evolution and dissipation in the flow, Turbulent Kinetic Energy (TKE) is calculated. TKE represents the mean kinetic energy per unit

mass associated with coherent structures in the turbulent flow and is calculated as half the sum of the turbulent normal stress.

$$TKE = \frac{1}{2}\left[\overline{(u')^2} + \overline{(v')^2} + \overline{(w')^2}\right] = \frac{1}{2}\left[u_{rms}^2 + v_{rms}^2 + w_{rms}^2\right] \qquad \text{2.7.8}$$

TKE can be decomposed into components of fluid shear production, mechanically generated eddies through wake production, turbulent transport, and viscous dissipation.

2.8   Quadrant Analysis

A quadrant analysis is performed to identify the dominant turbulent flow events in the flow field and to aid in identification of any potential coherent flow stuctures. Instantaneous flow velocity fluctuations are graphed on a *u'- w'* grid and categorized into quadrants according to the dominant data clustering (Lu and Willmarth 1973). The quadrants define the four modes of momentum transfer that may occur in a flow. Quadrants 2 (*u'<0; w'>0*) and 4 (*u'>0; w'<0*) indicate the dominance of ejection and sweep events, respectively. Events in quadrant 1 (*u'>0; w'>0*) are outward events while those defined by quadrant 3 (*u'<0; w'<0*) are inward. Sweep events (*Q4*) transport high velocity fluid from the outer flow regions toward the bed while ejections (*Q2*) transport low momentum fluid from the bed upward in the flow profile. Pairing of ejection and sweep events is common around LREs and provides a dominant mechanism for momentum transfer in the flow (Grass 1971; Nakagawa and Nezu, 1977; Reidenbach et al. 2010). defined a normalized instantaneous momentum flux fluctuation,

$$\tau_{i,H}(t) = \frac{\langle u'w' \rangle_{i,H}}{\overline{u'w'}} = \frac{1}{\overline{u'w'}} lim_{T\to\infty} \int_0^T u'w' I_{i,H}(t)dt \qquad \text{2.8.1}$$

in which the angle brackets denote a conditional average, H is the hole size; i defines the particular quadrant of interest ($i = 1, 2, 3, 4$); T is the time interval between measurements, and $I_{i,H}$ is the threshold indicator defined as

$$I_{i,H}(t) = \begin{cases} 1 & when \ |u'w'|_{i,H} \geq Hu_{rms}w_{rms} \\ 0 & otherwise \end{cases} \qquad 2.8.2$$

The hyperbolic hole function, H, in the $u'w'$ plane is applied to an analysis to enable a focus on only those velocity fluctuations with large contributions to Reynolds stress. The hole function defines a minimum velocity fluctuation value below which the data are not included in the quadrant analysis. The value of H is user defined, and past researchers have applied a range of H values to armored gravel beds (Lacey and Roy 2008b; Strom and Papanicolaou 2007). In this study threshold H values of 0 and 2.5 are used to characterize low and high magnitude turbulent events respectively (Buffin-Belanger and Roy 1998; Lacey and Roy 2008b). When $H = 0$, all contributions in terms of $u'w'$ are included within the quadrant analysis. When $H = 2.5$, only the high magnitude turbulent flows are considered.

2.9   Recirculating and Feed Flume

Flume experiments provide a basic but nonetheless comprehensive approach to model hydraulics, sediment transport, and the two types of armoring processes (Parker and Wilcock, 1993). When sediment is fed into the upstream end of the flume, the flume system adjusts the bed surface sediment composition, flow depth, and bed slope, to carry the imposed load. Mobility of coarse sediment is enhanced by accumulation on the surface until the grain size distribution for bedload and the supply are the same (Parker and Klingeman, 1982). With a higher flow rate, the armored layer breaks and the surface

sediment sizes become finer whereas the composition of bedload remains constant. In contrast, when the transported sediment at the downstream end of the flume is immediately returned to the upstream end, the sediment is recirculated. The flow rate and initial sediment grain size distribution are independent parameters while grain size distributions for transported and bed surface, total and fractional transport rates, and energy slope are free to adjust. Under higher flow rates, the transported sediment size tends to increase while the composition of the bed surface remains relatively constant (Figure 2.9.1 Parker and Wilcock, 1993). The equilibrium conditions for these two flume operations are very different. In the feed flume, all size fractions transport and fractional transport is less common. In the recirculating flume, size distributions for the sediment surface and bedload are free to adjust, enabling fractional transport as equal mobility is not required (Parker and Wilcock, 1993). For both feed and recirculating flumes, at low flow and sediment transport rates, the same general armoring trend occurs in that the sediment on the bed surface is coarser than the sediment transported (Figure 2.9.1 Parker and Wilcock, 1993).
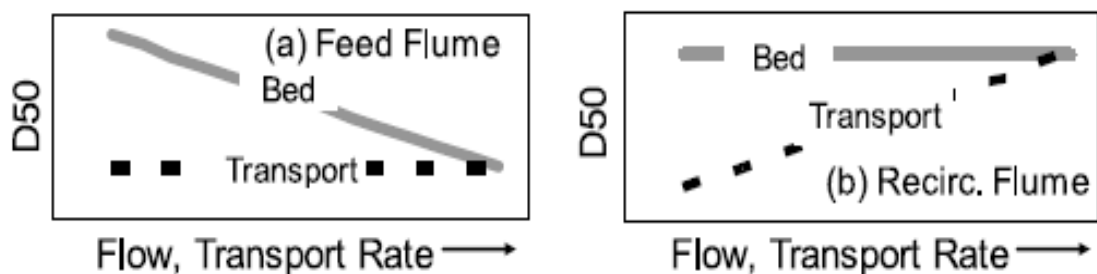
Figure 2.9.1 Schematic of bed surface and transport sediment size adjustment for feed and recirculating flume (Wilcock and DeTemple, 2005)

Natural streams and rivers behave as a combination of sediment recirculating and feed. The current bed state and sediment transport at any time reflects the interaction between the flow and bed surface at an earlier time (recirculating), but also the influence of the upstream sediment load (feed) (Parker and Wilcock, 1993). The presence of a static armor layer on the river bed surface is a common phenomenon downstream of dams and upstream of significant tributary inputs (Shen and Lu, 1983; Williams and Wolman, 1984; Richards and Clifford, 1991; Lamberti and Paris, 1992; Kondolf, 1997; Brandt, 2000; Grant, 2001; Vericat et al., 2006). A recirculating flume was chosen for this study which investigates the armoring process and impact of clusters in response to a series of specified flow rates and sediment compositions. Recirculating flumes better represent the field situation where the channel develops over extended temporal and spatial scales. Recirculating flume experiments simulate the low flow and sediment transport conditions where the flow rate and bulk sediment are non-varying spatially and temporally. Detailed information of the flume configurations will be addressed in Chapter 3.

Chapter 3.

EXPERIMENTAL WORK

3.1   Introduction

Experiments were performed in a sediment and water recirculating flume in the Sustainable Rivers Laboratory of the Department of Civil and Environmental Engineering. The experimental channel was 9 meters long 0.6 meters wide and 0.5 meters deep. A 3 meter long 1.5 meter wide and 1.7 meter deep tank was built up for water supply and recirculation. The flume is capable of a maximum flow rate of 0.12m^3/s, and flow passed through a set honeycomb meshes prior to entering the flow channel (Figure 3.1.1). A slurry system recirculated sediment clasts up to 16 mm, leaving the only the largest size fractions to accumulate on a wire screen at the entrance to the recirculation system. These larger sediments were recirculated manually. The flume represents a mid-section of a channel so that the influence of flow rate and channel sediment movement during bed armoring was measured directly.
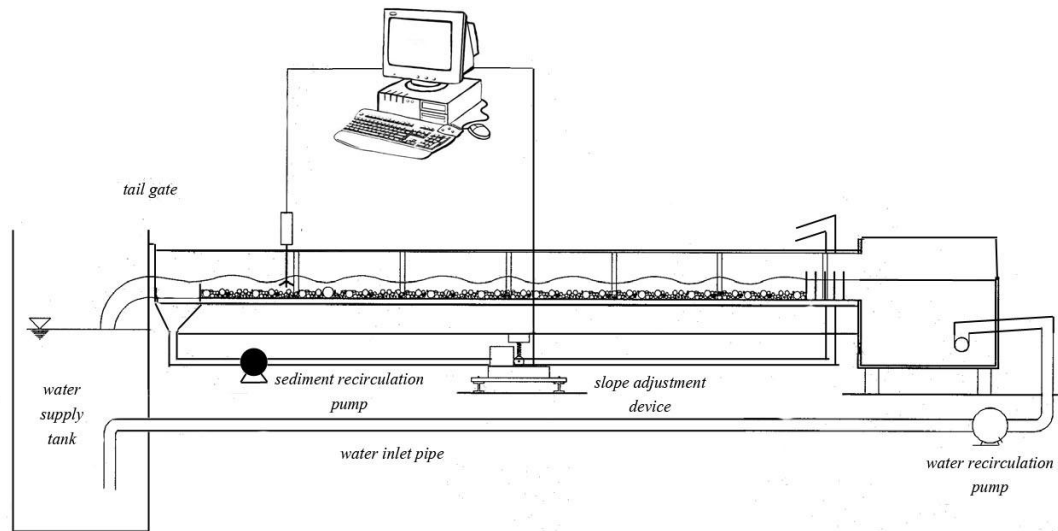
Figure 3.1.1 Schematic of flume set-up

Four experimental sediments were tested in these experiments. The first experiment used the sediment with the largest median grain size, and the median grain size of consecutive experimental sediments was decreased by adding sand into the bulk sediment used in the previous experiment. For each sediment mixture there were two to three runs with different flow rates. Table 3.1.1 shows the matrix of the experiments and the data that was collected from each experiment. By applying a matrix set-up for the experiments, I was able to test the influence of flow and sediment composition on cluster occurrence, distribution, and density separate from each other. The flow rates for these experiments were chosen to develop transport rates and shear stresses that would test the effect of flow rate on armoring. There were three different sets of flow rates tested against each of the four sediments. The flow rates maintained a subcritical flow, and flow depth was held constant at 10 cm throughout the experiments.

	Q: 0.07 m^3s^{-1} / Q_a: 0.035 m^3s^{-1}	Q: 0.09 m^3s^{-1} / Q_a: 0.045 m^3s^{-1}	Q: 0.11 m^3s^{-1} / Q_a: 0.055 m^3s^{-1}
100% gravel, 0% sand	Bed surface profiles		
	Cluster density in each 1-m section		
	Overall cluster density		
90% gravel, 10% sand	Maximum and average cluster spacing		
	Total stress for armored bed as a whole		
	Shields stress for an unclustered area of armored bed		
77% gravel, 24% sand	Time until transport initiated from armored bed		
	Grain size distribution of the initial bed surface		
	Grain size distribution of the armored bed surface		
65% gravel, 38% sand	Reynolds stress, TKE, TI around clusters of interest		
	Relative quadrant dominance around each cluster		

Table 3.1.1 Experiment Matrix

Each run consisted of three segments, defined by segment discharge. In segment 1, the flow rate created active transport of the sediment bed, with each size fraction either fully or partially mobile. This segment eliminated any bias introduced with the creation of the initial bed in the flume. Segment 1 continued until the bed reached a dynamic equilibrium state. Equilibrium was not expected to be static, and these runs were designed to achieve a dynamic equilibrium during which the channel bed was no longer aggrading or degrading. Dynamic equilibrium was determined to be when the bed and water surface profiles were parallel over the length of the flume. Segment 2 was designed to develop the armor layer on the channel bed. The flow rate was reduced by half from the rate used in Segment 1 and remained constant while the bed armored. Segment 3 assessed the stability of the armored bed by increasing the flow rate back to what it was

during Segment 1. The discharge in Segment 3 created active sediment transport and caused the armor layer to break. The flow rates for these runs were chosen from previous flume research. The flume runs described in Wilcock et al. (2001) and Wilcock and Crowe (2003) evaluated the transport rates of sediment beds which underwent an increase in sand content. The flow rates that correspond to mobile beds under bed substrates with sand contents near those being researched here were identified. These flow rates were used to set the flows for segments 1 and 3 of each of the experiments. With three segments for each of the 9 runs, there were a total of 27 separate flume run segments.

For each experiment, the flume slope was kept constant while the sediment bed slope was free to adjust. The flume slope was determined before each run through application of basic sediment transport, momentum and continuity equations:

$$q_b = 8\sqrt{(s-1)gD^3}\left(\frac{\tau_b}{(s-1)\rho gD} - \tau_{cr}^*\right)^{3/2} \qquad 3.1.1$$

$$\tau_o = \rho gZS \qquad 3.1.2$$

$$S = \frac{ff U^2}{8gh} \qquad 3.1.3$$

$$ff = \frac{8}{\left(2.5\ln\left(\frac{11Z}{2D}\right)\right)^2} \qquad 3.1.4$$

The initial flume slope was set in such a way that minimized the bed slope adjustments and time to reach the equilibrium state. All flume runs followed the 8-step approach outlined here.

1. Create initial bed. For each experiment, the desired sediment composition was created by adding sand into the bulk sediment if necessary. The sediment was thoroughly mixed and a sediment bed 10 cm thick was created over the length of the flume and screeded flat. For subsequent runs using the same sediment, the sediment grain size distribution does not change so only screeding was necessary.

2. Segment 1. Create the dynamic equilibrium sediment transport condition. The full discharge for the given run is used to mobilize the sediment bed. During this run segment, the bed surface and water surface elevations are measured. Segment 1 continues until the bed adjusts to a state of dynamic equilibrium. A transport sample was taken, analyzed, and recycled upstream every 10 minutes to determine the distribution and transport rate of the sediment.

3. Scan Bed. Following Segment 1 the flume is drained and the bed surface topography scanned. The bed cross-section topography is measured through every 2 mm using laser scans and the individual cross sections stacked to create a Digital Elevation Model (DEM) (Darboux and Huang, 2003; Zimmermann, 2009). These DEMs are used to depict the distribution of bed elevations above a standardized arbitrary reference datum and derive statistical metrics describing the surface roughness and geomorphic variability of the bed surface. Any bedforms on the bed surface are documented and measured. After the bed scan, the grain size distribution of the bed surface under equilibrium is determined using the grid by number method (Wolman, 1954).

4. Segment 2, create an armored bed surface. The flow rate is reduced by half from the rate used in Segment 1 and remained constant until the sediment bed has armored. Segment 2 continues until the rate of sediment transport as measured at the downstream end of the flume is less than 1% of the rate measured at the end of Segment 1. It is not possible to know with absolute certainty the point at which all particles have stabilized and will not transport, so the very low transport rate is used as a cut-off.

5. Flow field measurement. After the bed is fully armored, the 3-Dimensional (3-D) flow fields created by the armored bed both with and without clusters are measured. Clusters are expected to influence the flow patterns in their immediate area, and detailed measurements of the 3-D velocities in the region immediately around each cluster are taken.

6. Scan Bed. The armored bed surface is scanned using the same process as detailed in step 3. Clusters are identified from the DEMs created from these scans, and their geometric properties measured, including cluster length, height, and width. Using a digital camera, the entire bed surface is photographed. The different grain sizes creating each cluster are identified by clast color and the mean of the sizes of key clast of each cluster d_{sm} is determined. The armor ratio is not directly measured as that will necessarily destroy the armor and interfere with the goals of this research. Instead, the distribution of the larger grain size fractions and the percentage of bed area covered by sand are determined using the clasts colors and the digital

photos of the bed. These are compared to the surface grain size measured in step 3 as an assessment of the changes in the bed surface with formation of bed armor.

7. The DEMs also allow for the spatial location of each cluster to be identified and measured relative to other clusters on the bed. The clusters need to be spatially identified over the horizontal plane defined by the sediment bed which requires a means of locating within a 2-Dimensional (2-D) space that can include patterns that may be regular or irregular. Cluster density is measured over individual sections of the bed and for the overall bed surface. The 75mm of bed adjacent to the sidewalls is not included in the cluster density analysis because of potential sidewall effects. These effects have been shown to be minimal at 100mm from a smooth flume wall (Vanoni and Brooks, 1957). The number of clusters in each longitudinal meter of the bed was divided by the area of the bed surface in that section ($0.45m^2$). This process was repeated for the cluster density over the entire sediment bed ($2.8m^2$). Through these measures, any change in cluster density with distance downstream was identified along with the overall cluster density for the run.

8. Segment 3. The flow rate was increased to the same discharge as in Segment 1. For each 10 minutes, the flume run was paused and a DEM of the bed surface was created. These DEMs were stacked into an animation to track the migration of the bedforms and to identify motion patterns of the clusters measured in Segment 2. The bedload transport rate was measured from the sediment collected on the downstream wired screen to create a record of the rate of bed movement and timing of armor break-up. The number of the clasts in the four largest size fractions

in each sample was counted and the remainder of the sample weighed. Segment 3 continued until the bed armor had fully broken and the bed surface mobile.

3.2 Sediment

In this study, a natural gravel-bed sediment distribution was simulated. Sediment consisted of an increasing fraction of 0% ~ 38% sand of size under 2mm and smaller and a gravel fraction from 100% to 62% of the sediment which had a sediment size distribution between 2mm to 64mm,. The sediment distributions for each experiment are summarized in Table 3.2.1 by ½ ϕ fraction and illustrated in Figure 3.2.1. The sediment was remixed manually between each set of flow rates.

The largest five size fractions were painted to aid in their identification in the flume: 11.3mm-16.0mm, purple; 16.0mm-22.6mm, yellow; 22.6mm-32.0mm, green; 32.0mm-45.3mm, red; 45.3mm-64.0mm, blue. Similarly, the sand fraction (all grain sizes < 2mm, D_{50}=1.0 mm) was colored with all fractions brown. (Table 3.2.1) The addition of color assisted in identification of the key and component clasts in the clusters. Direct clast size measurements were not possible in these experiments as it would necessarily destroy the armored bed surface. By painting the large size fractions distinct colors, the sizes of the grains in the clusters could be visually identified. The sediment was used to create a bed 10cm thick over the length of the flume. This bed thickness is more than twice the length of the a-axis of the largest grain size. The upstream 2.5 meters long of the bed is not taken into account for measurement and data collection in order to ensure the flow is fully developed before it entered the test section, which is therefore 6.5 meters long. A screen at the downstream end of the flume captures large grain size (>16mm) sediment. Anything smaller than 16mm passes through the screen and is transported back to the upstream end of the flume by a sediment recirculation pump. The screen has an

opening of 16mm so that sediment colored by blue (45mm), red (32mm), green (22.5mm) and yellow (16mm) are captured.
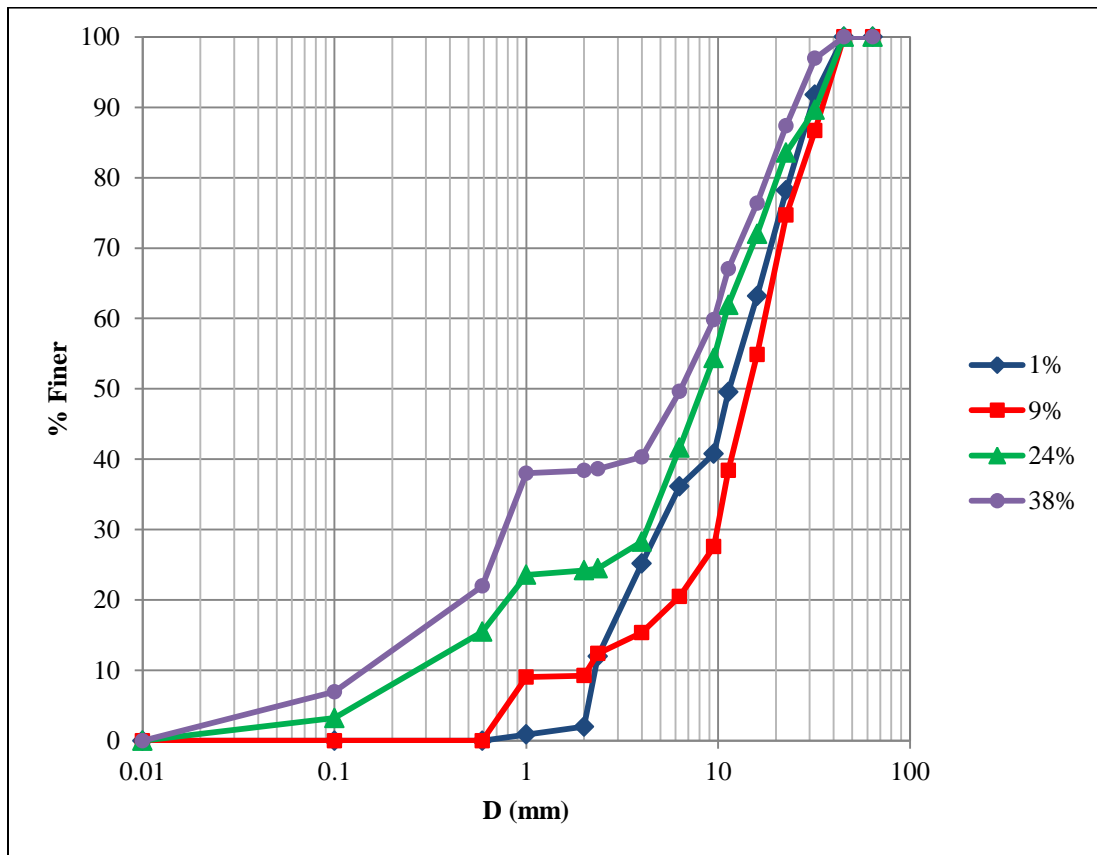
Figure 3.2.1 Grain Size Distribution for sediment with 10%~ 38% sand fractions

D (in)	D (mm)	Color	Type
2.520	64.00		cobble
1.782	45.25	Blue	very coarse gravel
1.260	32.00	Red	Very coarse/ coarse gravel
0.891	22.63	Green	coarse gravel
0.630	16.00	Yellow	coarse/ medium gravel
0.445	11.31	Purple	medium gravel
0.315	8.00	none	medium/ fine gravel
0.223	5.66	none	fine gravel
0.157	4.00	none	Fine/very fine gravel
0.111	2.83	none	very fine gravel
0.079	2.00	none	very fine gravel/very coarse sand
0.056	1.41	brown	very coarse sand
0.039	1.00	Brown	coarse sand
0.028	0.71	Brown	coarse sand

Table 3.2.1 grain size fractions with different colors

3.3   Bed Surface Elevation and Water Depth Measurement

The bed surface elevations were measured during the experiments. The elevations were read from rulers which were mounted every 50cm on the flume wall. Both the flume wall and the rulers were transparent so that the bed surface elevation could be read directly.

Water surface elevation was measured by using a point gauge. The point gauge was installed on the carriage that traveled along the rails on top of the flume. Water surface elevations were measured down the middle of the flume to avoid any influence of side walls. During the run, measurements were taken to monitor the flow and bed

development and plotted in a spreadsheet for visual comparison of the bed and water surface slopes. The averaged water surface slope and bed slope values for the entire test section were determined by taking the mean of all the local measurements. Dynamic equilibrium was determined in part as parallel water and bed surface slopes.

A DEM was created to represent the geomorphic characteristics of the armored surface and to document the movement of bedforms after the armored bed broke. DEMs for the equilibrium, armored and final bed surfaces were generated using a custom-built laser scanner for Run 1, 2, and 3. The laser scanner featured a laser line emitter and a scA1390-17gm Gigabit Ethernet camera manufactured by ©Basler Vision Technologies. The laser line was emitted perpendicular to the flume bottom and extended across the flume width to measure the cross-sectional bed topography. The camera was mounted on the carriage at an angle equal to the flume slope. A stepper motor moved the carriage in a 2mm step interval over 6500mm from the downstream to upstream end of the flume, taking pictures of the laser lines measuring the individual cross-sectional topography at each stop. The angle was determined in such a way that the entire cross-sectional laser line was visible in each image and it was kept fixed during the scanning process. Image data collection, processing, and DEM generation were all conducted through LabVIEW programming.

An ©MICRO-EPSILON scanCONTROL™ laser profiler was used for the rest of runs as a supplement and to generate an equally fine resolution DEM. The profiler was able to measure the bed surface topography to an accuracy of 2mm to be consistent with previous runs. The deployment of the profiler made detailed measurements of bed

elevations above a reference datum possible through the DEM. The scanner system was

be mobilized using a system of three stepper motors which moved the instrument exact

lengths over the armored bed area. To ensure a high level of accuracy, the scanned area is

limited to 200mm and two strips of measurements were taken and combined to create a

whole bed DEM. An unforeseen offset error occurred when combining the DEMs and

there was a slim gap of 25mm between the two sub-DEMs.

3.4 Flow Rate Measurement

A magnetic flow meter was installed to measure the water velocity through the

return pipe. When combined with the dimensions of the pipe, the average flow rate in the

flume was calculated using the equation:

$$Q = UA = \frac{Q_{pipe}}{\pi r^2} BZ \qquad\qquad 3.4.1$$

where Q_{pipe} is the discharge in water inlet pipe, r is the water inlet pipe radius, B is

the flume width and Z is the water depth in flume.

A ©Nortek AS Vectrino™ Acoustic Doppler Velocimeter was used to measure

the instantaneous three-dimensional velocity in the flow field around clusters of interest.

The detailed methods for data collection and analyze are addressed in the next sections.

The discharge in the flume was verified by the data measured by the Acoustic Doppler

Velocimeter.

3.5 Flow Velocity and Turbulence

To describe accurately the flow field generated around clusters, high spatial

resolution is needed for both velocity and topographic measurements (Lamarre and Roy,

2005). For this research, we employed the ©Nortek AS Vectrino™ Acoustic Doppler

Velocimeter (ADV) (Figure 3.5.1), which is able to measure near the bed surface at a fin resolution. A high rate of sampling was maintained (200Hz), enabling the collection of high resolution three-dimensional flow measurements. ADVs have become more common because of their ability to measure at a high resolution under a variety of conditions (Wren, personal comm.). Through the use of the Vectrino Velocimeter, the three-dimensional flow field generated by the structured armored beds and around individual clustered was able to be quantified.

Figure 3.5.1 Nortek AS© Vectrino™ Acoustic Doppler Velocimeter (ADV) (from Nortek AS© web site)

The configuration of the ADV probe enables the 3-D flow measurements (Figure 3.5.2). Areas of the armored bed where there were no clusters were measured in addition to those areas with clusters to allow for a comparison and analysis of the change to the flow profile due to cluster presence. Vertical flow profiles were taken by positioning the ADV first at 5mm (distance from the sensor to the sampling volume in Figure 3.5.2) above the highest point of the area to be measured and then increasing the height above

the bed by 5mm increments up to 100mm. Flow profiles were taken in locations with single clusters, where clusters are absent, and where clusters were grouped with different densities. The probe will be held at each location for a 120-second duration to allow the ADV to sample at a frequency that maintains equipment error of less than 1 mm/s. (Figure 3.5.3)

Figure 3.5.2 Vectrino ADV probe configuration and measuring volume position (from Vectrino™ ADV Manual)
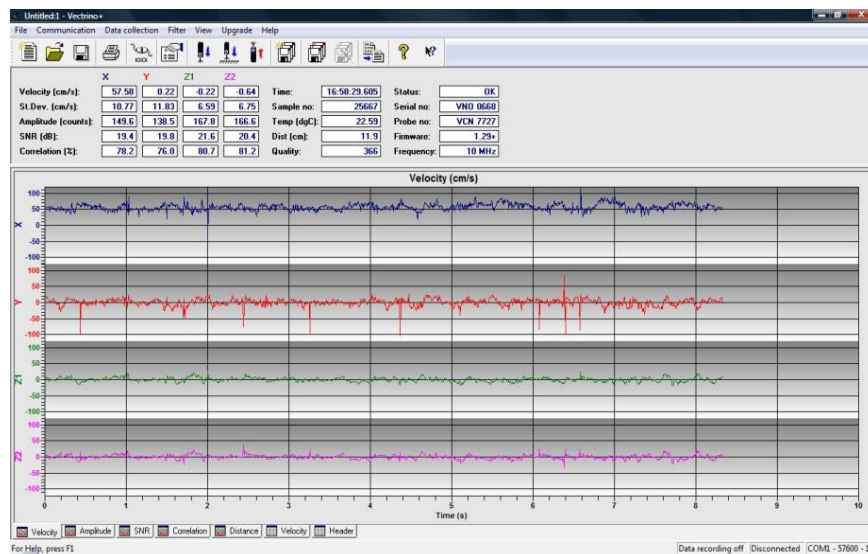
Figure 3.5.3 Screen Shot example of the measurement taken by the ADV showing the point instantaneous velocities (u,v,w) and fluctuations (u',v',w') over the bed surface

Velocity measurements were made in a 3-D grid pattern around each area of interest. The horizontal measurement areas extended over the clustered and non-cluster areas between the clusters as well as the wake zone for the isolated cluster. The velocimeter was attached to a system of three stepper motors which moved the instrument exact distances over the bed area of interest. The grid extended in the vertical as well as horizontal and transverse directions (Figure 3.5.4). Thus, the same Cartesian grid pattern was followed over the vertical flow profile. Each time the velocimeter was moved to a measurement location, or grid node, the three-dimensional velocity was measured over 120 seconds such that the velocimeter sampled at a frequency that maintained equipment error of less than 0.001m/s. Vertical spacing for the measurements was either 0.005 or 0.01m, while longitudinal and transverse spacing was 0.05m, which was slightly larger than the maximum clast. Measurement grids were centered over each area of interest.

Figure 3.5.4 Measurement grid shown over a single cluster; Flow velocity was measured at each grid node and the same grid was maintained through the flow profile. Overall grid size was adjusted to the size of the measurement area.

3.6   Velocity Time Series Data Quality

Velocity time series were initially inspected by eye for abnormalities and then de-spiked using the mean and standard deviations. Data values greater or lower than the mean velocity $\pm$ three standard deviation were truncated to achieve a relatively clean and regular time series. The Vectrino™ ADV signal correlation R_{adv} was used to detect unreliable data points. Manufacturers of both Sontek and Nortek ADVs recommend that velocity measurements for which the R_{adv} is less than 70% be considered acoustic noise and removed from the time series. However, others have reported that the signal quality is reduced at the region of high turbulent flow due to the shear in the sampling volume and the threshold correlation may be below 70% (Martin et al. 2002; Strom and Papanicolaou 2007). In recognition of this, we applied a filter designed to discard instantaneous velocity data points when the correlation R_{adv} <65%. Data with a correlation between 65% and 70% were maintained in the velocity time series to account for low correlation measurements caused by high turbulent events occurring in near bed regions.

3.7   Velocity and Turbulence Statistics

The time series data collected at each grid node were analyzed and several turbulence variables (e.g. Reynolds stress and Turbulent Kinetic Energy) quantified using the three-dimensional velocity data. Flow velocities are defined whereby u corresponds to the stream-wise direction x, v to the lateral (or transverse) direction y, and w to the vertical direction, z (Figure 3.7.1). As discussed in Section 2.7, the Reynolds stress refers to the stress acting over the stream-wise-vertical plane in the stream-wise direction and

the Turbulent Kinetic Energy (TKE) represents the mean kinetic energy per unit mass associated with coherent structures in the turbulent flow. These quantizes were calculated according to equations 2.7.4 and 2.7.6, respectively.
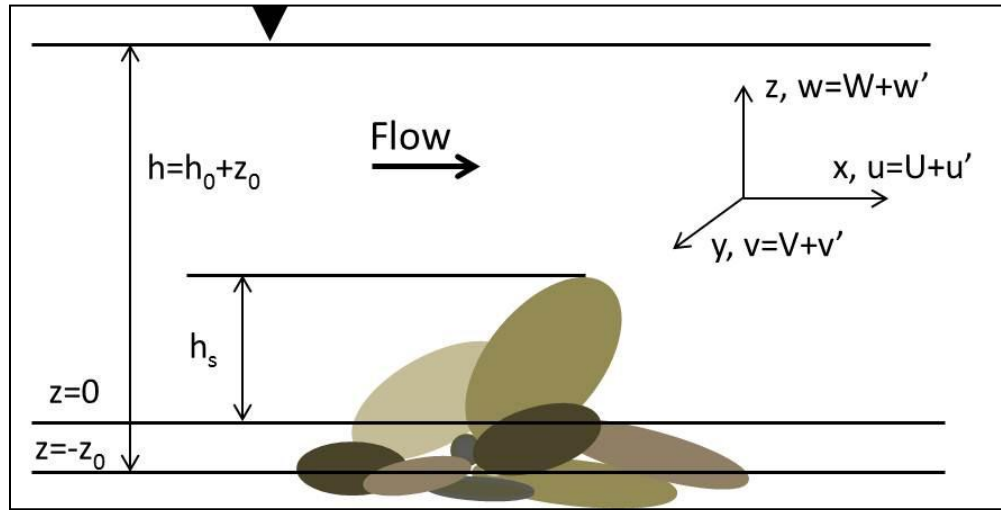
Figure 3.7.1 Definition sketch of a cluster on a bed surface and three-dimensional flow directions: h_s is height of cluster; $z=-z_o$ is the lowest elevation of the bed surface around the cluster; $z = 0$ at the mean bed elevation; h_o is the measured water depth

3.8 Quadrant Analysis

A quadrant analysis was performed to identify the dominance of turbulent flow events throughout the flow field generated around each cluster, group of clusters, and areas of open armored beds. The analysis was performed following the process outlined in Section 2.8, and the details are included in the following chapters where appropriate. Flow directions for all quadrant analyses are defined in Figure 3.7.1. The threshold hole values of 0 and 2.5 were used to characterize low and high magnitude turbulent events respectively (Buffin-Belanger and Roy 1998; Lacey and Roy 2008b). When $H = 0$, all contributions in terms of $u'w'$ were included within the quadrant analysis. When $H = 2.5$, only the high magnitude turbulent flows were considered.

3.9   Summary

A periodically repeated sequence of sediment transport samples were taken for both equilibrium sediment transport and armored bed sediment transport stages by collecting and counting the colored coarse gravels trapped at the downstream end and weighing the finer sediment recirculated at the upstream end. Three dimensional flow velocity measurements were made using an ADV over the full velocity distribution over both the armored bed and the different cluster arrangements. Using a laser displacement scanner to develop Digital Elevation Models (DEMs), clusters and other large scale bedforms were identified and their dimensional characteristics were measured. Critical shear stresses for the different sediment bed surfaces were calculated by reverse prediction from sediment transport rate data. Bed stability was evaluated through two approaches: qualitative assessment by recording the duration of a static armored bed surface after the flow rate brought back to original magnitude for each run, and quantitative bed stability was evaluated by the parameter of relative shear stress in terms of the ratio of boundary shear stress to critical shear stress. The turbulence variables of Reynolds stress and Turbulent Kinetic Energy were quantified around each area measured using the 3-D velocity data collected with the ADV. Quadrant analyses were performed to aid in the identification of coherent recirculation cells generated by the bed surface. When paired with the TKE and Reynolds stress values, the influence of different recirculation cells on the local flow field could be discerned.

Chapter 4.

EFFECT OF CLUSTER DENSITY ON HYDRODYNAMICS

Abstract

Gravel-bed rivers commonly form an armored surface layer within which cluster bedforms develop. Clusters can form in isolation or develop cluster groups of increasing density. Flume experiments are presented where a clustered, armored surface was formed on a gravel bed. Flows were measured over an area without a cluster, an isolated cluster, a coupled two clusters, and a grouped triple clusters. Turbulent flow parameters, Reynolds stresses and Turbulent Kinetic Energy, were calculated from Acoustic Doppler Velocimeter measured flows, as well as visualizations of the flow patterns around clusters. Flow separated over the cluster crest, creating an increase in the turbulent flow properties and a high turbulence intensity region when flow re-attached downstream. Turbulent Kinetic Energy increased around the coupled clusters, but around the grouped clusters, the flow field was distinguished by a high degree of uniformity. The net effect of increasing density of cluster grouping was an increase in the magnitude and variability of the turbulent flow field around coupled clusters followed by an overall dampening of turbulent flows around grouped clusters where the flow patterns generated interfered with each other and the cluster forms sheltered the bed surface.

4.1   Introduction

The river bed acts as an interface between channel flow and subsurface sediments, determining the sediment available for transport at the local scale. When the channel has a mobile bed, the presence or absence of bedforms becomes an important part of the bed surface topography. In a gravel bed river the bed surface is often additionally defined by whether or not it has an armored surface. A static armored bed condition develops as a result of an extended period of low flows over a mixed gravel bed. Low velocity flows generate shear stresses less than needed to entrain the largest particles but sufficient to transport fines, and over time, the fine sediment is either entrained from the bed surface or infiltrated into the substrate through kinetic sieving process (Frey and Church 2011). A coarse surface layer develops on the bed, effectively sheltering the finer substrate sediment from entrainment. Armor layers are common in gravel bed river reaches downstream of a dam and upstream of a significant tributary input (Brandt 2000; Grant 2001; Kondolf 1997; Lamberti and Paris 1992; Richards and Clifford 1991; Shen and Lu 1983; Vericat et al. 2006; Williams and Wolman 1984).

Armor layers increase the resistance of the bed surface to entrainment. Surface coarsening creates a bed surface with intergranular friction angles that increase the stresses necessary to entrain the bed surface (Buffington and Montgomery 1999; Parker et al. 1982; Vericat et al. 2006). Greater bed surface roughness impacts local channel hydraulics by increasing the frequency and magnitude of turbulent bursts (Papanicolaou et al. 2001), dissipating mean flow energy, and sheltering smaller grains from entrainment. Where a gravel bed river develops an identifiable surface structure, overall bed stability increases (De Jong 1991; Hassan and Reid 1990; Iseya and Ikeda 1987;

Lamarre and Roy 2005; Oldmeadow and Church 2006; Strom et al. 2004). Flow resistance increases over rough gravel beds through the formation of a turbulent flow field that includes formation of large scale, macroturbulent flow structures such as vortices (Buffin-Belanger and Roy 1998; Buffin-Belanger and Roy 1998; Hassan and Church 2000; Lamarre and Roy 2005). Turbulent wedges develop in the flow field that alternate between high and low speed, with high speed wedges traveling toward the bed surface and generating a temporary period of high shear stress. Coherent flow structures, including eddies, have been observed that scale with flow depth and the size and sorting of the bed surface (Hardy et al. 2009).

Clusters have long been recognized as part of the surface of gravel bed rivers (Judd and Peterson 1969; Brayshaw et al. 1983). Here we use the definition of clusters put forward by Strom and Papanicolaou (2004; 2007) that they are 'discrete, organized groupings of particles that sit above the average elevation of the surrounding bed surface.' The clusters extend above the bed surface and protrude into the flow area, affecting local hydraulics. Clusters have been shown to increase overall bed resistance (Brayshaw 1984; Hassan and Reid 1990; Canovaro et al. 2007) which has been quantified as an increased time to entrainment of the grains within the cluster form (De Jong 1991; Iseya and Ikeda 1987). In a study of the impact of the turbulence generated by isolated clusters, boulders, and cobbles, Lacey and Roy (2008a) found Reynolds stresses τ_{xy} and τ_{xz} were at a maximum near the bed on the immediate downstream side of the large clasts and also further downstream of the clast but in the upper portion of the flow profile. Turbulent kinetic energy (TKE) was also greater near the bed in the wake of a

clast, and three to four times greater than TKE over bed areas without clasts. An alternating pattern of positive and negative Reynolds stresses measured in the wake areas around isolated clasts indicated intense horizontal turbulent momentum exchange through the formation of counter-rotating vortices. These vortices generated Reynolds stresses more than twice what was measured over obstacle-free bed areas. The effect of the isolated clasts on hydraulic processes extended throughout the flow depth, as the turbulent structures were advected into the outer flow area (Hardy et al. 2009). A recirculation region formed around the clusters as a result of flow stagnation and separation immediately upstream of the cluster, which in turn generated vortices and large-scale coherent flow structures (Lawless and Robert, 2000, 2001a, 2001b).

The effect of bedforms on local and reach scale hydraulics depends on whether the bedform is isolated or part of a number of closely grouped bedforms. The influence of fixed object arrangement and packing density on flow hydraulics and coherent turbulent structures has been well documented for closed channel flow and aerodynamics (Brown et al. 2008; Jimenez 2004; King et al. 2008; Shao and Yang 2008), as well as open channels (Agelinchaab et al. 2009; Lyn 1993; Roussinova et al. 2009). The effect of variably spaced roughness elements on local hydraulics was used by Morris (1955) to classify flows in conduits. As flows passed over an element, a wake and vortex generating zone was created immediately downstream. An isolated flow is one for which any hydraulic effects are dissipated before the next object is encountered by longitudinal flow. If two elements are spaced such that the wake and vortex generation zone created by the first element is not fully developed prior to flow encountering the second element,

the flow is classified as wake interference flow. Turbulent mixing and intense vorticity accompanies this flow. The third flow type occurs when elements are so closely spaced that flow skims over the tops of the elements, behaving similar to flow in a smooth walled conduit. Vortices are formed between elements but remain stable in location between elements. These categories focus on classifying flows but also indirectly classify the roughness elements according to hydraulic impact within conduits. The same flow patterns were speculated to exist over naturally formed pebble clusters of varying spacing (Hassan and Reid 1990).

More recently, research has extended to examine the coherent flow patterns generated in open channels over sand beds (Yang and Tan 2008) and armored, rough gravel beds in open channels (e.g. Buffin-Bélanger et al. 2000; Hardy et al. 2010; Hardy et al. 2011; Roy et al. 2004). Dunes formed in sand bed channels present a potential analogue for defining the extent bedforms influence river hydraulics (Ojha and Mazumder 2010). Coherent turbulent flow structures generated by single, one-dimensional dune trains have been shown to interfere when multiple dunes are adjacent (Maddux et al. 2003a; Maddux et al. 2003b), altering the overall turbulence generated by the bedforms and demonstrating the importance of bedform spatial density. Studies of 3D dune bedforms showed that when dune crests are out-of-phase, overall turbulence was lowered (Maddux et al. 2003a; Maddux et al. 2003b; Venditti 2007). Total drag was reduced up to 20% over that of a smooth surface because the burst and sweep cycle was modified by the out of phase bedforms (Sirovich and Karlsson 1997; Venditti 2007). In a set of flume experiments, it was found that the spatial arrangement of pebbles on a gravel

bed had a significant impact on how and the extent to which the turbulent flow field was affected (Canovaro et al. 2007).

The purpose of this chapter is to demonstrate the effect of clusters on the flow over an armored gravel bed channel and to quantify the effect of cluster spatial arrangement on cluster-generated turbulent flows, as parameterized by the Reynolds stress and turbulent kinetic energy. We characterize the turbulent flow fields around clusters that were self-formed during gravel bed armoring as well as over an unclustered area of the armored bed. The clusters developed either as isolated clusters around a single anchor key stone, or as groupings of two to three clusters in close proximity on the bed surface. By comparing the flow around the clusters, we are able to quantify the effect of cluster density on turbulent channel hydraulics.

4.2   Methods

4.2.1   Experiment conditions

Experiments were performed in a sediment and water recirculating flume at the University of Virginia Sustainable Rivers Lab. The flume slope was kept constant while the sediment bed slope was free to adjust. Our flume represents the longitudinal middle section of a channel (Peakall et al. 1996; Sharp 1981), and does not simulate processes near channel banks. The flume allows for direct measurement of the influence of flow rate and bulk sediment size distributions on sediment movement and the hydrodynamics induced by variability in bed topography (Canovaro and Solari 2007; Curran and Wilcock 2005; Davies 1980; Wilcock et al. 2001).

The sediment used in the experiments was well graded gravel with grain sizes between 0.001m-0.0453m and either 24% or 38% sand content. The sediments differed only in the percent sand in the bulk mixture. The 24% sand content sediment had a bulk D50 of 0.0084m and D84 of 0.0233m. The 38% sand sediment had the same gravel distribution but the additional sand lowered the D_{50} to 0.0064m and D_{84} to 0.0191m. The lower sand content sediment was used in the experiments forming the armor bed with the clusters while the armored, cluster free open bed area was measured from a run using the 38% sand mixture. Direct clast size measurements were not possible in these experiments as it would have destroyed the armored bed surface. Therefore, the largest five grain size fractions were painted to aid in their identification in the flume. Similarly, the sand fraction (all grain sizes < 0.002m, D_{50}=0.001m) was colored with all fractions brown (Table 3.2.1). The addition of color aided in identification of the key and component clasts in the clusters (Wilcock et al. 2001; Curran 2005).

For all experiments, a 0.1m thick bed was created and screeded flat over the length of the flume as an initial step. This bed thickness is more than twice the length of the a-axis of the largest grain size. Two distinct flow rates were used in the experiments. An initial flow rate of 0.11m^3/s fully mobilized the sediment and was employed to create a gravel bed under equilibrium transport condition. Dynamic equilibrium was determined to exist when the channel bed was no longer aggrading or degrading, as measured by parallel water and bed surface profiles over the length of the flume. At the end of this first run segment, a sediment transport sample was collected from the downstream end of the flume. This part of the experiments was completed to correct for any bias in cluster

location that could result from the creation and screeding of the sediment bed. Once equilibrium transport conditions were established, the flow was lowered to $0.055\text{m}^3/\text{s}$, half the initial value. This flow rate was held constant for 12 hours while the bed surface armored. During this time, the sediment transport rate was measured by collecting the sediment exiting the flume over set time intervals. Samples were collected in 5 minute intervals and compared to the sample taken at the conclusion of the dynamic equilibrium portion of the run. Armoring was considered complete when the transport rate was less than 1% of the rate measured during the equilibrium condition. Because it was not possible to know with absolute certainty the point at which all particles had stabilized, a very low transport rate was used to define the armored bed condition. Flow depth was maintained at 0.015m during both run segments by adjusting a tail gate on the flume. Table 4.2.1 shows the final experimental conditions under which velocity measurements were made for all experiments.

	No Cluster	Isolated cluster	Coupled cluster	Grouped cluster
λ (cluster spacing) (m)	N/A	N/A	0.20	0.22
D_{50} of bulk sediment (m)	0.0064	0.0084	0.0084	0.0084
Froude Number **Fr**	0.26	0.43	0.33	0.29
Reynolds Number **Re**	51968	61360	45980	44800
Longitudinal double averaged velocity U (m/s)	0.33	0.52	0.38	0.35
Mean water depth h_o (m)	0.16	0.118	0.121	0.128
Max. Cluster length L_s (m)	N/A	0.25	0.16	0.17
Max. Cluster width W_s (m)	N/A	0.170	0.160	0.120
Max. cluster heights h_s (m)	N/A	0.018	0.039	0.042
Ratio of cluster height to width	N/A	0.11	0.24	0.35
water depth, h_o / D_{50}	25.00	14.05	14.40	15.24
water depth, h_o / d_s	N/A	2.62	3.78	4.00
water depth, $h_o /$ cluster height	N/A	6.56	3.10	3.04

Table 4.2.1 Experimental parameters and measurements around clusters

4.2.2   Streambed Topographic Analysis

The armored bed surface was analyzed through the combined use of a digital elevation model (DEM), a panoramic photograph, and visual inspection. The DEM was generated from bed elevation data collected with a Micro-Epsilon laser profiler, which has an accuracy of 0.002m. A panoramic photo of the armored bed surface was created from individual photos of the bed surface, and the surface grain size distribution was

determined by identifying the color of 400 surface grains, and hence their sizes, using the modified grid by number method on the panoramic photo (Rice and Church 1996; Wolman 1954). Clusters and any other bedforms present on the armored bed were identified through the combined use of the DEMs, the panoramic photos, and visual inspections of the armored sediment bed. Following the definition of a cluster, each cluster consisted of an identifiable key clast around which at least two smaller grains deposited and was elevated above the surrounding bed area, making the DEMs a particularly useful tool in identification. The geometric properties of the clusters were measured from the photos and DEMs, including cluster length L_s, maximum height h_s, width W_s, and key clast size d_s (Table 4.2.1). The ratio of cluster height to width is also given as a way to compare the aspect ratios between cluster densities. As aspect ratio increases, coherent turbulent flow structures have been shown to transform from a wake interference flow regime to skimming flows (Baik and Kim 1999). Similar to the correlation function developed by Strom and Papanicolaou (2008) to define cluster spacing, λ (Equation 4.2.1) was defined in this case as the distance from individual cluster to the nearest cluster along a downstream diagonal direction:

$$\lambda = \sqrt{\lambda_x{}^2 + \lambda_y{}^2} \qquad\qquad\qquad 4.2.1$$

where λ_x is the downstream cluster-to-cluster spacing for which $\Delta y = 0$ and λ_y is the transverse cluster-to-cluster spacing for which $\Delta x = 0$. For natural clustered beds, x and y are taken to be the streamwise and cross-stream directions respectively.

The spacing between neighboring clusters within cluster groups was defined using the cluster spacing λ. Earlier experiments using the same key clast size showed the area

of influence by a cluster over the flow field to be 0.30m (Curran and Tan, 2010), which is approximately seven times the maximum clast size (0.0453m). Clusters separated by more than seven times ds were considered "isolated", and clusters with smaller spacing were categorized as "multiple" clusters.

There exist different approaches to classifying groups of bedforms. As discussed in the introduction, Morris (1955) classified according to hydraulic effects, while Maddux et al. (2003a; 2003b) defined dunes from the dimensional arrangement of multiple dunes on the bed surface. Our hydraulics analysis makes use of time-averaged turbulence parameters, which precluded direct analysis of the movement of coherent flow structures around clusters. Thus, we use the geometric arrangement and spacing between individual clusters on the bed surface to classify clusters as isolated, coupled, or grouped. Isolated clusters are those spaced further than *7ds* from any other cluster. Coupled clusters and grouped clusters were distinguished by the number of clusters found within a radius of *7ds* for each cluster of interest. Coupled clusters consist of a pair of clusters close together and a group contained three clusters within a *7ds* radius.

4.2.3 Velocity Measurement

High resolution velocity measurements were necessary to describe accurately the flow field generated around clusters (Lamarre and Roy 2005). For this research, we employed a ©Nortek AS Vectrino™ Acoustic Doppler Velocimeter (ADV), which has a manufacturer reported accuracy of 0.5%. Individual velocity measurement error as estimated by a duplicate w-velocity measurement was ±0.001m/s. A high rate of sampling was maintained (200Hz), enabling high resolution three-dimensional flow

measurements. Previous research has shown that a stationary time series develops in turbulent flow within 60 seconds (Buffin-Belanger and Roy 2005; Hardy et al. 2009; Thoroddsen et al. 2008), and our measurements showed the sampling duration of 120 seconds to be sufficient.

Velocity measurements were made in a 3-D grid pattern around each area of interest. The horizontal measurement areas extended over the clustered and non-cluster areas between the clusters as well as the wake zone for the isolated cluster. The velocimeter was attached to a system of three stepper motors which moved the instrument exact distances over the bed area of interest. The grid extended in the vertical as well as horizontal and transverse directions (Figure 3.5.4). Thus, the same Cartesian grid pattern was followed over the vertical flow profile. Each time the velocimeter was moved to a measurement location, or grid node, the three-dimensional velocity was measured over 120 seconds such that the velocimeter sampled at a frequency that maintained equipment error of less than 0.001m/s. Vertical spacing for the measurements was either 0.005 or 0.01m, while longitudinal and transverse spacing was 0.05m, which was slightly larger than the maximum clast. Measurement grids were centered over each area of interest. For coupled and grouped clusters, the grid included profiles over the center of each cluster and the mid-point between clusters.

4.2.4 Velocity Time Series Data Quality

Velocity time series were initially inspected by eye for abnormalities and then de-spiked using the mean and standard deviations. Data values greater or lower than the mean velocity $\pm$ three standard deviation were truncated to achieve a relatively clean and regular time series. The Vectrino ADV signal correlation R_{adv} was used to detect

unreliable data points. Manufacturers of both Sontek and Nortek ADVs recommend that velocity measurements for which the R_{adv} is less than 70% be considered acoustic noise and removed from the time series. However, others have reported that the signal quality is reduced at the region of high turbulent flow due to the shear in the sampling volume and the threshold correlation may be below 70% (Martin et al. 2002; Strom and Papanicolaou 2007). In recognition of this, we applied a filter designed to discard instantaneous velocity data points when the correlation $R_{adv} < 65\%$. Data with a correlation between 65% and 70% were maintained in the velocity time series to account for low correlation measurements caused by high turbulent events occurring in near bed regions.

4.2.5   Velocity and Turbulence Statistics

The time series data collected at each grid node were analyzed and several turbulence variables (e.g. Reynolds stress and Turbulent Kinetic Energy) quantified using the three-dimensional velocity data. Turbulent Kinetic Energy (TKE) represents the mean kinetic energy per unit mass associated with coherent structures in the turbulent flow and was calculated as half the sum of the turbulent intensities (Equation 4.2.2).

$$\text{TKE} = \frac{1}{2}\left[\overline{(u')^2} + \overline{(v')^2} + \overline{(w')^2}\right] = \frac{1}{2}\left[u_{rms}^2 + v_{rms}^2 + w_{rms}^2\right] \qquad 4.2.2$$

The time averaged Reynolds stress was calculated using the covariance of two of the three flow dimensions, where ρ is the water density. The Reynolds stress tangential over the streamwise-vertical plane in the streamwise direction provides a measure of the anisotropic structure in the flow, and is calculated as in Equation 4.2.3.

$$\tau_{xz} = \tau_{Re} = -\rho\overline{u'w'} \qquad 4.2.3$$

Because the stream-wise-vertical stress is the only component of the Reynolds stress tensor used in this manuscript, we refer to it here as the Reynolds stress.

4.2.6   Quadrant Analysis

A quadrant analysis was performed to identify the dominance of turbulent flow events throughout the flow field and to aid in the identification of any potential coherent flow structures in the downstream direction. Instantaneous flow velocity fluctuations were graphed on a *u'*- *w'* grid and categorized into quadrants according to the dominant data clustering (Lu and Willmarth 1973). The quadrants define the four modes of momentum transfer that may occur in a flow. Quadrants 2 (*u'*<0; *w'*>0) and 4 (*u'*>0; *w'*<0) indicate the dominance of ejection and sweep events, respectively. Events in quadrant 1 (*u'*>0; *w'*>0) are outward events while those defined by quadrant 3 (*u'*<0; *w'*<0) are inward. Sweep events (*Q4*) transport high velocity fluid from the outer flow regions toward the bed while ejections (*Q2*) transport low momentum fluid from the bed upward in the flow profile. Pairing of ejection and sweep events is common around LREs and provides a dominant mechanism for momentum transfer in the flow (Grass 1971; Reidenbach et al. 2010). Nakagawa and Nezu (1977) defined a normalized instantaneous momentum flux fluctuation,

$$\tau_{i,H}(t) = \frac{\langle u'w'\rangle_{i,H}}{\overline{u'w'}} = \frac{1}{\overline{u'w'}} \lim_{T\to\infty} \int_0^T u'w' I_{i,H}(t)dt \qquad 4.2.4$$

in which the angle brackets denote a conditional average, H is the hole size; i defines the particular quadrant of interest (i = 1, 2, 3, 4); T is the time interval between measurements, and $I_{i,H}$ is the threshold indicator defined as

$$I_{i,H}(t) = \begin{cases} 1 & when \ |u'w'|_{i,H} \geq Hu_{rms}w_{rms} \\ 0 & otherwise \end{cases} \qquad 4.2.5$$

The hyperbolic hole function, *H*, in the *u'w'* plane is applied to an analysis to enable a focus on only those velocity fluctuations with large contributions to Reynolds stress. The hole function defines a minimum velocity fluctuation value below which the data are not included in the quadrant analysis. The value of *H* is user defined, and past researchers have applied a range of *H* values to armored gravel beds (Lacey and Roy 2008b; Strom and Papanicolaou 2007). In this study threshold *H* values of 0 and 2.5 are used to characterize low and high magnitude turbulent events respectively (Buffin-Belanger and Roy 1998; Lacey and Roy 2008b). When $H = 0$, all contributions in terms of *u'w'* are included within the quadrant analysis. When $H = 2.5$, only the high magnitude turbulent flows are considered.

4.3   Results

Detailed flow measurements were recorded over four different bed areas: an isolated cluster, a coupled cluster, a grouped cluster, and an area of armored bed without any clusters.   Measurements over the open, cluster free armored bed were included to create a baseline case against which the influence of clusters on flow patterns was discernible. The topographies of each area of investigation are illustrated by a plan view photo of the bed surface and the corresponding DEM (Figure 4.3.1). The isolated cluster was located 0.52~0.60m from the downstream end of the study reach. The coupled cluster was a pair of clusters with spacing parameter. The clusters were longitudinally aligned and located 3.2~3.7m from the downstream end of the study reach. The grouped cluster consisted of three individual clusters with an average spacing parameter. The

grouped clusters were located 6~6.5m from the downstream end of the study area.

Velocities were measured at each of the four different sites.

a

b

c

d
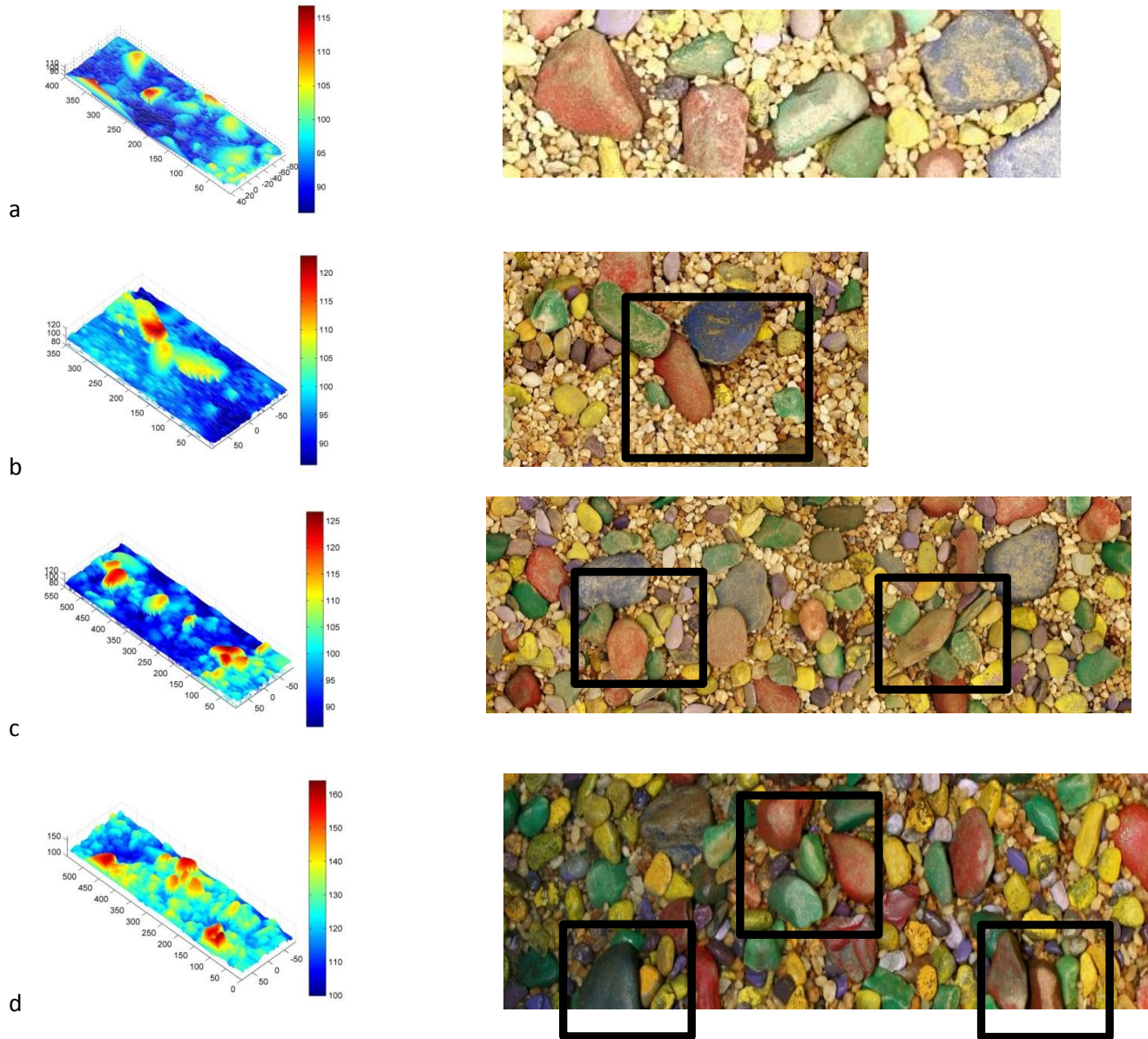
Figure 4.3.1 Plan view photo of the surface and corresponding DEM for (a) area of bed without a cluster, (b) isolated cluster, (c) coupled cluster, and (d) grouped cluster. Clusters are marked in the plan view photos by black boxes.

Values of Reynolds stress τ_{xz} or τ_{Re} and TKE were computed over the flow

region around each area measured and contour maps were created from which vertical

and horizontal profiles could be examined (Figure 4.3.2– Figure 4.3.5). TKE production involves interactions of the Reynolds stresses with the mean velocity gradient (Tennekes and Lumley 1972). Vertical profiles were analyzed over the centerline of each cluster as well as over the open bed area between clusters. A horizontal profile was analyzed at the z* elevation corresponding to the crests of the clusters, where z* is the non-dimensional elevation defined as the local depth normalized by total flow depth. This elevation provides a plan view plot of the flow just above the tops of the cluster forms and illustrates flow processes in the near bed region.
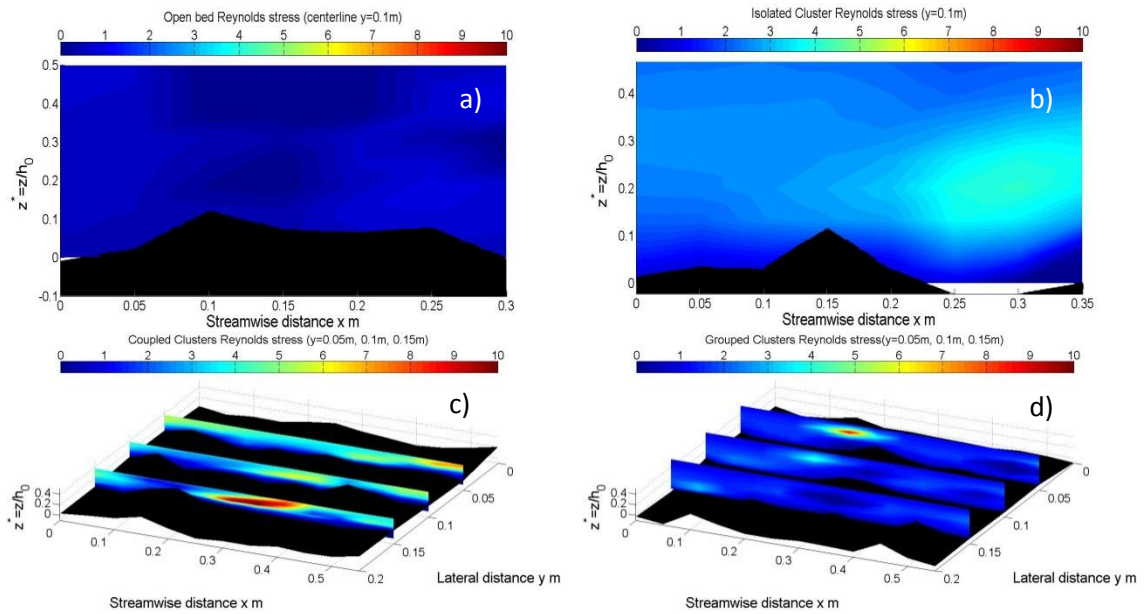
Figure 4.3.2 Reynolds shear stress (Pa) contour maps showing the x-z flow plane over the centerline of the area for a) open bed without a cluster, b) isolated cluster, c) coupled clusters, d) grouped clusters;
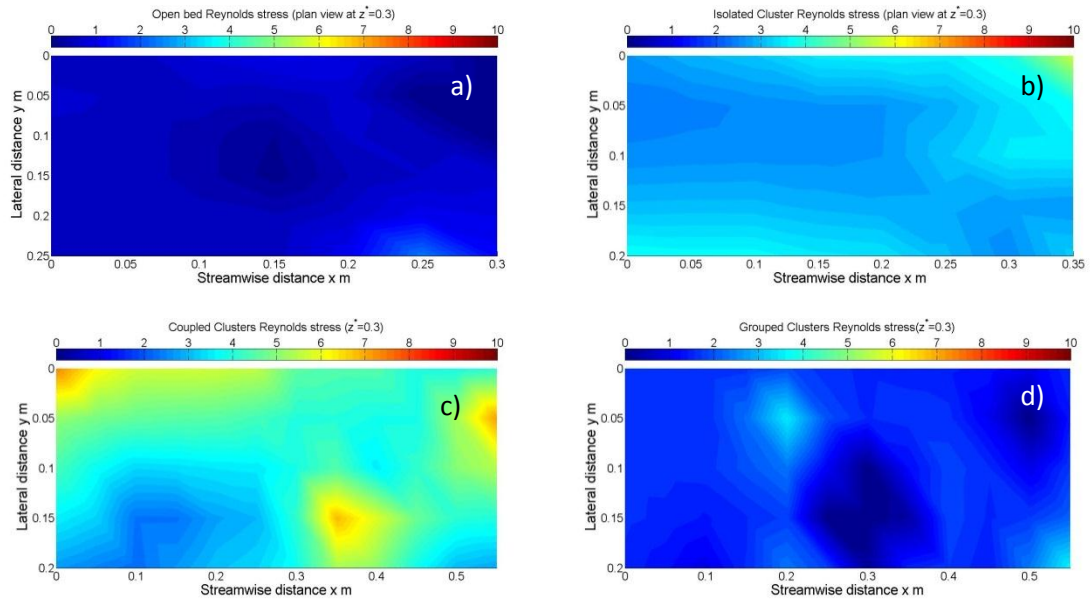
Figure 4.3.3 Figure 5 Reynolds shear stress (Pa) plan view contour maps of the x-y flow measured at an elevation of z*=0.3 for a) open bed without a cluster, b) isolated cluster, c) coupled clusters, d) grouped clusters;
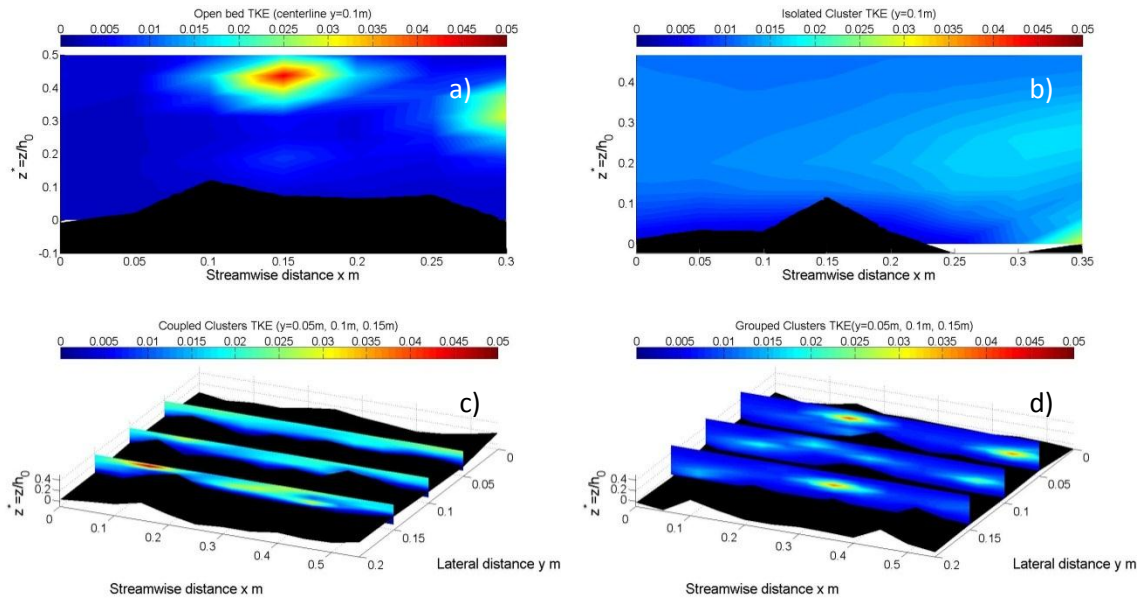
Figure 4.3.4 Turbulent Kinetic Energy (m^2s^{-2}) contour maps of the x-z flow measured over the centerline area for a) open bed without a cluster, b) isolated cluster, c) coupled clusters, d) grouped clusters;
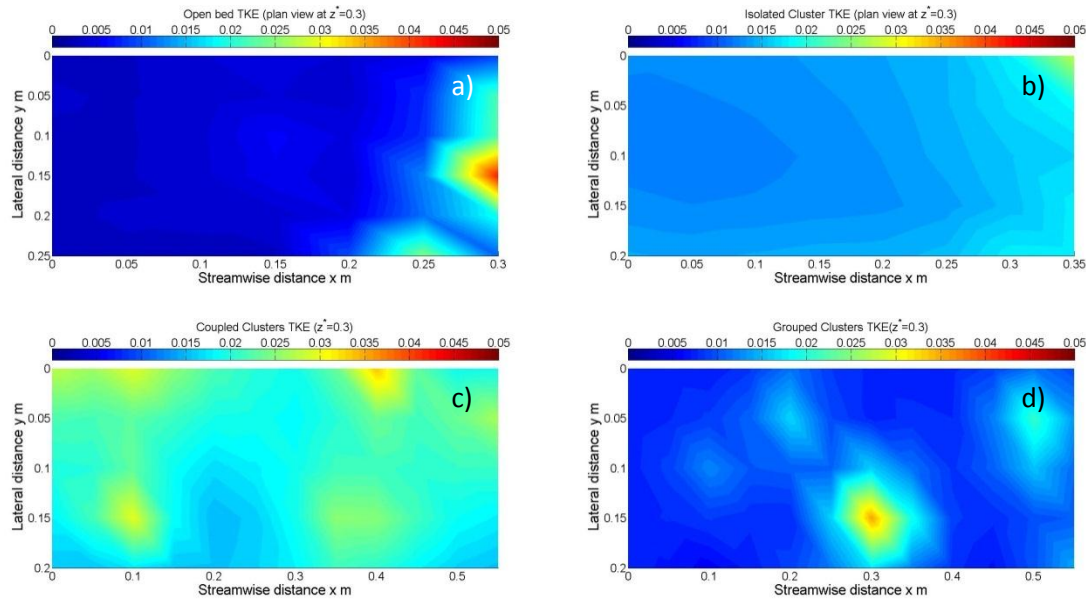
Figure 4.3.5 Turbulent Kinetic Energy (m^{2}s^{-2}) plan view contour maps of the x-y flow measured at an elevation of z*=0.3 for a) open bed without a cluster, b) isolated cluster, c) coupled clusters, d) grouped clusters;

4.3.1 No Cluster

The flow over the armored bed without any clusters showed minimal changes in Reynolds stress and TKE (Figure 4.3.2a and Figure 4.3.4a). Turbulence in the near bed flow region showed an overall uniformity, indicating little energy and momentum exchange near the bed. Reynolds stress averaged 0m^2/s^2, further indicative of an absence of the momentum exchange needed for the formation of large coherent flow structures scaled with flow depth. Changes in TKE were confined to the near bed region where TKE magnitude increased due to the roughness of the armored bed topography. A small, 0.01m high roughness feature on the bed surface induced an increase in the local TKE value near bed to a maximum value of 0.05m^2/s^2. This feature was not a cluster as there were not a number of small grains grouped around a large, key clast. The irregularity on the armored gravel bed was the result of an isolated large clast and not a defined bedform.

The effects of the bed irregularity on the flow hydraulics were limited to the near bed flow region as the relative submergence of the bed roughness feature was h_o/h_s =16. For comparison, the average cluster submergence was between 3 and 6. Figure 4.3.3a and Figure 4.3.5a show a horizontal slice through the x - y flow field plane at an elevation of z* = 0.3. What is noticeable in all three figures is the uniformity of the flow. Once outside the near bed region, there was little to no influence on the flow field by the bed surface irregularity.

4.3.2   Isolated Cluster

Turbulent flow around the isolated cluster was characterized by a localized area of increased τ_{Re} and TKE (Figure 4.3.2b and Figure 4.3.4b). The isolated cluster crest peak occurred at z*=0.15, or 0.018m above the mean bed surface. The peak Reynolds stress of 4.99Pa occurred at z*=0.2 and x=0.3m. The Reynolds stress increased by 2Pa over the cluster crest and continued to increase on the downstream side of the cluster to 3Pa greater than values upstream of the cluster. A similar pattern was measured for values of TKE, with peak values of 0.017m^2/s^2 occurring at the same location as the peak τ_{Re}. Immediately downstream of the cluster crest and extending downstream and upward in the flow profile was a localized increase in turbulence parameters that can be defined by an increase in the averaged momentum flux in the vertical direction due to turbulent flows (Figure 4.3.4b).

The plan view plots of the near bed flow area show a consistent increase in τ_{Re} and TKE as flow traveled over and downstream of the cluster peak (Figure 4.3.3b and Figure 4.3.5b). The plan view also illustrates that the influence of the cluster form over

flow hydraulics extends beyond the near bed flow region. In contrast to the uniformity in the plan view plots over an area of open, armored bed surface, the cluster had a clear influence throughout the inner flow region. However, the effects of the isolated cluster on the surrounding flow dynamics were localized and limited to approximately 0.10m laterally around the cluster. The cluster width was 0.17m, making the width of the entire area of influence 0.27m, or 6ds. The aspect ratio for the isolated cluster was the lowest of any of the clusters measured.

4.3.3   Coupled Clusters

Vertical profiles of τ_{Re} and TKE were measured around the coupled clusters at y= 0.05, 0.10, and 0.15m (Figure 4.3.2c and Figure 4.3.4c). The coupled cluster crests are at x=0.15m, y=0.15m and x=0.4m, y=0.1m. Because of the higher density of these cluster patches, three profiles are shown in each figure: one over the centerline of each cluster and an additional profile between clusters. From the vertical profiles of τ_{Re} at y=0.15m, a turbulent flow structure with maximum Reynolds stress was identified at 0.20m<x<0.40m which extended from the crest of the upstream cluster to the downstream cluster. The τ_{Re} values from the horizontal layer at z*=0.2 showed an increase from 1.3Pa to 3.84Pa as flow passed over the clusters, with the minimum occurring directly over the cluster peaks. TKE transitioned abruptly from low magnitude in the near bed flow region to a maximum in the outer section of the inner flow region as flow was forced over the cluster crests. In the region between the cluster crests, a coherent flow structure was not indicated and TKE values were lower, and there was a general lack of distinguishable patterns within the longitudinal TKE profiles which

indicated limited energy production and dissipation in the inner flow area. However, a band of elevated τ_{Re} was measurable between the coupled clusters.

The plan view contour maps of τ_{Re} and TKE illustrate a strong influence of coupled clusters on flow hydraulics in the outer flow and extending laterally from the clusters (Figure 4.3.3c and Figure 4.3.5c). τ_{Re} increased to a maximum value of 6.5Pa, indicating momentum transfer and movement downstream of the cluster form. TKE values were also elevated in the areas around the cluster crests. While the clusters were aligned longitudinally, the centers were off-set laterally, causing the turbulent flow structure generated around the coupled cluster to display an asymmetric pattern in the plan view. The spacing between the coupled clusters was 0.2m or $4.4d_s$, which is less than the size of the known area of influence of an isolated cluster. However, the aspect ratio was larger than for the isolated cluster.

4.3.4   Grouped Clusters

The grouped cluster consisted of three clusters located at x - y coordinates of: 0.1m, 0.18m; 0.25m, 0.05m; 0.45m, 0.20m. The first and third clusters were aligned longitudinally with the larger middle cluster off-set laterally. Spacing between the clusters averaged 0.22m, or $4.9d_s$, which is less than the size of the known area of influence of an isolated cluster. The area measured was focused around the clusters and the area over which clusters had the greatest influence. Vertical profiles over the centerline of each cluster illustrate the influence of the grouped cluster on local flow patterns (Figure 4.3.2d and Figure 4.3.4d). Reynolds stresses in the near bed region (z*=0.3) illustrated overall spatially uniform, with localized areas where τ_{Re} ranged from

a minimum of 0Pa to a maximum of 3.41Pa (Figure 4.3.2d). A similar uniformity through the flow profile was apparent for TKE. Despite this overall uniformity in the vertical profiles, the effects of the grouped cluster were identifiable in the plan view of the flow area over the cluster crests (Figure 4.3.3d and Figure 4.3.5d). Peaks in τ_{Re} and TKE occurred in the immediate areas downstream of each cluster crest, although there was little difference between the average and peak values. Maximum TKE values corresponded to the region adjacent to the middle cluster and between the upstream and downstream clusters. The same pattern was measured for the minimum τ_{Re} values with the overall minimum occurring in the region between the clusters. The grouped cluster had the largest aspect ratio of those measured.

4.3.5   Quadrant Analysis

A quadrant analysis was performed over the isolated, coupled, and grouped clusters to identify the dominant turbulent events contributing to momentum transfer through the flow. The same profiles used for analysis of the turbulent characteristics were applied to the quadrant analysis. Following the flow directional definitions, we applied threshold H values of 0 and 2.5 to characterize low and high magnitude turbulent events.

4.3.5.1 *Hole size H = 0*

The hole size *H* was set to 0 so that all the turbulent fluctuations, regardless of magnitude, were included in the analysis. The centerline vertical profile over the isolated cluster illustrates a dominance of paired ejection and sweep events (Figure 4.3.6a). In the near bed and downstream areas, ejections (Q2) were dominant with the exception of the area immediately downstream and adjacent to the cluster crest. In the outer flow, sweep events paired to the ejections near the bed. Neither inward nor outward events were

dominant at any location in the profile. At the coupled clusters, when hole size H=0 (Figure 4.3.6b), ejections were dominant in the lower flow were paired with sweeps (Q4) in the outer flow and around the crests of both clusters. Inward and outward events became apparent in areas between or immediately adjacent to the clusters. On the downstream side of each cluster, a dead zone formed near the bed characterized by outward (Q1) and inward (Q3) events which we interpreted to be a wake area created by the cluster. Above the wake areas, flow ejections were dominant. At each cluster crest, there was an isolated area of outward flow events. The flow profiles over the grouped clusters had an almost uniformity of ejection events near the bed underlying sweep events in the outer flow, $z^* \geq 0.3$ (Figure 4.3.6c). Outward events were present in the immediate region around each cluster, indicating formation of a wake region adjacent to and downstream of each cluster. There was only one area where inward events were dominant, on the immediate downstream side of the larger, middle cluster.
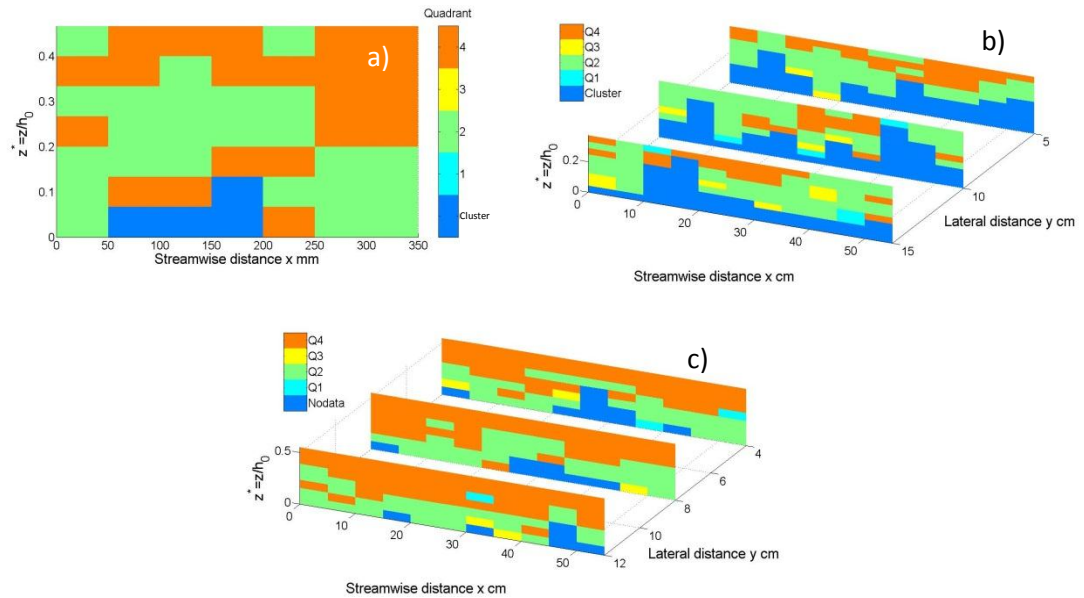
Figure 4.3.6 Profiles showing the quadrant analysis with hole size *H*=0 for the x-z flow plane measured over the centerline of the crest of a) isolated cluster; b) coupled clusters; c) grouped clusters

4.3.5.2 *Hole size H = 2.5*

A hole size of *H*=2.5 was used in the quadrant analysis to determine the dominant flow patterns associated with only the large magnitude velocity fluctuations. Thus, those flow events contributing most to the formation of coherent flow structures were isolated and identified. As a result, the general dominance by specific quadrants was inverted from what was observed when the hole size was zero. Around the isolated cluster, sweep events became dominate in the near-bed region and were paired with ejection events in the outer portion of the flow (Figure 4.3.7a). At the coupled clusters, the pairing of ejection and sweep events dominant in the flow profile was similar to that observed with a zero hole size but with the sweep events near the bed and the ejections in the outer flow (Figure 4.3.7b). Immediately adjacent to the bed and adjacent to the cluster form, outward and inward events were prevalent. The general pattern of quadrant dominance

where ejections in the outer flow profile paired with sweeps near the bed was also observed around the grouped clusters (Figure 4.3.7c). Similar to the coupled clusters, immediately adjacent to the bed and adjacent to the clusters form, outward and inward events were prevalent.
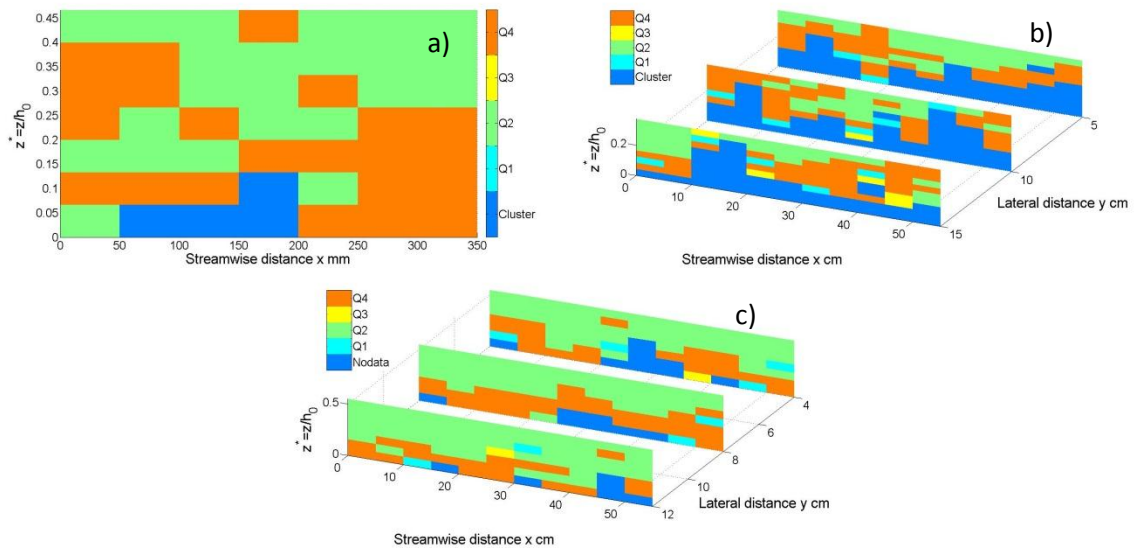
Figure 4.3.7 Profiles showing the quadrant analysis with hole size *H*=2.5 for the x-z flow plane measured over the centerline of the crest of a) isolated cluster; b) coupled clusters; c) grouped clusters

4.4   Discussion

Armored gravel-bed rivers typically have an uneven bed surface due to the variable sizes of the gravel clasts that make up the bed surface and the lack of sand filling voids on the surface. In the case of the armored bed without a cluster, the natural variability of surface grains created a roughness element that extended 0.01m into the flow. The effect was the formation of a flow structure, identifiable primarily by TKE (Figure 4.3.4a). The flow structure attached to the top of the roughness feature and extended to a height of z*=0.2 in the flow, thus remaining entirely within the near bed flow region. The influence of the armored bed is similar to what has been measured for

sand channels. For flows over a flat sand bed, the Reynolds stress increases from zero at the water surface to a maximum value at the bed with no along stream variation (Venditti 2007). The armoring process creates an uneven surface that can generate small scale turbulent flow structures, but the turbulence generated by these small roughness features does not transfer momentum and energy to the outer flow field and the overall impact on channel hydraulics remains limited to the near bed region.

Visualizations of the flow field around the isolated cluster show a clear influence of the cluster on the turbulent character of the flow that extends throughout the profile (Figure 4.3.2b and Figure 4.3.4b). In measurements around clusters formed in an armored gravel bed river in the field, Buffin-Belanger and Roy (1998) found that TKE increased toward the water surface and, as flow passed over the cluster crest, local flow acceleration contributed to a minimum in TKE immediately over the cluster. Our results show low TKE and τ_{Re} values as the flow approaches the cluster crest and then increased values on the downstream side of the cluster (Figure 4.3.4b). TKE did increase over the cluster crest, forming a local area of increased TKE and τ_{Re} at approximately z*=0.15 as flow passed over the cluster. Minimum TKE values occurred in the flow near, but not immediately adjacent to, the bed and extended from upstream of the cluster to the location of the cluster crest. TKE and τ_{Re} increase to a maximum values downstream of the cluster crest, indicating increased flow momentum and energy transfer occurring immediately downstream of the cluster and formation of a possible flow structure. These findings are in partial agreement with those of Lacey and Roy (2008a), who measured maximum τ_{Re} values near the bed downstream of the cluster and also in the downstream

flow profile. We measured TKE values 1.5-2 times greater than the average TKE over the unclustered armored bed, which is less than the four-fold increase measured by Lacey and Roy. The differences in our results may stem from the experimental conditions. Lacey and Roy (2008a; 2008b) measured clusters in a field setting whereas we performed our measurements in a laboratory flume with controllable flow rates and depths.

The turbulent flow patterns from our experiments indicate the cluster crest caused local flow acceleration and an associated increase in flow energy and momentum transfer with the formation of a recirculation cell generated downstream from the crest. This finding is similar to those made around sand dunes for which the maximum τ_{Re} and TKE values occurred at and just downstream of the reattachment zone formed along the shear layer (Maddux et al. 2003a; Venditti and Bennett 2000). The presence of a recirculation cell at the cluster can be interpreted physically. Measured patterns of low to high values of TKE are mimicked by the flow vectors around a cluster (Figure 4.4.1). Flow contracts and expands when passing over the cluster crest in a pattern that coincides with the measured band of elevated TKE values which expanded throughout the flow profile with distance downstream from the cluster. The flow reattachment point was at a location (x=0.2m) coincident with the upstream edge of maximum TKE values and the leading edge of an apparent shear layer from the cluster crest. The association between flow lines, recirculation cell formation, and cluster presence indicates a physical interpretation the formation of turbulent flows over clusters on armored beds. The presence of the cluster caused the flow to separate as it passed over the crest, creating an increase in the

turbulent flow properties and the formation of a recirculation zone where flow re-attached

downstream of the cluster.

a)

b)

c)

d)
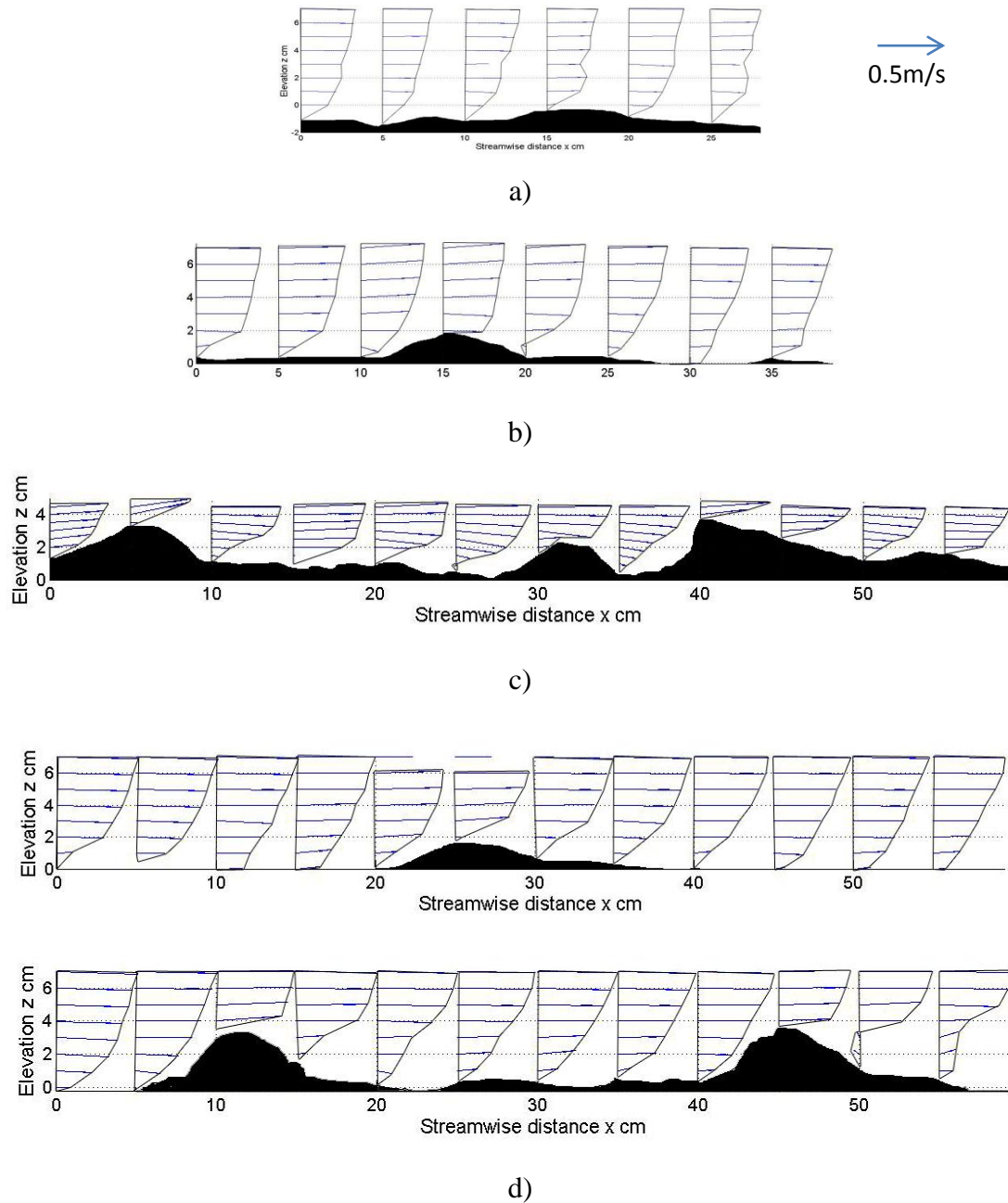
Figure 4.4.1 Flow vectors over a) open bed w/o clusters; b) the isolated cluster; c) coupled clusters; d) grouped clusters;

The velocity profiles over different cluster arrangements and open areas were plotted and compared in Figure 4.4.1. Recirculation cells and flow reattachment point were visible in the wake regions of isolated clusters at x=20cm; in the region between the coupled clusters at x=25cm, and in the wake region of triple clusters downstream element at x=50cm. The velocity profiles over open bed area without cluster bedforms are more logarithms shaped than any of the profiles over cluster bed areas.

A region of elevated TKE and τ_{Re} similar to the one measured downstream of the isolated cluster formed at each of the clusters in the coupled and grouped clusters (Figure 4.3.2c,d and Figure 4.3.4c,d). Recirculation cells occurred at the crest of each cluster and expanded downstream and upward in the flow profile. These structures formed consistently on the downstream side of the clusters, at an elevation of 0.3<z*<0.4 in the flow profile. The effect of cluster grouping on the turbulent hydraulics becomes apparent when comparing the momentum and energy fluxes around the clusters. The flow field around the coupled clusters had the highest magnitude τ_{Re} and TKE of any measurements, indicating large amounts of vertical momentum movement downstream of the upstream cluster. The turbulent flow structures were centered below the elevation of the cluster crests, and the plan view (Figure 4.3.3c and Figure 4.3.5c) showed τ_{Re} reached a maximum between cluster crests and minimums were over cluster crests. The downstream recirculation cell attained a lower maximum τ_{Re} (Figure 4.3.2c) than the upstream cluster. The difference in Reynolds stress maximums between the two clusters may result from the spatial arrangement. Because we allowed the clusters to form naturally, the coupled cluster did not align longitudinally. In the coupled cluster, the

upstream cluster was larger and laterally off-set from the downstream cluster. We interpret the reduction in turbulent flow strength downstream of the second cluster to be a result of the limited flow area between the two clusters. TKE values around the coupled clusters showed similar trends, with peak magnitudes following the upstream cluster.

The extent of hydraulic influence of cluster formation and cluster density on flows in the upper part of the flow profile provides a means for assessing the movement of energy and momentum to the outer flow area and an indication of cluster influence over the larger flow area. TKE and τ_{Re} values were averaged over the horizontal plane of the measurement grid at a z* elevation just above the cluster crests, as defined in the results section, to provide spatially averaged τ_{Re} and TKE values for the inner flow area. The averaging was repeated at a z* elevation twice that used for the inner flow area, generally z*≥0.4, for the outer flow region. Overall, spatially averaged τ_{Re} and TKE values increased with the formation of a cluster on an otherwise unclustered bed surface (Figure 4.4.2). As the number of closely spaced clusters increased to form a pair of coupled clusters, TKE and τ_{Re} increased for flows in both the near bed and outer flow regions when compared to measurements from flows around the isolated cluster. TKE magnitudes were highest over the coupled clusters, averaging 6% and 50% greater than over the isolated cluster for the inner and outer flow fields, respectively (Figure 4.4.2b). Upon an increase in cluster density to grouped clusters, all the turbulent flow parameters measured decreased. In the inner flow region, the spatially averaged τ_{Re} and TKE values were either approximately equal to or less than those measured over the cluster-free bed surface, and for the outer flow region, turbulent flows were reduced when compared to

flows over the isolated cluster. The addition of a third closely spaced cluster and the associated change from coupled to grouped cluster form reduced the inner flow field τ_{Re} by 63% and the outer flow field by 51% (Figure 4.4.2a). TKE values in both the inner and outer regions of the grouped cluster were reduced from the same areas of the coupled cluster. The disparate effects of isolated, coupled, and grouped clusters on flow hydraulics indicate that the classification of Morris (1955) may be applicable to these clusters and that there may be similarity in the behavior of flow over roughness elements in both conduits and open channels. Hassan and Reid (1990) speculated on the transition in flow patterns from isolated, through wake interference, to skimming flow with increased particle cluster density. These results are measuring a similar adjustment in flow hydraulics as clusters become more closely spaced. Coupled clusters, with increased turbulent parameters, created a hydraulics pattern similar to that described for the wake interference flows. Despite overall mixing, upstream turbulent flow recirculation cells were not fully developed before reaching the downstream cluster, which is consistent with the definition of Morris. Further supporting the correlation between our coupled clusters and the wake interference flows of Morris comes from the aspect ratio. The increase in aspect ratio for the coupled cluster indicates wake interference flows have developed (Baik and Kim 1999). Grouped clusters showed a reduction in turbulence such that the spatially-averaged TKE and τ_{Re} values were closer to the values measured over the unclustered bed area than to any of the other cluster configurations. Morris (1955) classified closely spaced groups of roughness elements as flow skimming elements because the flow skimmed along the tops of the roughness forms, much as it would over

a smooth boundary. Our turbulent measurements indicate that skimming of flows across the cluster tops may be occurring for the grouped cluster. Because our measurements are averaged, we can only speculate on whether flow skimmed over the cluster crests. However, the high aspect ratio indicates skimming flows with stable vortices formed between clusters (Baik and Kim 1999), possibly extending the application of previous work of naturally formed clusters in armored beds. A reduction in Reynolds stress similar to that measured around the grouped cluster was also measured around sand dunes and was attributed to flow interference due to the proximity and dimensionality of dunes when arranged in a three-dimensional pattern on a sand bed (Maddux et al. 2003b).

A comparison of turbulent flow parameters as measured for the inner ($z^* \leq 0.3$) and outer ($z^* \geq 0.4$) flow regions (Figure 4.4.2) allows for quantification of the influence of the bed surface on the near bed flows, the influence of the near bed flow on the outer flow region, and the movement of energy and momentum within the flow field. The flow field over the unclustered bed area had consistently lower turbulent flow magnitudes in the outer flow when compared to the inner flow area. This finding supports our observations of a limited influence by the rough armored bed surface over the flow. The turbulent flow parameters around the coupled and grouped clusters exhibited spatial variability with noticeable differences between the values of the turbulent parameters when averaged over the entire measurement areas and the same parameters when limited to only the bed areas between clusters. Flows around the isolated and grouped clusters as well as the area between the clusters of the grouped cluster had near equal levels of TKE in the inner and outer flow regions (Figure 4.4.2b). However τ_{Re} measurements show a

larger amount of momentum in the outer flow regions and a transfer of momentum outward for all but the isolated cluster (Figure 4.4.2a).

Within the inner flow area of the coupled cluster, TKE increased while τ_{Re} experienced a near negligible decrease in value, and the opposite pattern was measured for the outer flow area. Thus, around the coupled cluster, the outer flow area had greater magnitude TKE and τ_{Re} than the inner flow region. TKE measurements indicate a large amount of energy and momentum movement occurred around and between the clusters. The overall exchange of energy from the outer to inner flow regions ranged between 0% and 38%. The recirculation zone created by the upstream cluster was characterized by large turbulent flow properties, and the slight increase in turbulent flows in the downstream bed area may be a reflection of the highly turbulent flows encountering a downstream obstacle. For the grouped clusters, turbulent flow interference and sheltering slightly reduced the measured turbulence parameters in the area between clusters with the exception of the τ_{Re}, which increased near the bed but decreased in the outer flow region (Figure 4.4.2a). The amount of change in turbulent flow parameters between the inner and outer flow regions was large, varying from 19~70% reductions and 6~47% increases, but the overall magnitude of the turbulent parameters remained small in comparison to the isolated and coupled cluster cases. There was little TKE transfer from the inner flow to outer flow for either the entire clustered area or the area between the clusters. However, there was a significantly greater transfer of momentum (evaluated by τ_{Re}) from the inner to outer flow for the flows measured over the entire cluster area (82%) than from the areas between the clusters (5%). Around the grouped cluster, individual cluster proximity

prevented the formation of a high magnitude turbulent flow field and reduced measured turbulent flow properties to magnitudes near those measured over an armored bed without any clusters. When these values were compared to energy and momentum patterns over the armored cluster-free bed area, it was found that while the overall effect of coupling and grouping clusters was to increase the movement of energy and momentum from the inner to the outer flow. If considered in absolute terms, the percent movement was greater from the regions over clusters than from the areas between clusters. The majority of the energy movement appeared to have occurred in the flow field around the coupled clusters, although a large amount of momentum movement is also apparent in the flow field over the grouped cluster.
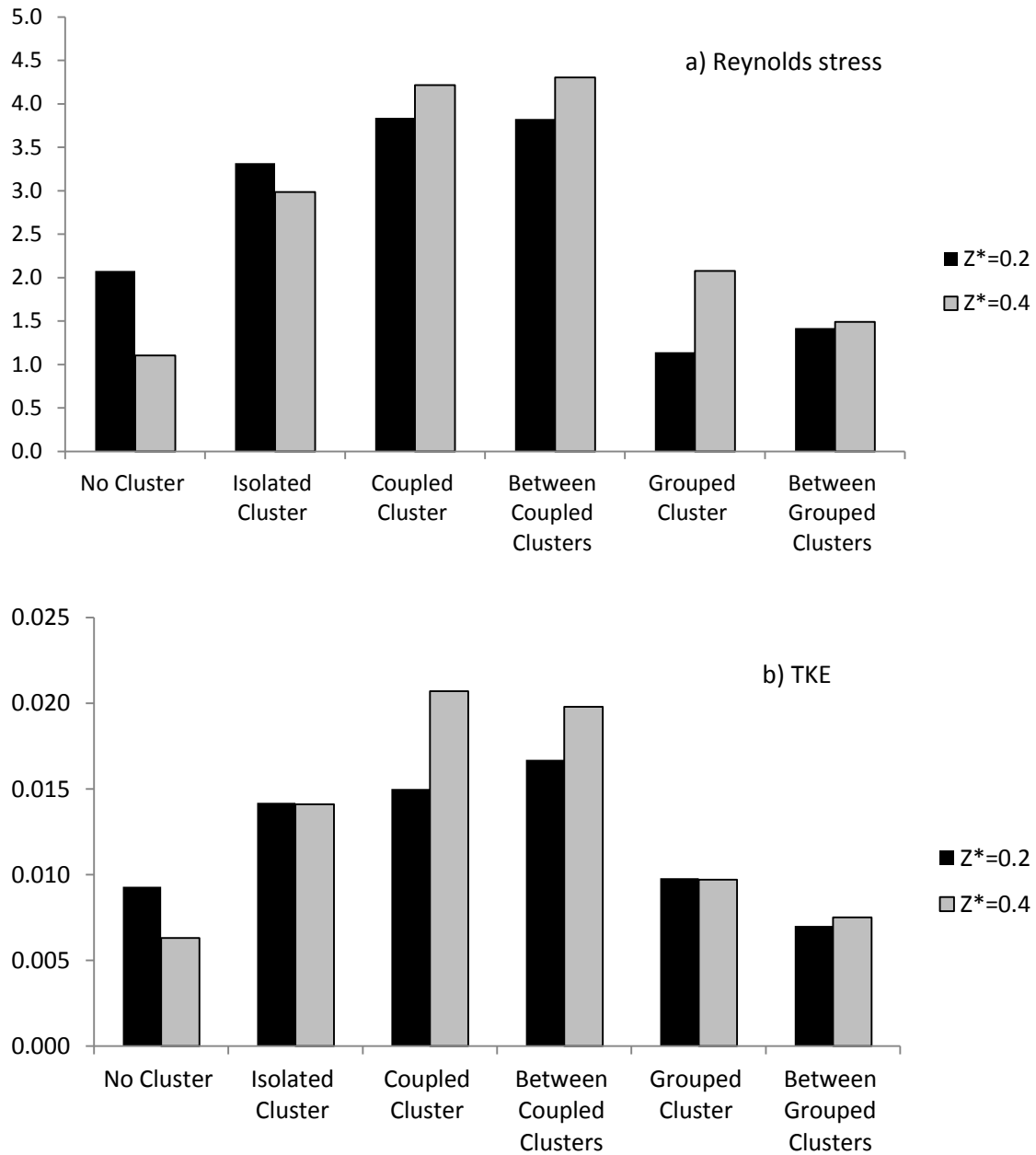
Figure 4.4.2 Spatially and temporally averaged a) τ_{Re} and b)Turbulent Kinetic Energy values for the open area of armored bed, isolated cluster, coupled cluster, the open bed area between the clusters in the coupled cluster, the grouped cluster, and the open bed area between the clusters in the grouped cluster. Two flow planes are compared. The inner flow region, measured immediately above the cluster crests at z*=0.2 or z*=0.3 depending on cluster height (darker column) and the outer flow region measured at z*=0.4 (lighter column).

Quadrant analysis provided a context for understanding how the turbulent fluctuations contributed to the distribution of energy and momentum around the measurement areas and to the flow patterns visualized in the flow profiles. The flow field around the isolated cluster was dominated by ejection (Q2) and sweep (Q4) events regardless of whether the hole size was zero or 2.5 (Figure 4.3.6). When combined with the high measured values of τ_{Re}, the interaction between ejections and sweeps indicated that the flow patterns represented the formation of intense, laterally oriented vortices around the cluster. For the multiple clusters, regardless of hole size, ejections around the crests of the clusters were paired with sweeps on either side of the clusters at $z^*=0.3$, a pattern indicative of vortex shedding from the cluster crests (Figure 4.3.6 and Figure 4.3.7). This location corresponded to the flow recirculation structure seen in the τ_{Re} and TKE plots. On the lee side of each cluster, a dead zone formed near the bed where outward (Q1) and inward (Q3) events dominated, which corresponded to the area of lower τ_{Re} immediately adjacent to the cluster form. The overall pattern of changing quadrant dominance upon increasing the hole size to 2.5 supports the interpretation of increased turbulence and energy transfer in the flows around coupled clusters (Figure 4.3.7b). The pattern of quadrant dominance around the grouped clusters (Figure 4.3.7c) was similar to that for the coupled clusters, but with an overall reduction in variability. The reduced variability in quadrant dominance is in agreement with the spatially averaged turbulence statistics, thus illustrating an overall reduction in turbulence and energy movement in the flow field over grouped clusters and the possibility that flow was skimming over the tops of the clusters.

4.5   Conclusion

Detailed laboratory measurements were made of the turbulent flows around clusters naturally formed during the armoring process in a gravel bed channel. We characterized the turbulent flow field around clusters that were self-formed during gravel bed armoring as well as over an unclustered area of the armored bed. The clusters naturally developed either as an isolated cluster, a pair of clusters immediately adjacent to each other forming coupled clusters, or a group of three clusters in close proximity forming grouped clusters. By comparing the flows around the clusters, we quantified the effect of increased cluster configuration on the turbulent flow field in a setting for which the clusters were not manipulated in any way.

The impact of cluster presence on the flow field was assessed by comparison to measurements over an area of armored bed surface without clusters. The cluster form extends above the local, mean bed surface and into the flow field farther than the topography created by individual clasts on an uneven armored surface. The impact of small scale roughness associated with the armoring process was limited to the inner flow region, increasing turbulent flows only near the bed. Where a cluster was present, the impact of flow hydraulics extended throughout the flow field as turbulent flows near the bed transferred momentum and energy to the outer flow area. The presence of the cluster caused the flow to separate as it was forced over the cluster crest, creating an increase in the turbulent flow properties and formation of a flow recirculation cell where the flow re-attached downstream of the cluster.

As the number of closely spaced clusters increased to form coupled and grouped clusters, the effect of increasing cluster density was measured in the magnitudes and patterns of the Reynolds stresses and TKE in the turbulent flow field. The formation of coupled clusters increased the overall turbulence in the flow field. Flow structures formed around the coupled clusters had magnitudes of τ_{Re} 16% greater than over the isolated cluster. Maximum τ_{Re} values were centered in the recirculation cell formed from the crest of the upstream cluster, while minimum τ_{Re} values were associated with the flow wake immediately downstream of each cluster. Quadrant analysis around the coupled clusters confirmed the wake area as a dead zone near the bed where outward and inward events dominated. With an increase in density to grouped clusters, the turbulence statistics showed a weak energy and momentum flux in a flow field distinguished by a high degree of uniformity, especially when compared to flows around the coupled clusters. Recirculation cells were limited in size and the differences between minimum and maximum turbulent flow parameter values were small. The reduced variability was apparent in the pattern of quadrant dominance, which also illustrated an overall reduction in flow variability. The net effect of increasing cluster density was an increase in the magnitude and variability of the turbulent flow field as the bedform transitioned to coupled clusters, followed by an overall dampening of turbulent flows with an increase to a grouped cluster pattern, where the turbulent flows generated around individual clusters interfered with each other and the cluster forms sheltered the bed surface. Flows may have developed an interference pattern around the coupled cluster that increased overall

turbulent flow hydraulics and a skimming pattern over the tops of the grouped cluster for which the flow differed little for that over a rough boundary without clusters.

Increased cluster density created a variable turbulent flow pattern as bed areas over clusters transferred a larger amount of energy and momentum from the inner to outer flow. As a consequence, inner flow turbulence statistics over the areas between clusters had greater magnitudes than the turbulence statistics directly over the cluster crests. The open bed areas between the clusters experienced large transfers of energy and momentum from the inner to outer flow regions, consistent with the formation of vortices over the open bed area. A larger amount of energy transfer occurred in the flow field over the coupled clusters, while momentum transfer was greater through the flow field over the entire grouped clusters. When compared to energy and momentum magnitudes across the flow field over the armored but unclustered bed area, it was found that the overall effect of clusters was to increase transfer to the outer flow.

Chapter 5.

EFFECT OF BULK SAND CONTENT ON THE TURBULENT

FLOWS ASSOCIATED WITH CLUSTERS

Abstract

As the surface of a gravel bed river armors, a structure develops that can be characterized by the presence of clusters. Individual clusters are known to exert a significant influence over the spatial and temporal flow processes acting in the vicinity of the bed. A series of flume experiments investigated the turbulent structures around clusters formed during the armoring process. Armored beds were created using four different bulk grain size distributions which progressively increased in the percent sand in the bed sediment from one to 38% of the bulk bed. Turbulent flow parameters, Reynolds stress and turbulent kinetic energy, were calculated from Acoustic Doppler Velocimeter measured flows around each cluster. The results indicated that for all sediment beds, the cluster created an increase in momentum and energy in the flow, as measured by TKE and Reynolds stress. Local flow around the cluster was altered to a different degree depending on the sand content of the bulk bed from which the armor formed.

For similarly shaped clusters, as sand content increased, the difference between the average and maximum TKE values between the near bed and distant portions of the flow profile also increased. Recirculation cells formed downstream of the cluster remained below the elevation of the cluster crest. This finding indicated that less energy

and momentum were transferred from the inner to outer flow regions as the sand content of the bed increased. The morphology of the cluster also had a role in the extent of flow alteration around the cluster. Where the cluster created an abrupt elevation transition over a low sand content bed, the effect on turbulent flows extended across the flow depth. However, at high sand content, the influence of the sand content over the turbulent flow profile reduced the influence of the cluster shape. Thus, despite a cluster morphology that at a lower sand content would have impacted turbulent flows over a large portion of the flow depth, a high bulk bed sand content creates a cluster and armored bed situation where the turbulent flows remain primarily within the lower part of the flow depth.

5.1   Introduction

A river bed surface acts as an intermediary between channel flow and bed sediments, determining the sediments available for transport. In a gravel river with mixed sediment sizes in the bed, the bed often develops an armored layer whereby the larger clasts are over represented on the bed surface when compared to their population in the subsurface. A static armored bed condition forms as a result of an extended period of low flow over a mixed gravel bed. These low flows generate shear stresses less than that needed to entrain the largest particles but large enough to transport the fines, and over time the fine sediments are winnowed from the bed surface. A coarse surface layer forms on the bed surface, effectively sheltering the finer substrate grains from entrainment (Jain 1990; Parker and Sutherland 1990). The presence of an armor layer on the bed surface is a common phenomenon in rivers subject to seasonal low flows, and also in the reach downstream of a dam and upstream of a significant tributary input (Brandt 2000; Grant

2001; Kondolf 1997; Lamberti and Paris 1992; Richards and Clifford 1991; Shen and Lu 1983; Vericat et al. 2006; Williams and Wolman 1984).

An armor layer creates a structure on the surface of the gravel bed river which in turn increases the resistance of the bed surface to entrainment. Coarsening creates a rougher surface with greater intergranular friction angles which increase the stresses necessary to entrain the bed surface (Buffington and Montgomery 1999; Parker et al. 1982; Vericat et al. 2006). Large grains on the bed surface often arrange to create clusters as part of as part of the process of developing the armor on the bed surface (Brayshaw 1984; Church et al. 1998; Oldmeadow and Church 2006). Here, we use the definition of clusters put forward by Strom and Papanicolaou (2004; 2007) that they are 'discrete, organized groupings of particles that sit above the average elevation of the surrounding bed surface.' The occurrence, topography, distribution, and relative mobility of clusters are continuing topics of research (i.e. Madej 2001; Strom and Papanicolaou 2009). An increase in overall bed resistance (Brayshaw 1984; Canovaro et al. 2007) has been documented as an increased time to entrainment of the grains within the cluster microform (De Jong 1991; Iseya and Ikeda 1987).

The influence of the armored surface topography on the turbulent flow field has been investigated using visualization studies (i.e. Imamoto and Ishigaki 1986; Schvidchenko and Pender 2001) which have more recently combined with quantitative measurements of the turbulence parameters (i.e. Hardy et al. 2009; Lacey and Roy 2007; Reidenbach et al. 2010). The generation of turbulent flow structures around clusters has been confirmed in field studies (Roy et al. 1999; Roy and Buffin-Belanger 2001).

Clusters have been shown to effect local channel hydraulics by inducing the formation of coherent turbulent flow structures (Buffin-Belanger and Roy 1998; Hassan and Church 2000; Lamarre and Roy 2005). Using detailed measurements and analysis of the flows over isolated pebble clusters in a natural river, Buffin-Belanger and Roy (1998) identified distinct regions corresponding to flow acceleration, recirculation, shedding, reattachment, upwelling, and flow recovery. Of these, the authors defined downstream vortex shedding as a primary consequence of cluster presence. Lateral momentum exchange was measured in the wake just downstream of the cluster form (Lacey and Roy 2008b; Strom and Papanicolaou 2007). Using video during injection of flow tracers upstream of a cluster, Lacey and Roy (2008) observed eddies along the top of the cluster and a separation zone downstream. Counter rotating vertical vortices around clusters were indicated by large amounts of horizontal turbulent momentum exchange, identifying a distinctly three-dimensional component to the turbulence generated around clusters.

Armor layers and clusters form under a wide array of circumstances and thus, under a range of bed sediment grain size distributions. The presence of sand in the bed sediment or supplied to a gravel bed channel is known to have an effect on transport rates, particularly when the sand content is increased beyond 14% (Curran and Wilcock 2005; Wilcock et al. 2001; Wilcock and Crowe 2003). The effects of increasing sand content to an armored gravel bed remain less well defined. Through flume experiments adding sand to a water-worked gravel bed, Hardy et al. (2010) showed the importance of relative roughness to the magnitude and extent of coherent flow structures generated in the turbulent flow field. These experiments focused on quantifying the change in turbulence

parameters with decreases in effective roughness as sand content increased and grain protrusion decreased.

The purpose of this research presented here was to examine the influence of increasing bulk sediment sand content on the turbulent patterns generated by clusters formed during bed armoring. Through a series of flume runs, we created armored beds and clusters using gravel sediment to which sand was added to create grain size distributions of 1, 9, 23, and 38% sand. Each bed was allowed to armor naturally and clusters were self-formed. Using an Acoustic Doppler Velocimeter (ADV), the turbulent flows were measured around clusters formed on each armored bed as well as over an unclustered area of armored bed. This chapter presents research quantifying the effect of increasing bulk bed sand content on the turbulent flow patterns generated over the armored bed surface and around clusters formed during bed surface armoring.

5.2   Methods

Experiments were performed in a sediment and water recirculating flume at the University of Virginia Sustainable Rivers Lab. The experimental channel is 11 meters long, 0.6 meters wide, and 0.5 meters deep. The flume slope was kept constant while the sediment bed slope was free to adjust. The four experimental sediments were created by adding an increasing amount of sand to a constant gravel mixture. In this manner, each mix had the same gravel distribution but sand content of 1%, 9%, 24%, or 38%. Gravel sizes ranged from 2.0mm to 45.3mm and sand from 0.10mm and 2.0mm (Figure 5.2.1). The largest five grain size fractions were painted to aid in their identification in the flume. Similarly, the sand fraction (all grain sizes < 2mm, D_{50}=1.0 mm) was colored with all

fractions brown. The addition of color aided in identification of the key and component clasts in the clusters. Direct clast size measurements were not possible in these experiments as it would have necessarily destroyed the armored bed surface.
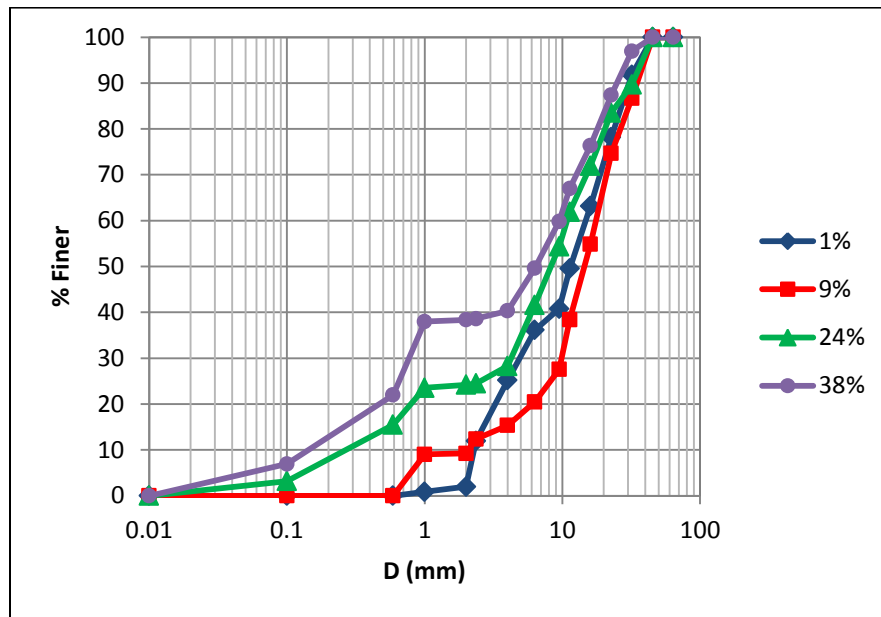
Figure 5.2.1 Grain size distributions curves of the experimental sediments.

Each experiment was set-up using the same procedures but with a different sediment mixture. An initial 10cm thick bed was created over the length of the flume and screeded flat. This bed thickness is more than twice the length of the a-axis of the largest grain size.

A series of initial flow rates of 0.07, 0.09 and 0.11m3/s fully mobilized the sediment and were employed to establish a dynamic equilibrium transport condition. Dynamic equilibrium was determined to exist when the channel bed was no longer aggrading or degrading, as measured by parallel water and bed surface profiles over the length of the flume. This initial experimental step was undertaken to eliminate possible bias in cluster formation due to the creation and screeding of the sediment bed. When this

step was complete, the flow rate was lowered to half the initial values. The 0.035, 0.045 and 0.055m^3/s flow rate was held constant for 36 hours while the bed surface armored. Armoring was considered complete when the transport rate was less than 1% of the rate measured during the equilibrium condition. Because it was not possible to know with absolute certainty the point at which all particles had stabilized, a very low transport rate was used to define the armored bed condition. The flow depth was maintained at 15cm during both run segments by adjusting a tail gate on the flume. We applied the same flow conditions to each of the sediment mixtures, for a total of 9 flume runs (27 total segments) where gravel beds were allowed to armor and develop clusters without external influence. Table 5.2.1 shows all the clusters measured and the experimental hydraulic conditions for each measurement. The clusters were respectively named after combinations of digitals representing the flow rate and sand content under which they were created plus an alphabet to distinguish clusters that were measured in the same flume experiment.

Three levels of flow rates were applied in this research. The same flow rates were applied to each subset of experiments to exclude the effect of flow rate magnitude on flow field turbulence. For simplicity, we analyzed highest same flow sequence consisting of two distinct flow rates (0.055 and 0.11m^3/s) instead of all three flow rate levels and this study served as an example for research on sand content effects. Results including turbulence statistics from the other two levels of flow rate experiments can be found in Appendix II.

ID	Q (m³/s)	Run#	sand %	d_s (mm)	h_o (m)	h_s/h_o	Armor Ratio	Fr	Re ×10⁴
1101open	0.11	2	1	NA	0.25	NA	1.83	0.234	9.2
1101A	0.11	2	1	45.3	0.15	0.32	1.83	0.234	9.2
1109B	0.11	4	9	32	0.15	0.13	1.26	0.504	9.2
1109C	0.11	4	9	32	0.1	0.2	1.26	0.504	9.2
1124open	0.11	7	24	NA	0.2	NA	1.73	0.704	9.2
1124D	0.11	7	24	45.3	0.2	0.06	1.73	0.704	9.2
1138E	0.11	9	38	32	0.25	0.16	1.42	0.457	9.2
1138F	0.11	9	38	45.3	0.21	0.17	1.42	0.457	9.2
1138open	0.11	9	38	NA	0.1	NA	1.05	0.457	9.2
0724open	0.07	5	24	NA	0.25	NA	1.24	0.589	5.8
0724G	0.07	5	24	32	0.22	0.14	1.24	0.589	5.8
0724H	0.07	5	24	45.3	0.2	0.22	1.24	0.589	5.8
0738I	0.07	8	38	32	0.1	0.3	1.05	0.589	5.8
0901J	0.09	1	1	32	0.25	0.13	1.28	0.192	7.5
0909open	0.09	3	9	NA	0.18	NA	1.26	0.192	9.2
0909K	0.09	3	9	45.3	0.16	0.2	1.26	0.192	9.2

Table 5.2.1 Details of the all measured isolated clusters and hydraulic conditions for each experiment

5.3   Cluster Identification

The armored bed surfaces were analyzed through the creation of digital elevation models (DEM) and panoramic photos. A DEM of each bed surface was generated from bed elevation data collected with a Micro-Epsilon laser profiler, which has an accuracy of 2mm (Lane 2005; Michael and Gerhard 2006; Nikora et al. 1998). Digital photos of the bed surface were taken and stitched together to create a panoramic photo of the armored bed surface. The bed surface grain size distribution was determined by identifying the color of 400 surface grains, and hence their sizes, using the modified grid by number

method (Rice and Church 1996; Wolman 1954) on the panoramic photo. Bed armor ratios for each experiment were calculated using information from the pebble counts and the bulk sediment size distribution (Table 5.2.1).

The DEMs, panoramic photos, and visual inspection were used to identify clusters that developed on the armored sediment bed. Each cluster consisted of an identifiable key clast around which at least two smaller grains deposited. Clusters were elevated above the surrounding bed area, making the DEMs a particularly useful tool in identification (Figure 5.3.1). The geometric properties of the clusters were measured from the photos and DEMs, including maximum cluster height hs, and key clast size ds (Table 5.2.1). Similar to the correlation function developed by Morris (1955) and Strom and Papanicolaou (2008) to define cluster spacing, a spacing parameter λ (Equation 5.2.1) was defined in this case as the distance from individual cluster to the nearest cluster along a downstream diagonal direction:

$$\lambda = \sqrt{\lambda_x{}^2 + \lambda_y{}^2} \qquad\qquad 5.2.1$$

where λ_x is the downstream cluster-to-cluster spacing for which $\Delta y = 0$ and λ_y is the transverse cluster-to-cluster spacing for which $\Delta x = 0$. For natural clustered beds, x and y are taken to be the streamwise and cross-stream directions respectively. Initial experiments identified 30cm as the minimum distance between clusters necessary for a cluster to be considered isolated. This corresponds to $\lambda \geq 7d_s$ and is approximately seven times the maximum clast size (4.53cm) in the bed.
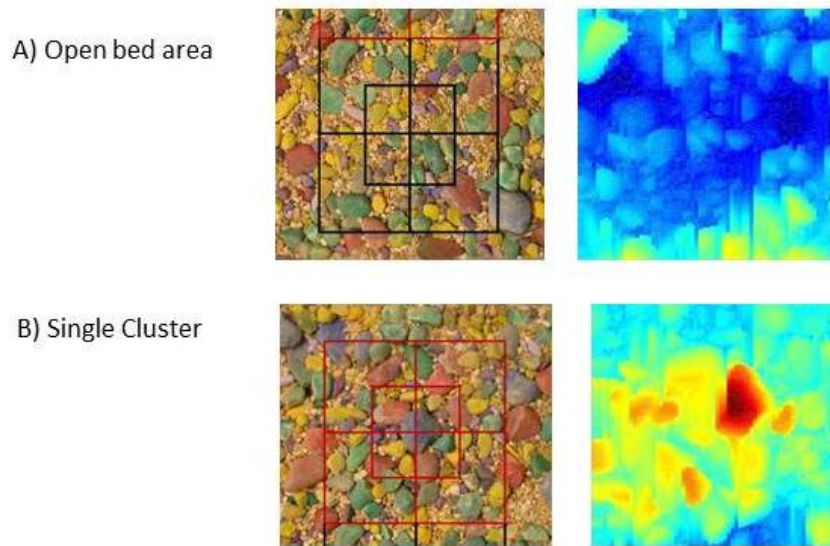
Figure 5.3.1 Measurement grid and associated DEM for the armored bed with 1 % sand. A) area of bed without a cluster. B) Single cluster where the keystone clast is in the center of the measurement grid

5.4 Velocity Measurements

High resolution velocity measurements were necessary to describe accurately the flow field generated around the clusters (Lamarre and Roy 2005). For this research, we employed a ©Nortek AS Vectrino™ ADV which has a manufacturer reported accuracy of 0.5% measured value ±1 mm/s and measures over a sampling volume 4.9 cm from the probe. A high rate of sampling was maintained (200Hz), enabling high resolution three-dimensional flow measurements. Previous research has shown that a stationary time series develops in turbulent flow within 60 seconds (Buffin-Belanger and Roy 2005; Hardy et al. 2009; Thoroddsen et al. 2008), and our measurements showed the sampling duration of 120 seconds to be sufficient. Thus, all of our measurements are temporally averaged over 2 minutes.

Velocity measurements were made around five clusters formed on armored surfaces and two areas of armored bed surface without clusters were measured. Detailed measurements were ensured by following a grid of measurements around one cluster from the 1% sand bed (Cluster 1101A), two from the 9% sand bed (Clusters 1109B and 1109C), one from the 24% sand bed (Cluster 1124D), and two from the 38% sand bed (Clusters 1138E and 1138F). The open, armored bed areas from were measured from both the 1% sand bed (1101open) and the 24% sand bed (1124open) to create baselines against which the influence of clusters on flow patterns could be compared.

The flow pattern was defined by making velocity measurements following a grid pattern where measurements made at each node in a 3-D grid with the cluster at the center of the grid (Figure 5.3.1). The velocimeter was attached to a system of three stepper motors which moved the instrument exact distances. The grid extended in the vertical as well as horizontal and transverse directions so that the same Cartesian grid pattern was measured at each position in the vertical flow profile. Vertical spacing for the measurements was either 0.5 or 1 cm, while longitudinal and transverse spacing was 5 cm, which was slightly larger than the maximum clast size.

5.4.1   Velocity Time Series Data Quality

Velocity time series were initially inspected by eye for abnormalities and then de-spiked using the mean and standard deviations. Data values greater or lower than the mean velocity $\pm$ three standard deviation were truncated to achieve a relatively clean and regular time series. The Vectrino ADV signal correlation R_{adv} was used to detect unreliable data points. Manufacturers of both Sontek and Nortek ADVs recommend that velocity measurements for which the R_{adv} is less than 70% be considered acoustic noise

and removed from the time series. However, others have reported that the signal quality is reduced at the region of high turbulent flow due to the shear in the sampling volume and the threshold correlation may be below 70% (Martin et al. 2002; Strom and Papanicolaou 2007). In recognition of this, we applied a filter designed to discard instantaneous velocity data points when the correlation R_{adv} <65%. Data with a correlation between 65% and 70% were maintained in the velocity time series to account for low correlation measurements caused by high turbulent events occurring in near bed regions.

5.4.2   Turbulence Parameters

The time series data collected around each cluster and open bed area were analyzed and several turbulence variables quantified using the time averaged three-dimensional velocity data. Flow velocities are defined whereby u corresponds to the streamwise direction x, v to the lateral (or transverse) direction y, and w to the vertical direction, z (Figure 5.4.1).
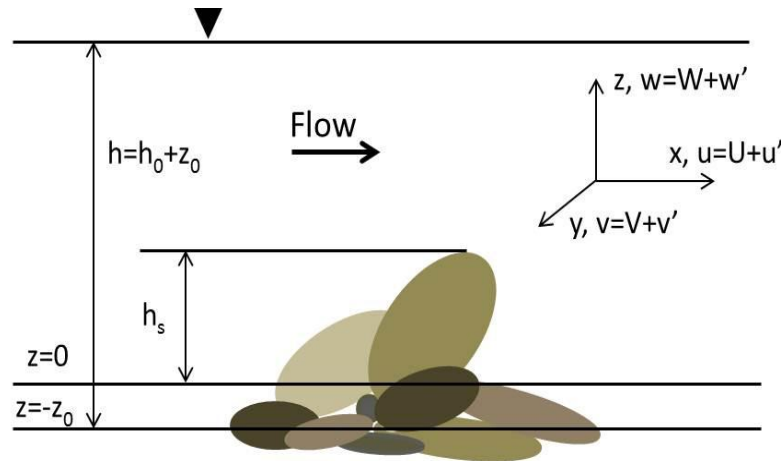
Figure 5.4.1 Definition sketch of a cluster on a bed surface and three-dimensional flow directions. hs is height of cluster; zo is the lowest elevation of the bed surface around the cluster; z=0 at the mean bed elevation; ho is the water depth measured from the zero elevation.

Turbulent Kinetic Energy (TKE) represents the mean kinetic energy per unit mass associated with coherent structures in the turbulent flow and was calculated as half the sum of the turbulent intensities in all three dimensions for each grid node (Equation 5.2.2).

$$\text{TKE} = \frac{1}{2}\left[\overline{(u')^2} + \overline{(v')^2} + \overline{(w')^2}\right] = \frac{1}{2}\left[u_{rms}{}^2 + v_{rms}{}^2 + w_{rms}{}^2\right] \qquad 5.2.2$$

The Reynolds stress in the xz direction was calculated using the covariance of two of the three flow dimensions, where   is water density. The x-z direction Reynolds stress provides a measure of the momentum exchange in the flow, and was calculated according to Equation 5.2.3. Because only the x-z direction Reynolds stress was used in this analysis, it is referred to here as the Reynolds stress τ_{Re}.

$$\tau_{xz} = \tau_{Re} = -\rho\overline{u'w'} \qquad 5.2.3$$

5.4.3   Quadrant Analysis

A quadrant analysis was performed to identify the dominant types of turbulence events throughout the flow field and to aid in the identification of any coherent flow structures created around the clusters. Instantaneous flow velocity fluctuations were graphed on a u',w' grid (Figure 5.4.2) and categorized into quadrants according to the dominant data clustering (Lu and Willmath, 1973).
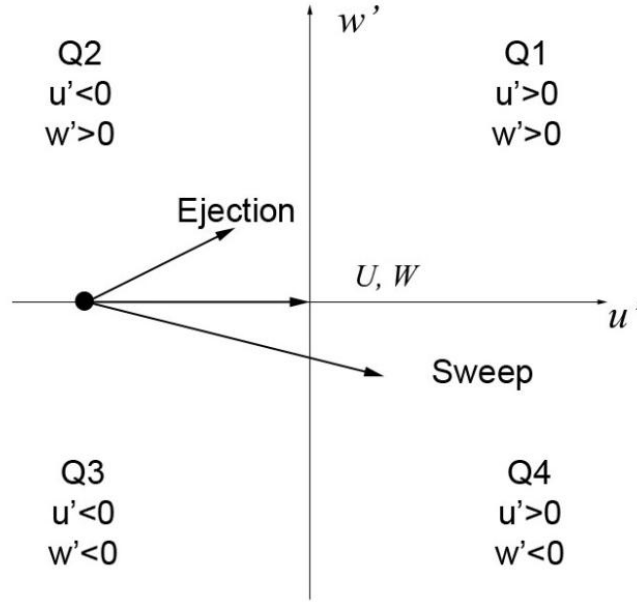
Figure 5.4.2 Schematic of Quadrant Analysis

The quadrants define the four modes of momentum transfer that may occur in a flow. Quadrants 2 (u'<0; w'>0) and 4 (u'>0; w'<0) indicate the dominance of ejection and sweep events, respectively. Events in quadrant 1 (u'>0; w'>0) are outward events while those defined by quadrant 3 (u'<0; w'<0) are inward. Sweep events (Q4) transport high velocity fluid from the outer flow regions toward the bed while ejections (Q2) transport low momentum fluid from the bed and upward in the flow profile. Pairing of ejection and sweep events is common around roughness features and provides a dominant mechanism for momentum transfer in the flow (Grass 1971; Reidenbach et al. 2010). Nezu and Nakagawa (1977) defined a normalized instantaneous Reynolds shear stress fluctuation, Equation (5.2.4),

$$\tau_{i,H}(t) = \frac{\langle u'w'\rangle_{i,H}}{\overline{u'w'}} = \frac{1}{\overline{u'w'}}\lim_{T\to\infty}\int_0^T u'w'I_{i,H}(t)dt \qquad\qquad 5.2.4$$

where the angle brackets denote a conditional average, H is the hole size; i defines the particular quadrant of interest ($i=1$, 2, 3, 4); T is the time interval between measurements, and $I_{i,H}$ is the threshold indicator defined as

$$I_{i,H}(t) = \begin{cases} 1 & \text{when } |u'w'|_{i,H} \geq Hu_{rms}w_{rms} \\ 0 & \text{otherwise} \end{cases}$$ 5.2.5

The hyperbolic hole function, H, in the *u'-w'* plane is applied to the analysis to enable a focus on only those velocity fluctuations with large contributions to Reynolds shear stress. The hole function defines a minimum velocity fluctuation value below which the data are not included in the quadrant analysis. The value of H is user defined, and past researchers have applied a range of H values to armored gravel beds through the application of equation (5.2.6) (Lacey and Roy 2008b; Strom and Papanicolaou 2007).

$$H = \frac{|u'w'|}{u_{rms}w_{rms}}$$ 5.2.6

In this study threshold H values of 0 and 2.5 were used to characterize low and high magnitude turbulent events respectively. When $H = 0$, all contributions in terms of *u'w'* were included within the quadrant analysis. When $H = 2.5$, only the high magnitude turbulence events were considered.

5.5   Turbulence Statistics Results

The time averaged values of TKE (Equation 5.2.2), and Reynolds stress (τ_{Re}; Equation 5.2.3) were computed at each of the grid nodes where the 3-D velocity was measured around each area of interest. Specific measurement details concerning the three dimensional velocities, TKE, and τ_{Re} in the flow area above the clusters of interest and the open armored bed areas without any cluster are provided in Table 5.5.1. The

minimum, maximum, and spatially averaged TKE and τ_{Re} values from each grid area illustrate the variability in turbulent flow parameters between the clusters and the open bed area (Figure 5.5.1 and Figure 5.5.2). The vertical flow scale was made non-dimensional to ensure comparison across the experiments. The non-dimensional parameter z^* is defined as the local depth over the bed at that point divided by total depth h_o (i.e. $z^*=z/h_o$). The elevation at $z^*=0.3$ typically corresponded to the flow just above the cluster form. We use this elevation as a measure of flows near bed surface and the cluster form. At $z^*=0.5$ the flow was well above the cluster where the flow was no longer directly influenced by the bed surface or cluster form. By analyzing the measurements at $z^*=0.3$ and $z^*=0.5$, we measured any change in the magnitude of turbulent flow parameters with elevation in the flow profile. To distinguish these regions in this discussion we label the elevation at $z^*=0.3$ near bed and at $z^*=0.5$, distant.
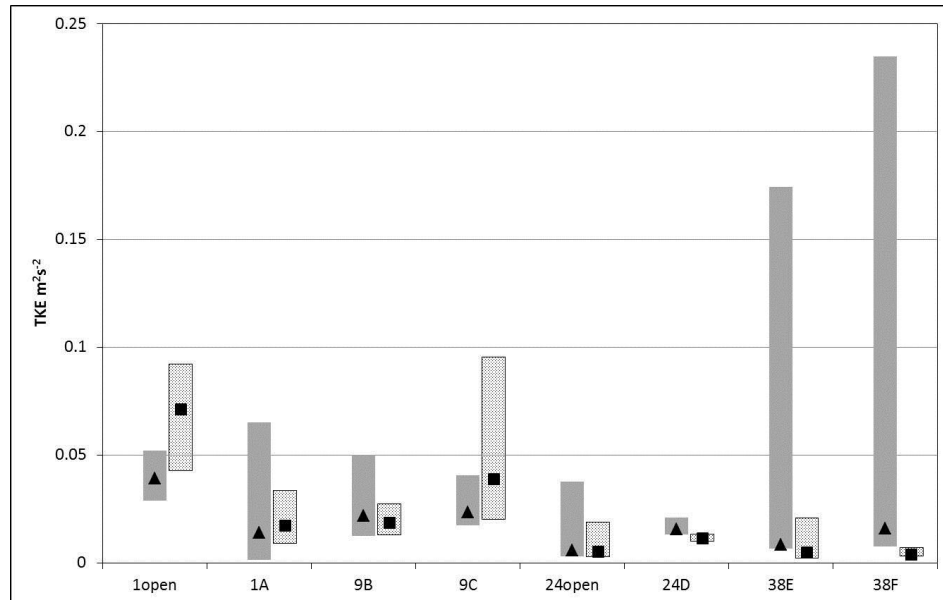
Figure 5.5.1 TKE measurements from the near bed (solid) and distant (patterned) flow areas. The near bed was measured at elevation $z^*=0.3$ and the distant flow at $z^*=0.5$. Solid markers indicate mean value
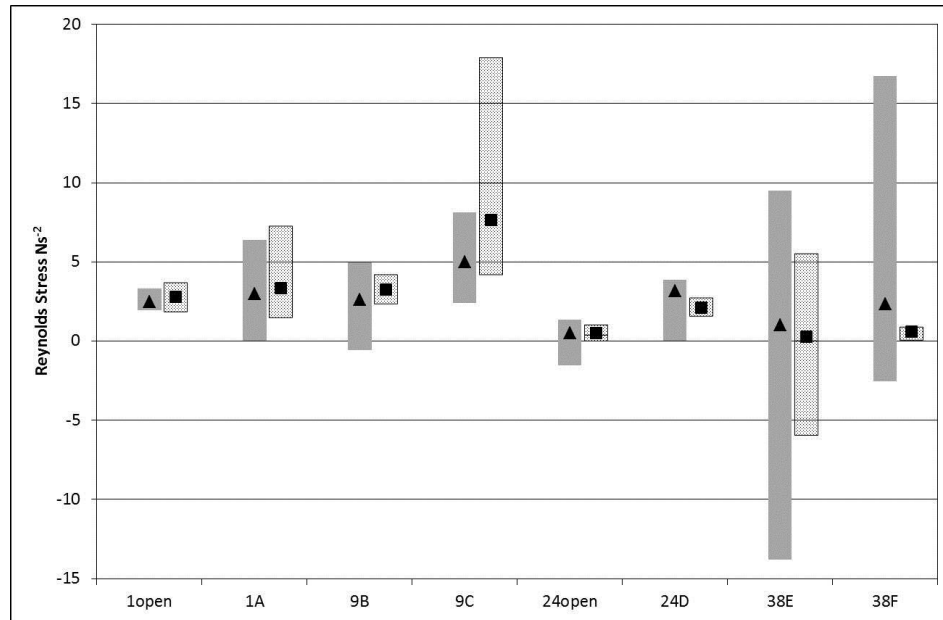
Figure 5.5.2 Measurements of Reynolds stress in the xz-direction from the near bed (solid) and distant (patterned) flow areas. The near bed was measured at elevation z*=0.3 and the distant flow at z*=0.5. Solid markers indicate mean values

The TKE and τ_{Re} values computed at the grid nodes were used to create contour plots of the turbulent flow parameters around the clusters and open bed areas (Figure 5.5.4; Figure 5.5.5; Figure 5.5.6). Each of the clusters showed a similar pattern of influence over flows in the immediate area, thus only selected contour plots are included. In each case a recirculation cell of locally elevated TKE and τ_{Re} formed downstream of and at an equal elevation to the cluster crest. The cell size and the values of the turbulent flow parameters changed with the different clusters, but a similarly located cell developed at every measured cluster. Paired with the contour plots is an x,y-plot of the horizontal flow plane just above the cluster crest, at z*=0.3. By isolating the flow just over the cluster crest, the plot visualizes the lateral extent of the cluster's influence over the flow.

108

ID	Time and Space Averaged Velocity(m/s)			TKE at z*=0.3	τ_{Re} at z*=0.3	TKE at z*=0.5	τ_{Re} at z*=0.5
	$\bar{U}$	$\bar{V}$	$\bar{W}$	Max Average Min	Max Average Min	Max Average Min	Max Average Min
1101open	0.321	0.0072	0.0003	0.051 / 0.039 / 0.0287	3.3381 / 2.4528 / 1.9294	0.0911 / 0.071 / 0.0429	3.6628 / 2.7752 / 1.8406
1101A	0.62	0.0123	0.002	0.064 / 0.0139 / 0.0012	6.3958 / 2.9722 / 0.1175	0.0328 / 0.0171 / 0.0092	7.2296 / 3.3334 / 1.5011
1109B	0.63	0.0206	-0.013	0.049 / 0.0219 / 0.0125	4.9814 / 2.5947 / -0.5858	0.0265 / 0.0186 / 0.0131	4.1605 / 3.2458 / 2.3554
1109C	0.92	0.0151	-0.015	0.0396 / 0.0234 / 0.0173	8.1146 / 4.987 / 2.425	0.0946 / 0.0389 / 0.0201	17.867 / 7.6476 / 4.1749
1124open	0.23	0.0108	0.0007	0.0367 / 0.0059 / 0.0029	1.3659 / 0.5148 / -1.513	0.018 / 0.0051 / 0.003	1.0324 / 0.5211 / 0.3577
1124D	0.44	-0.007	-0.004	0.0198 / 0.0154 / 0.013	3.8884 / 3.1426 / 2.6579	0.0123 / 0.0114 / 0.0101	2.6941 / 2.0992 / 1.55
1138E	0.35	0.0003	-0.004	0.1732 / 0.0085 / 0.0066	9.5166 / 1.0273 / -13.817	0.0198 / 0.0047 / 0.0024	5.511 / 0.2953 / -5.956
1138F	0.37	0.0003	-0.004	0.2339 / 0.016 / 0.0076	16.744 / 2.3326 / -2.5284	0.0061 / 0.0037 / 0.0031	0.8635 / 0.6018 / 0.039

Table 5.5.1 3-D velocities and turbulence statistics for measured clusters and open bed areas in experiment with equilibrium flow rate = 0.11m³/s

5.5.1 1% Sand Bed

Detailed flow measurements were recorded over two different areas of the armored bed created from the bulk sediment with 1% sand content. One area was an open region of the armored bed surface without a cluster 1101open and the other was around

an isolated cluster 1101A. The cluster-free open bed area measured was a 0.2×0.2m square located 0.4m from the downstream end of the flume bed. This area was chosen because it aligned transversely with the measured cluster. Thus, the open bed area and cluster were equidistant from the upstream end of the flume.
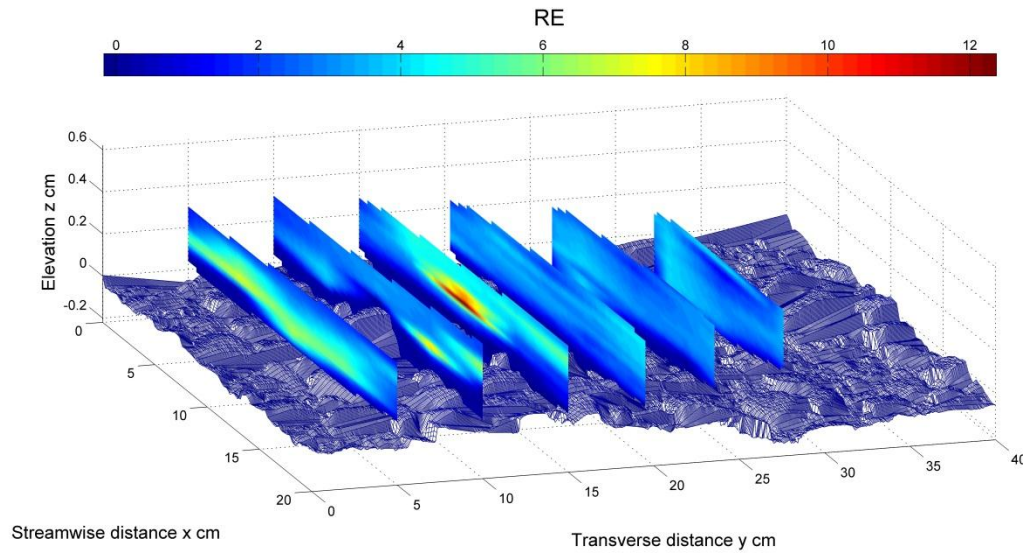
Figure 5.5.3 Reynolds stress measurement over 1101open and 1101A; flow direction is perpendicular and outward from the paper; 1101A is located in the left part of the figure, and 1101open is the area in the right with lower elevation.

The flow field over the cluster-free armored bed was distinctive for its uniformity (Table 5.5.1 and Figure 5.5.3). There was minimal variability in the magnitude of τ_{Re} in the flow field over the bed in either the near bed or distant flow regions (Figure 5.5.2 and Figure 5.5.3). When averaged spatially over the horizontal flow plane, the Reynolds stress was near 0Pa in both the near bed and distant flow regions. The TKE profile was equally uniform near the bed but elevated over part of the distant flow, increasing the size of the bar in Figure 5.5.1. The extent of the area of higher TKE values did not increase until reaching an elevation $z^* \geq 0.3$, indicating that the change in turbulent energy was not the result of the flow interaction with the bed surface. TKE averaged near $0m^2/s^2$ in the

near bed flow region. The consistent and low magnitudes of Reynolds stress and TKE near the bed indicated a limited influence of the unclustered, armored bed surface on local turbulent flow parameters.

The cluster developed during the armoring of the bulk sediment with 1% sand content had a keystone clast that was from the largest grain size available in the sediment with secondary clasts from the D_{84} grain size. This cluster extended further into the open flow area than any other measured cluster (Table 5.5.1). The greatest magnitude values of both TKE and τ_{Re} were measured within the recirculation cell downstream of and level with the cluster crest. The recirculation cell was within the area we defined as the near bed flow region and the increase in TKE at the recirculation cell was the difference between the average, $0.014 m^2/s^2$, and maximum, $0.064 m^2/s^2$, TKE values (Figure 5.5.1, Table 5.5.1). The range in TKE values was larger near the bed than in the distant flow region, with larger magnitudes near the bed. Average Reynolds stress measurements were near equal average in the near bed and distant flow areas (Figure 5.5.2).

5.5.2   9% Sand Bed

Two isolated clusters were measured from the armored bed created from bulk sediment with 9% sand content. Both clusters formed around a D_{84} size keystone clast, had similar widths, but differed in profile as cluster 1109C extended further into the flow field. Contour plots of the vertical flow profile over cluster 1109B (Figure 5.5.4 A and C) illustrate the pattern of a high magnitude recirculation cell adjacent and downstream of the cluster peak.

Figure 5.5.4 Turbulent flow parameters measured around Cluster 1109B. A) Centerline profile of Reynolds stress. B) Centerline profile of TKE. C) Plan view Reynolds stress in the xy plane measured at z*=0.3. D) Plan view TKE in the x-y plane measured at z*=0.3. In all, the x-axis is streamwise distance (m). In A and B the y-axis is the z* value. In C and D, the y-axis is the lateral distance (m). In each figure, the color scale extends from a low of 0 (dark blue) to high (red) values.

The Reynolds stress varied between 2-4Pa for the majority of the flow profile with the exception of a recirculation cell where values increased to near 10Pa. There were two smaller recirculation cells in the distant flow area at a z* elevation between 0.3 and 0.4 which had τ_{Re} values near 5Pa. The same pattern of recirculation cells within an otherwise consistently low magnitude profile was measured in the TKE plot (Figure 5.5.4). TKE magnitudes increased two orders of magnitude in the recirculation cell formed immediately downstream of the cluster crest. The plan view measured at z*=0.3 illustrated the effect of the cluster on the pattern of TKE and τ_{Re} in the region around it (Figure 5.5.4 B and D). The plots were centered over the cluster and although the cluster was not visible at this flow level, the influence on energy and momentum distribution in

the flow field was indicated by elevated magnitude contour patterns above and downstream of the cluster.

Cluster 1109C had a ratio of cluster peak elevation to flow depth of $z* = 0.20$ and exerted a larger influence on the surrounding flow field, as shown in the flow profiles of the turbulent parameters (Figure 5.5.5). The cluster morphology formed a distinct peak with a more abrupt elevation transition than did Cluster 1109B. In response, recirculation cell at Cluster 1109C formed with higher magnitude turbulence. Reynolds stress increased from 2.4Pa for the flow near the bed to a peak of 17.9Pa in the center of the recirculation cell. The recirculation cell was also larger, extending downstream and upward in the flow. TKE values showed a similar increase in value in the recirculation cell downstream of the cluster peak, but the area of elevated TKE also extended upstream.
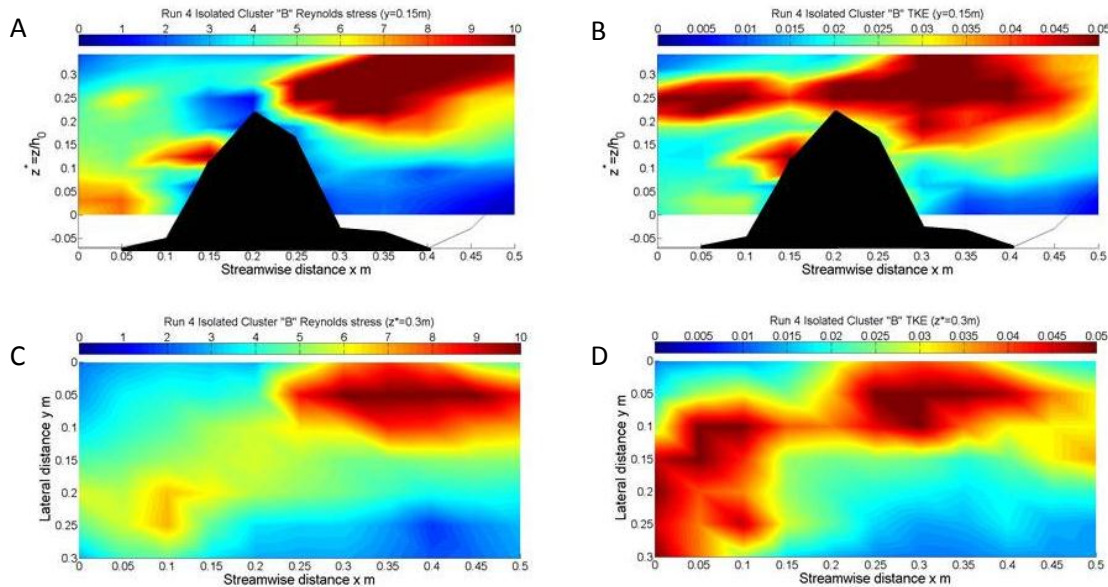
Figure 5.5.5 Turbulent flow parameters measured around Cluster 1109C. A) Centerline profile of Reynolds stress. B) Centerline profile of TKE. C) Plan view Reynolds stress in the xy plane measured at z*=0.3. D) Plan view TKE in the xy plane measured at z*=0.3. In all, the x-axis is streamwise distance (m). In a and b the y-axis is the z* value. In c and d, the y-axis is the lateral distance (m). In each figure, the color scale extends from a low of 0 (dark blue) to high (red) values.

The extended recirculation cells at Cluster 1109C were apparent in the plan view plots of TKE and τ_{Re} measured above the cluster, at z*=0.3. The Reynolds stress plot (Figure 5.5.5A, C) had a single large, but distinct area of elevated τ_{Re} measurements matching the location of the cluster. A smaller area of increased τ_{Re}, was measured upstream of the cluster and may have been associated with a bed feature upstream. The TKE plan view (Figure 5.5.5D) showed two areas of elevated TKE, one at a location downstream of the cluster and the other laterally across the flow area upstream of the cluster. There may have been a recirculation cell formed from an upstream bed feature that traveled downstream and was measured in the area around Cluster 1109C. Because we focused our measurements around single clusters, we can only speculate on the origin of the upstream recirculation cell. However, it does appear to be distinct from the cell associated with the cluster.

5.5.3   24% Sand Bed

With the increase in bulk sediment sand content to 24%, an open area of the armored bed was measured in addition to the cluster. Similar to the flow field over the cluster free bed area of the 1% sand sediment mixture, the turbulent parameters were highly uniform (Table 5.5.1) as shown in the TKE and τ_{Re} profiles (Figure 5.5.6). There was almost no variability in the magnitude of the τ_{Re} in the flow field across the flow profile and Reynolds stress values averaged 0Pa. TKE values were also minimal and uniform near the bed but elevated at an apparent recirculation cell in the distant flow, at z*≥0.4. The location of the cell in the outer flow region indicated that it was not formed through flow interaction with the immediate bed surface.

114
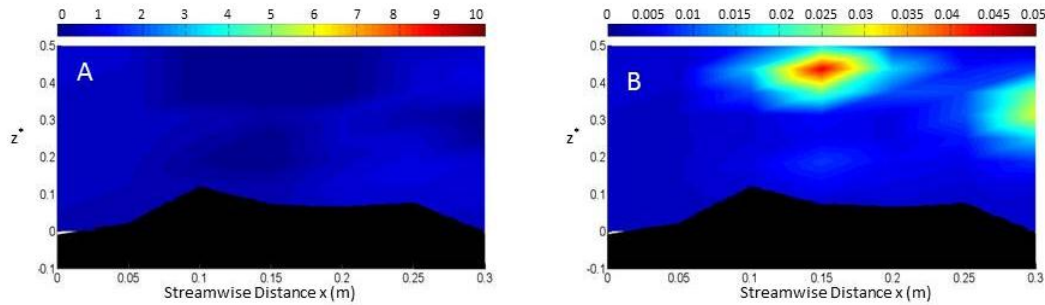
Figure 5.5.6 Turbulent flow parameters measured over the 1124open. A) Centerline profile of Reynolds stress. B) Centerline profile of TKE. The x-axis is streamwise distance (m) and b the y-axis is the z* value. In each figure, the color scale extends from a low of 0 (dark blue) to high (red) values.

The cluster measured was comprised of a keystone from the largest grain size available with two adjacent clasts in the D_{84} size range. While distinctive on the bed surface and in the DEMs, it was much lower in profile than clusters generated from beds with lower sand contents (Table 5.5.1) Maximum values of Reynolds stress and TKE in the recirculation cell downstream of the cluster were also lower reaching 3.9 Pa and $0.02m^2/s^2$, respectively (Figure 4.3.2 and Figure 4.3.4). The Reynolds stress increased by 2Pa over the cluster crest and continued to increase on the downstream side of the cluster to 3Pa greater than values upstream of the cluster. A similar pattern was measured for TKE values, with peak values occurring at the same location as the peak τ_{Re}. The ranges in τ_{Re} and TKE in the flow area around the cluster were the smallest measured around clusters (Table 5.5.1; Figure 5.5.1 and Figure 5.5.2).

5.5.4 38% Sand Bed

The largest bulk sand content tested was 38% and from this armored bed, two clusters were measured. The first was comprised of four D_{84} grain sizes grouped on the bed while the second was distinguished by a keystone from the maximum grain size available with three D_{70} grains adjacent.
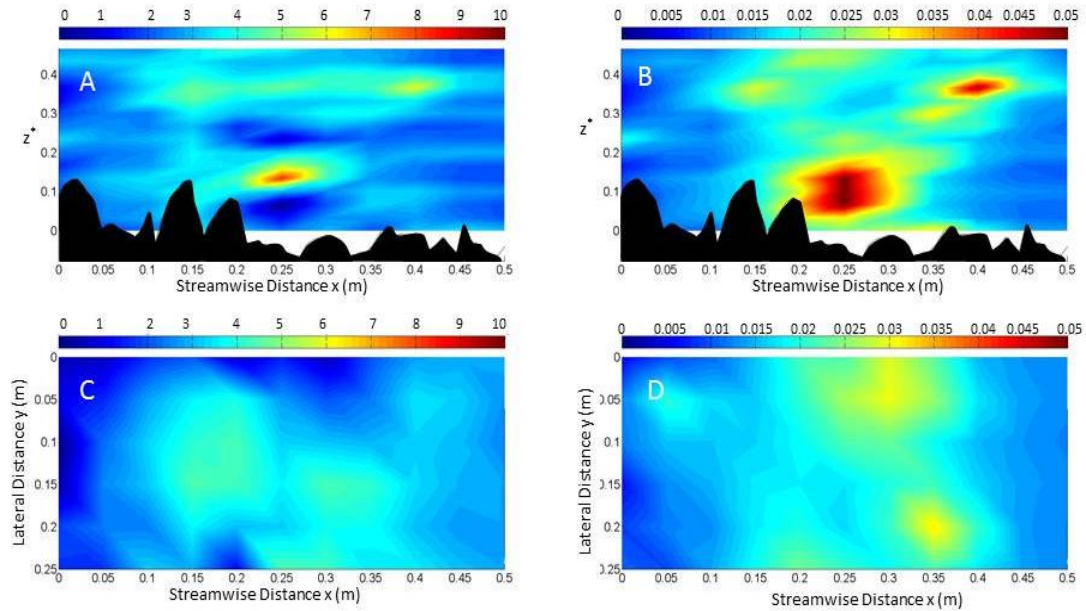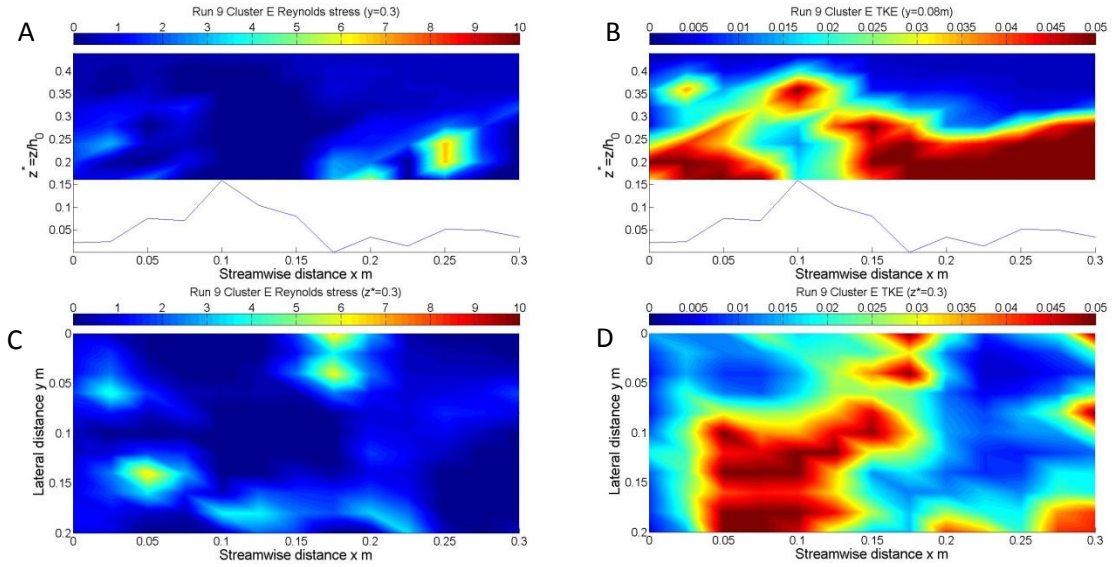
Figure 5.5.7 Turbulent flow parameters measured around Cluster 1138E. A) Centerline profile of Reynolds stress. B) Centerline profile of TKE. C) Plan view Reynolds stress in the xy plane measured at z*=0.3. D) Plan view TKE in the xy plane measured at z*=0.3. In all, the x-axis is streamwise distance (m). In and b the y-axis is the z* value. In c and d, the y-axis is the lateral distance (m). In each figure, the color scale extends from a low of 0 (dark blue) to high (red) values.
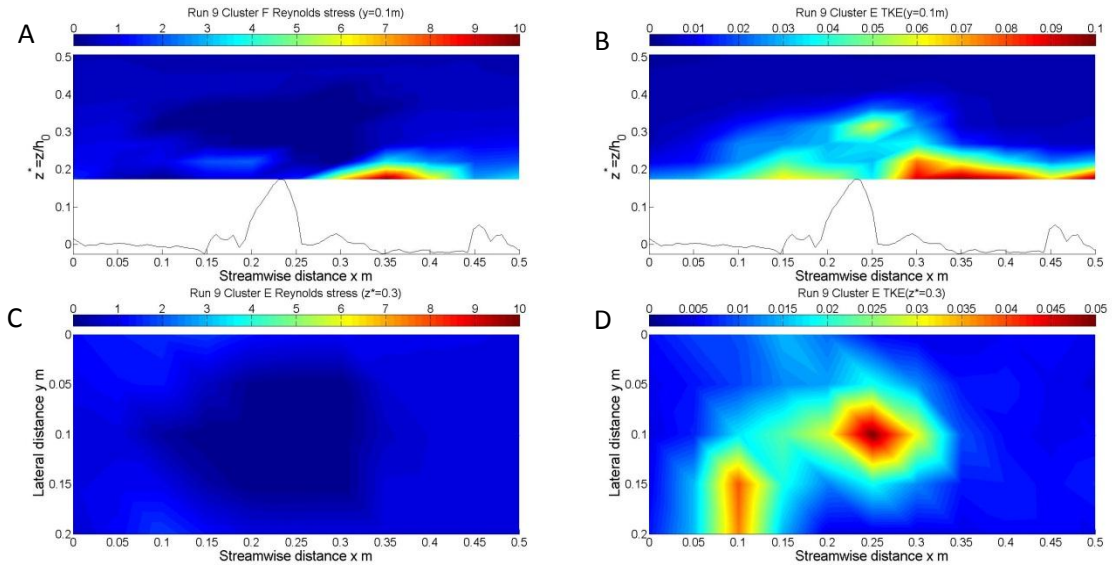
Figure 5.5.8 Turbulent flow parameters measured around Cluster 1138F. A) Centerline profile of Reynolds stress. B) Centerline profile of TKE. C) Plan view Reynolds stress in the xy plane measured at z*=0.3. D) Plan view TKE in the xy plane measured at z*=0.3. In all, the x-axis is streamwise distance (m). In and b the y-axis is the z* value. In c and d, the y-axis is the lateral distance (m). In each figure, the color scale extends from a low of 0 (dark blue) to high (red) values.

The clusters reached similar maximum elevations from the bed surface and showed a similar impact on the surrounding turbulent flow. Recirculation cells of high magnitude Reynolds stress and TKE were formed downstream of both cluster peaks. TKE increased from near zero to maximums of 0.17 m^2/s^2 and 0.23 m^2/s^2 in the recirculation cells formed downstream of Clusters 1138E and 1138F, respectively (Table 5.5.1, Figure 5.5.1, Figure 5.5.7, and Figure 5.5.8). These were the largest TKE values measured in these experiments. TKE was also elevated in the distant flow area, although by much less. The majority of the change in TKE occurred within the region near the bed and only a limited difference in turbulent energy was measured in the outer flow (Figure 5.5.1). The Reynolds stresses showed a similarly large range in values within the near bed flow area around the clusters. Values increased from -13Pa to 9.5Pa in the recirculation cell downstream of Cluster 1138E and from -2.5Pa to 14.4Pa in the cell associated with Cluster 1138F (Figure 5.5.2). In both cases, elevated Reynolds stress values were only measured in the near bed region. Once distant from the clusters, there was less change in the Reynolds stress in the flow field which averaged near 0Pa in the distant flow region.

5.6   Quadrant Analysis Results

A quadrant analysis was performed over each cluster and open bed area to identify the dominant turbulent events contributing to momentum transfer through the flow. The same profiles used for analysis of the turbulent characteristics were applied to the quadrant analysis. Two threshold *H* values, 0 and 2.5, were employed in separate quadrant analyses. When the hole size was set to 0 all the turbulent fluctuations,

117

regardless of magnitude, were included in the analysis. A hole size of *H*=2.5 was used in the quadrant analysis to determine the dominant flow patterns associated with only the large magnitude velocity fluctuations. For every region analyzed, the flow profiles were dominated by ejection (Q2) and sweep (Q4) events. Similar patterns were measured around the different clusters so while all are summarized here, a limited number of representative images are shown.

5.6.1   Hole size *H* = 0

When all the turbulent fluctuations, regardless of magnitude, were included in the analysis, the centerline vertical profile illustrated a dominance of paired ejection and sweep events with a minority of events corresponding to inward (Q3) and outward (Q1) events (Figure 5.6.1). Over the unclustered, armored bed surface the quadrant analysis showed a flow field dominated by flow ejections (Figure 5.6.1a). There was no distinct flow pattern linked to the bed surface. However, where an isolated area of outward events was dominant in flow profile over the open bed with 24% sand, this location was coincident with the local peak in TKE (Figure 5.5.6), indicating a recirculation cell formed within the flow field due to a phenomenon unrelated to the immediate bed area.

The flow area above the clusters was dominated by bursts and sweeps with the majority of the inward and outward events restricted to an elevation below that of the cluster height. On the downstream side of each cluster, a dead zone formed near the bed characterized by outward (Q1) and inward (Q3) events which was interpreted to be a wake area created by the cluster. This pattern was repeated over all the clusters measured. Clusters 1109B and 1109C also illustrated the impact of cluster morphology on the turbulent flows, mimicking the patterns of TKE and τ_{Re} discussed in Section 5.5.2.

Cluster 1109B (Figure 5.6.1b) had a distributed cluster profile as it was comprised of a grouping of D_{84} size particles. The quadrant analysis showed the distant region of the flow profile was almost entirely composed of sweep events, with alterations in the area of the recirculation cell downstream of the cluster. Cluster 1109C was characterized by a single large particle that extended as an isolated form into the flow area. The quadrant analysis, similar to the pattern of turbulent flow parameters, reflected a more varied turbulent flow pattern where the flow field was dominated by paired bust and sweep events (Figure 5.6.1c). Areas dominated by inward flows were limited to near the bed and below the elevation of the cluster crest.
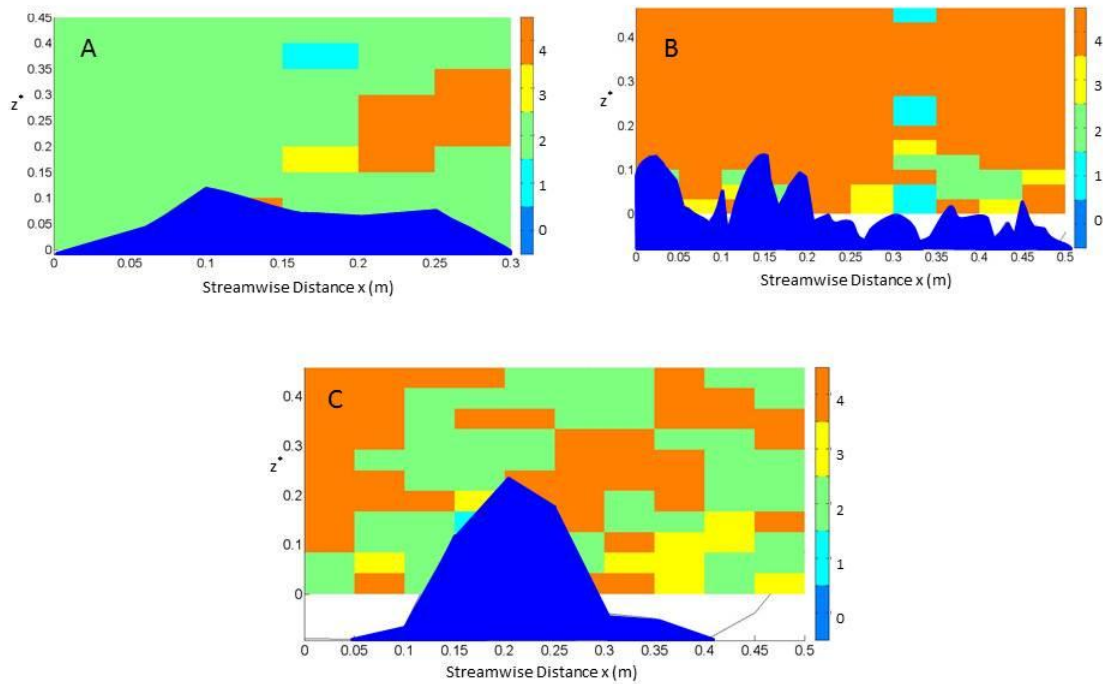
Figure 5.6.1 Profiles showing the quadrant analysis over the centerline profile with hole size H=0 for an 1101open (A), over Cluster 1109B, and (C) Cluster 1109C. The x-axis is streamwise distance (m) and b the y-axis is the z* value. In each graph the dark blue area labeled 0 represents the cluster.

5.6.2 <u>Hole size *H* = 2.5</u>

A hole size of $H = 2.5$ limited the quadrant analyses to those flow events contributing most to the formation of turbulent flow structures. As a result, the general dominance by specific quadrants was inverted from what was observed when the hole size was zero. Over the armored, unclustered bed areas the pattern remained one of alternating burst and sweep events without any clear connection to the bed surface (Figure 5.6.2A). Over the clusters, the burst and sweep pattern continued to dominate with limited regions of inward and outward events downstream of the cluster and near the bed surface. The distributed cluster morphology of Cluster 1109B generated a flow field dominated by flow ejections with areas of flow sweeps near the bed and downstream of the main cluster form (Figure 5.6.2B). Wake areas formed along the bed surface were limited in size. Cluster 1109C generated a flow field representative of a cluster morphology characterized by a distinctive profile (Figure 5.6.2C). There was greater variability in the distribution of ejection and sweep events when compared to the pattern measured over the diffuse cluster morphology. The inward and outward events around Cluster 1109C formed a distinct pattern immediately downstream of the key cluster particle and adjacent to the bed, characteristic of a wake area downstream of a large object.

120
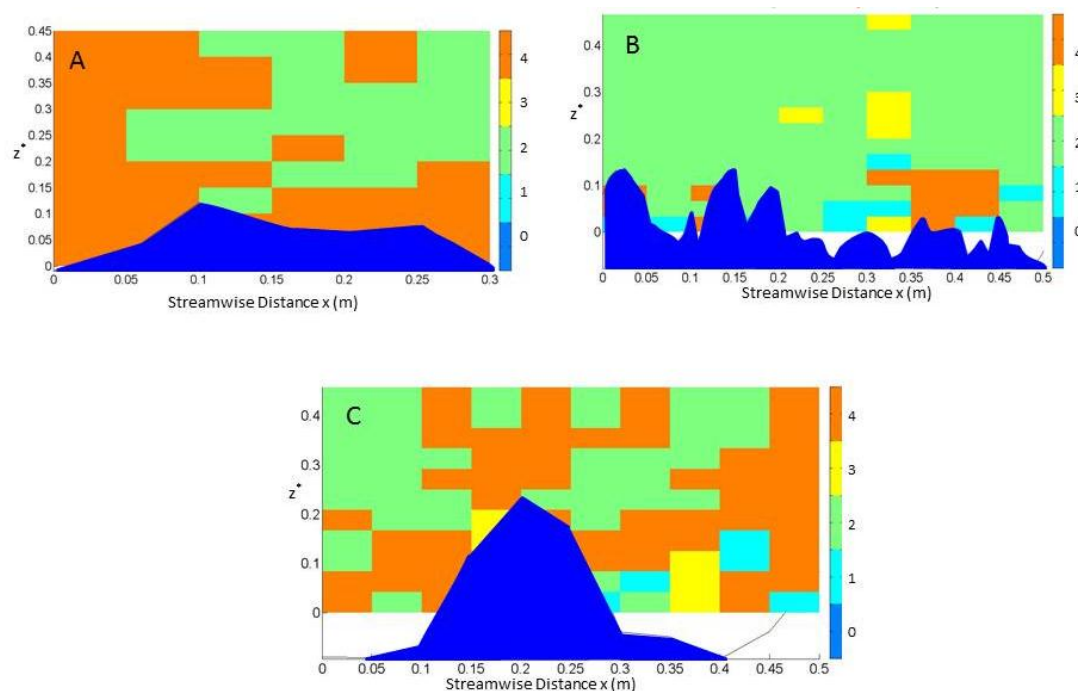
Figure 5.6.2 Profiles showing the quadrant analysis over the centerline profile with hole size H=2.5 for an 1101open (A), over Cluster 1109B(B), and Cluster 1109C(C). The x-axis is streamwise distance (m) and b the y-axis is the z* value. In each graph the dark blue area labeled 0 represents the cluster.

5.7   Discussion

Clusters form within the structure of the bed surface when a gravel bed river armors. Because the cluster form extends above the mean bed surface and into the open flow area, it has been shown to affect the near bed turbulence and generate coherent turbulent flow structures (Buffin-Belanger and Roy 1998; Hassan and Church 2000; Lamarre and Roy 2005). Hardy et al. (2009) linked the coherent flow structures that developed over gravel beds to interaction of the near bed flow with the bed surface. We measured the effects of isolated clusters formed during the armoring of channel beds that ranged in sand content. In each case, we found results similar to those described from field experiments where flow acceleration, recirculation, shedding, and reattachment

were measured around clusters (Buffin-Belanger and Roy 1998). At each cluster, we identified a recirculation cell at the level of the cluster crest which extended downstream in the flow. The methods used in this study precluded the real-time measurements necessary to identify the recirculation cells as shedding vortices, but the measured cells were similar to vortices previously identified as shedding from the downstream side of clusters (Buffin-Belanger and Roy 1998; Lacey and Roy 2008b).

All the bed surfaces, including the unclustered bed areas, had some effect on the measured turbulent flow parameters. By measuring across the flow profile, we are able to separate the impact on the near bed and distant flow areas and identify how both were affected by clusters and bulk bed sand content. Rough beds have been shown to increase turbulent flow parameters near the bed (Hardy et al. 2009), and also in the outer flow regions as the roughness of the bed surface increased (Wang et al. 2012). The magnitude of the increased turbulence was limited over a gravel bed river in the field where no clusters were present (Lacey et al. 2007). Our results showed that for both the 1% and 24% sand bed cases, the unclustered armored bed had a limited measurable impact on the near bed flows, elevating the TKE and Reynolds stress immediately over the bed but not in the distant flow region. The increase in turbulence parameters could not be associated with any particular location on the bed as the mean value was coincident with the median in both cases. The lack of variability in the range of energy (Figure 5.5.1) and momentum (Figure 5.5.2) as measured over the open bed regions indicated a uniformly affected flow that was characteristic to the unclustered, armored bed surface. When the measurements from the 1% and 24% open bed areas were compared, the influence of increased sand

content in the sediment bed became noticeable as a lowering of both TKE and Reynolds stress. The armor ratio also decreased from 1.83 to 1.73. Our finding of a reduction in turbulent flow parameters for a bed with increased bulk sand content confirms and extends the findings of Hardy et al. (2010) who found that as the bed surface smoothed, the overall turbulence as measured by TKE decreased. Sweep events have been shown to be more prevalent and stronger in the flow over smooth beds (Bomminayuni and Stoesser 2011), and our quadrant analysis showed sweep (Q4) events dominated the flow over the open bed areas (Figure 5.6.2).

The clusters impacted their immediate flow area by increasing the Reynolds stress and TKE in the near bed region and in most cases the distant flow region as well. The measured flow structures indicated movement of momentum and energy between the near bed and distant flow regions around the clusters. The effect of isolated clasts on hydraulic processes has been previously shown to extend throughout the flow depth, as the turbulent structures were advected into the outer flow area (Hardy et al. 2009). In a study of the impact of the turbulence generated by isolated clusters, boulders, and cobbles, Lacey and Roy (2008a) found Reynolds stresses were at a maximum both near the bed on the immediate downstream side of the clasts and also further downstream but in the upper portion of the flow profile. TKE was three to four times larger near the bed in the wake of a clast. An alternating pattern of positive and negative Reynolds stresses measured in the wake areas around isolated clasts indicated intense horizontal turbulent momentum exchange through the formation of counter-rotating vortices in the flow (Lawless, 2004). In our experiments, the presence of the cluster caused the flow to separate as it was

forced over the cluster crest, creating an increase in the turbulent flow properties and formation of a flow recirculation cell with a flow re-attachment point downstream of the cluster. What differed with the change in bulk bed sand content was the magnitude of the turbulence generated around each cluster, as measured through TKE and τ_{Re}. The range in TKE measurements (Figure 5.5.1) around the clusters in the near bed region showed an increased range and difference between maximum and average TKE values for the end member sand contents. The range in TKE values for the near bed flow field decreased as the sand content of the bulk bed increased from 1% to 24% sand. This trend reversed at the highest sand content, 38% of the bulk bed sediment. For both clusters measured over the 38% sand bed, the inner flow TKE values reached maximum values that were an order of magnitude greater than the average. Reynolds stress in the near bed region (Figure 5.5.2) showed a similar increase in range for the 38% sand bed, with the maximum τ_{Re} eight times greater than the average value at Cluster 1138F. At lower sand contents the ranges in near bed τ_{Re} values were either constant or much smaller. The distant flow region had more variable patterns of both TKE and τ_{Re}, with the lowest outer region values measured when the sand content of the bed was high. The size of the ranges in TKE and τ_{Re} values could not be attributed to changes in the relative heights of the clusters on the bed surface, a finding in contrast to what has been previously measured over gravel beds (Hardy et al. 2010). Cluster 1101A had the largest relative roughness (Table 5.5.1) but not the largest range, maximum, or average TKE or τ_{Re} values. Although inconsistent with respect to a correlation with relative bed roughness, the influence of sand in the bulk bed sediment did appear to influence the

turbulent flow events around the clusters. The quadrant analysis provided an indication of the influence of a progressively smoother armored bed surface in the presence of clusters. When the hole size was set to 0, sweep events dominated across the flow depth as illustrated by Cluster 1109B (Figure 5.6.1). The prevalence of sweep events was consistently measured as the sand content in the bed increased, an observation in agreement with previous findings over smooth bed (Bomminayuni and Stoesser 2011).

The difference in TKE and τ_{Re} ranges between the near bed and distant flow regions provided a method for evaluating the movement of momentum and energy through the flow profile. The balance between the turbulent parameter values in the distant and near bed areas varied as the amount of sand in the bulk bed changed. With the exception of Cluster 1109C, the average and maximum TKE values were lower in the distant flow region than near the bed. As sand content increased, the difference between the average and maximum TKE values also increased, indicating that less energy was transferred from the near bed to distant flow regions as the sand content of the bed increased. This was especially evident for the clusters from the 38% sand bed. Maximum TKE values for the distant flow area decreased 89% and 97% when compared to the near bed flow area around Clusters 1138E and 1138F, respectively. Similar recirculation cells formed at these clusters but remained near the bed surface and did not extend into the outer flow area. The Reynolds stress measurements showed a similarly low amount of momentum transfer from the near bed to distant flow regions. The exceptions were the average values at Clusters 1101A, 1109B, and 1109C; although around Cluster 1109B the range of Reynolds stress values in the distant region was much smaller than for near the

bed. The decrease in momentum transfer away from the bed was greatest for the clusters from the 38% sand bed, matching the findings for energy transfer and conforming to the observation that the recirculation cell was located near the bed and lower in the flow profile than those cells measured around clusters on beds with lower sand contents.

The exception to the general trend of decreasing movement of energy and momentum away from the near bed region with increasing sand bed content was Cluster 1109C. This cluster developed with a distinctive geometry and an abrupt elevation transition. This was not the cluster with the largest relative roughness but its prominence in the flow profile was a likely factor in the increased values of both τ_{Re} and TKE in the distant flow region. The recirculation cell associated with Cluster 1109C remained elevated in the flow profile with the bulk of the cell level with or higher than the cluster crest. This recirculation cell was characterized by an alternating pattern of sweeps and ejections in the quadrant analysis (Figure 5.6.1). Changing the hole size used for the quadrant analysis inverted the dominance of sweeps and ejections, but in both cases, sweeps and ejections were paired throughout the flow profile. There was a second recirculation cell visible on the TKE image (Figure 5.5.5) on the upstream side of the cluster. While this cell may help explain the elevated TKE values in the outer flow region, it was not apparent on the Reynolds stress image. The results around Cluster 1109C indicate that the morphology of a cluster may have a greater impact on the magnitude of the turbulent flow parameters and the transfer of energy and momentum across the flow profile than has been previously reported. However, it cannot provide a full explanation. The morphology of Cluster 1138F had similar characteristics and relative roughness

values as Cluster 1109C, with a distinct peak and cluster keystone. Unlike Cluster 1109C, there was almost no movement of either energy or momentum outward in the flow profile. The recirculation cell that formed at the cluster crest remained in the lower portion of the flow profile, approximately level with or below the cluster crest. The similarities in cluster profile geometries but difference in cluster effect over the flow profile indicate that at high amounts of bed sand content, the influence of the sand content over the turbulent flow profile becomes greater than the influence of the cluster shape. Thus, despite a cluster morphology that at a lower sand content would have impacted turbulent flows over a large portion of the flow depth, a high bulk bed sand content results in a cluster and armored bed situation where the turbulent flows remained primarily within the lower part of the flow profile.

5.8   Conclusion

Clusters form within the structure of the bed surface when a gravel-bed river armors. Because armored river beds are generated from sediment beds of different sand content, and the focus of this study was to evaluate the impact of the clusters formed from beds of varying sand content on the flow field. To do this, we conducted lab experiments where an armor layer was created using sediment beds of 1, 9, 24, and 38% sand content. Every bed surface was mobilized and then armored under the same combination of flow rates and clusters formed without interference as part of the bed surface structure. Flows were measured around clusters from each armored bed surface and over two areas of unclustered armored bed. We collected 3-D flow measurements

following a grid pattern which allowed for calculation of the turbulent parameters, TKE and Reynolds stress across the flow profile and area around each cluster.

The results indicated that for all sediment beds, the presence of a cluster increased the momentum and energy in the flow, as measured by TKE and the τ_{Re} . Where the armored bed areas without clusters were measured, there was limited increase in turbulent parameters. The influence of sand on the armor layer that formed was indicated by a reduction in turbulent parameters as the sand content of the bed increased and the armor ratio decreased.

The clusters impacted their immediate flow area by increasing the Reynolds stress and TKE in the near bed region around each cluster. Flow separated as it passed over a cluster, creating an increase in the turbulent flow properties and formation of a flow recirculation cell with a flow re-attachment point downstream of the cluster. Local flow around the cluster was altered to a different degree depending on the sand content of the bulk bed from which the armor layer and clusters formed. As sand content in the bulk sediment increased, the vertical transfer of momentum and energy showed a general decreasing trend as indicated by the comparison of Reynolds stress and TKE variability and magnitude measured in the near bed and distant flow regions. Variability in TKE and τ_{Re} values for the near bed flow field decreased as the sand content of the bulk bed increased to 24% sand, and the average and maximum TKE values were lower in the distant flow region than near the bed. As sand content increased, the difference between the average and maximum TKE values also increased, indicating that less energy was transferred from the near bed to distant flow regions as the sand content of the bed

increased. This was especially evident for the clusters from the 38% sand bed for which the variability and difference between maximum and average turbulent flow parameters increased near the bed. Recirculation cells formed at these clusters but remained near the bed surface and did not extend into the outer flow area.

Cluster morphology appeared to be as important a factor in the degree of flow alteration as the sand content of the bulk bed. Most of the clusters had a low profile and were composed of a number of near equal size clasts, but some formed with a single, large key clast prominent in the bed profile. Where the clast morphology was of the latter type and the sand content in the bed low, the recirculation cell associated with the cluster remained elevated in the flow profile with the bulk of the cell level with or higher than the cluster crest. A similarly shaped cluster was measured from the 38% sand bed, but in this case the recirculation cell remained below the cluster crest and there was minimal movement of either energy or momentum outward in the flow profile. Thus, at low sand content, the prominence of cluster height increased the vertical advections of energy and momentum, whereas at higher sand content, the effect of cluster morphology on flow energy and momentum transfer between inner and outer flow was dampened.

Chapter 6.

FLOW RATE, SEDIMENT AND BED STABILITY

6.1   Introduction

Bed stability for gravel-bed rivers can be served as a good indicator for in-channel habitat quality (Kaufmann, 1999). A Relative Bed Stability index (RBSI) was defined as the ratio median particle size of the substrate to the diameter of the largest particle the stream could theoretically move at bankfull flow conditions (Kaufmann, 2008):

$$RBSI = \frac{D_{50}}{D_{cbf}}$$

where: $RBSI$ = Relative Bed Stability Index

D_{50} = median grain size for substrate particles

D_{cbf} = critical grain size of transport at bankfull flows

Although the equation illustrate the correlation of bed stability with the sediment material size and flow boundary conditions, it did not consider the armored bed conditions where the surface material is much coarser than the substrate material. Furthermore, the lack of consideration of flow resistance induced by LREs including cluster bedforms and the effect of their size, shape, and spacing on bed stability prohibited the equation application in most gravel-bed rivers where armored bed layers are common.

In previous chapters, the influence of clusters, cluster density, and the bulk sediment sand content on near bed turbulent hydrodynamics were discussed. These effects are limited to a local scale. To better estimate the influence of sediment input on

the downstream river morphology and ecosystem, an improved understanding of the relationship among hydraulics, cluster characteristics, and bed stability over the reach scale is necessary.

The bed stability can also be considered the resistance of the bed surface to flow induced mobility. One of the most widely used parameters to represent this resistance is the Darcy-Weisbach (*ff*) coefficient, detailed in Chapter 3, which is calculated here using the hydraulic radius and double averaged flow velocity.

The flow resistance coefficient *ff* reflects the channel bed roughness which is in turn associated with the structure of the bed surface and influences the measured bedload transport rate at a given flow rate. Shear stresses generated by flow over the bed surface are responsible for sediment movement and are counteracted by the summation of grain and form roughness. That portion of the shear stress associated with grain resistance is responsible for bedload transport (Yalin, 1977, 1992; Richard, 1982). Because the critical shear stress (see Chapter 2 and equation 2.2.3) is the minimum required to initiate sediment motion, this shear stress portion is often quantified as the amount of shear stress in excess of critical.

Bed stability for an armored bed can be determined either qualitatively through the time for the armor layer of the bed surface to mobilize or quantitatively through the magnitude of the ratio of the nondimensional boundary shear stress over the nondimensional reference shear stress. The statistical properties of the topography of an armored gravel bed act as indicators of bed stability and are a function of hydraulic conditions in the channel. As long as the link between the hydraulic variables, bed

topographic statistics, and cluster spatial arrangements is established, a numerical model to predict entire bed stability can be developed. Therefore, the effect of channel conditions -- average flow rate and sediment composition in this case -- on the armored bed roughness and cluster spatial distribution were evaluated by comparing the results of semivariogram analyses of bed surface profiles, linear regression modeling, and through two-way Analysis of Variance (ANOVA). On each armored bed, local cluster density varied more than the total number of clusters in the reach, indicating that when evaluating local bed stability, local cluster density may be more important than the total number of clusters. Thus the local bed stability can be predicted through the cluster density which is also a feedback of flow rate, sediment bedload transport rate, and bed surface geometric properties.

Preceding studies have focused on the formation of surface texture over a range of applied discharge durations (Marion et al., 1997, 2003; Pender et al., 2001; Ockelford et al., 2010). The formation of surface clusters under threshold flow conditions was quantitatively analyzed and studied (Piedra et al., 2012). However, the effects of constant discharge magnitude and sediment grain size distribution on sediment surface topography and overall bed stability have not been fully analyzed. Thus this chapter investigates the response of cluster quantity, overall and local cluster density, and cluster spacing under the influence of alternative discharge and sediment sand proportion.

6.2   Experimental Set-up and Techniques

The flume experiments were conducted as described in Chapter 4 and 5. A series of steady discharges ranging from 0.07 m^3/s to 0.11 m^3/s were applied to four sediment mixtures with different sand proportions (Figure 6.2.1). The coarsest five size fractions of each sediment mixture were manually painted in order to be easily identified by eye from panoramic photos of the bed surface. Each experiment began from an initial bed without any imposed structure. Thus the experimental setting was considered as appropriate to avoid the complexities stemming from the interdependent and multiple environmental variables within a natural river (Piedra et al., 2012).
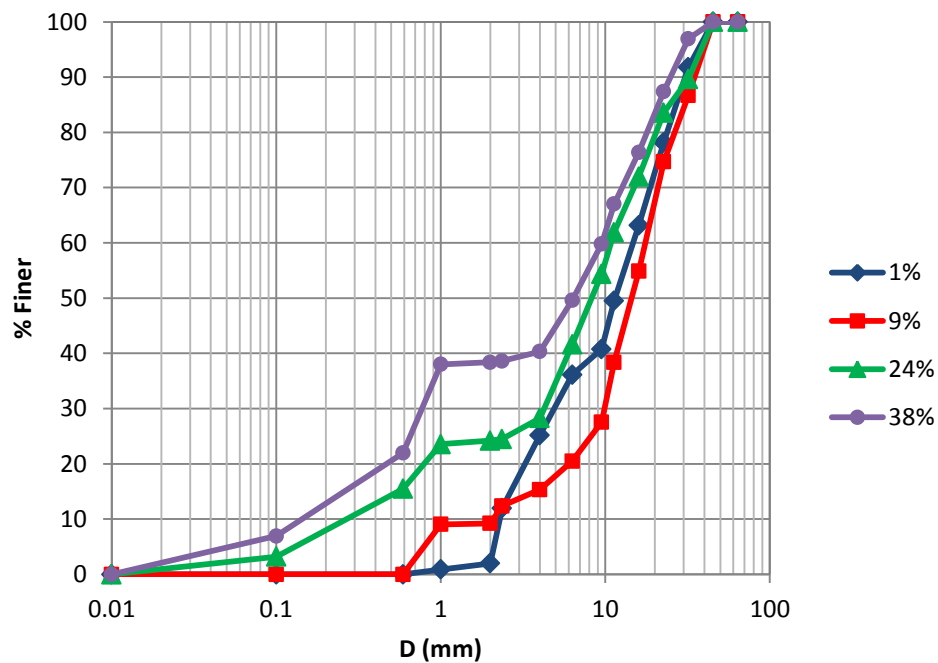
Figure 6.2.1 Grain Size Distribution for sediment mixtures with 10%~ 38% sand fractions

Digital Elevation Models (DEMs) were generated to analyze the spatial distribution of clusters and to enable calculation of elevation statistics for each armored bed surface. A laser profiler was used to scan the downstream 6 meters of the flume, from

downstream to upstream, using a sampling interval of 2 mm. The width of the laser scan was set to 0.0225 m and scans were repeated to the right and left side of the centerline. The two sets of scanned data were combined together and the finalized DEM data were composed of three numerical columns corresponding to the three dimensional coordinates: x, y, and z. Bed elevation data (z-direction data) were extracted from the DEM matrix for detailed statistical analysis. The number and spatial distributions of clusters on each armored surface were determined through the combined use of DEMs and panoramic photographs. The sediment bed was mixed between each experiment to eliminate the possible bias from an initial uneven or well sorted surface. Therefore the locations of clusters and spacing between neighboring clusters were stochastic and independent. The time required for the armored bed to break was recorded for each experiment to qualitatively evaluate the armored bed stability created under each distinct hydraulic and sediment condition.

6.3 Data Analysis

The relations between bed stability and bed surface profile properties were analyzed statistically using experimental semivariograms, linear regression modeling, multiple linear regression modeling, and two-way ANOVA technique. Profile properties analyzed include the surface elevation statistics, characteristic surface roughness, cluster spacing and density, the multivariate effect of flow rate magnitude, and the sediment grain size distribution on the bed topographic properties and cluster spatial distributions.

6.3.1 Statistical Properties of Gravel-bed Profiles

Semivariogram and zero-crossing analysis are common in the analysis of bed surface profile properties and bedform geometrical parameters (Robert, 1988). As a result of irregularity of gravel-bed river bed surfaces, the semivariogram is often used to investigate the fractal properties of bed profiles, obtain the characteristic roughness of each length scale, and provide a basis for zero-crossing analysis of grain and form scale wavelength and amplitudes (Robert 1988, Clifford, et al., 1992). The semivariogram was developed and advocated for the analysis of spatially-dependent random geomorphological variables (Matheron, 1971; Oliver and Webster, 1986, Clifford, et al., 1993). Following Carr (1995), the 2-D semivariance, $\gamma(\Delta s)$, of a vector point elevation $\left(e(x_i, y_i)\right)$ at location i is defined as half of the variance of the increment:

$$[e(x_i + \Delta s, y_i + \Delta s) - e(x_i, y_i)]$$

and is written as:

$$2\gamma(\Delta s) = Var[e(x_i + \Delta s, y_i + \Delta s) - e(x_i, y_i)] = E[e(x_i + \Delta s, y_i + \Delta s) - Z(x_i, y_i)]^2$$

where Δs is the lag distance, and E represents the expected value. The shape of the semivariogram plot describes the spatial dependence between samples Z as a function of the lag distance. The semivariance increases with the lag distance over a distance which represents the "range" of the process, identified as Δs_{max}, to a maximum value, or "sill", after which it remains constant. For gravel-bed rivers, the semivariogram log-log plot (Figure 6.3.1) often presents two distinct linear ranges. The two fractal bands on the semivariogram correspond to a grain roughness scale and a form roughness scale at which cluster bedforms are dominant (Clifford, et al., 1992). The break in slope on the

semivariogram is defined as Δss or the value above which the effect of cluster bedforms on profile roughness becomes dominant.
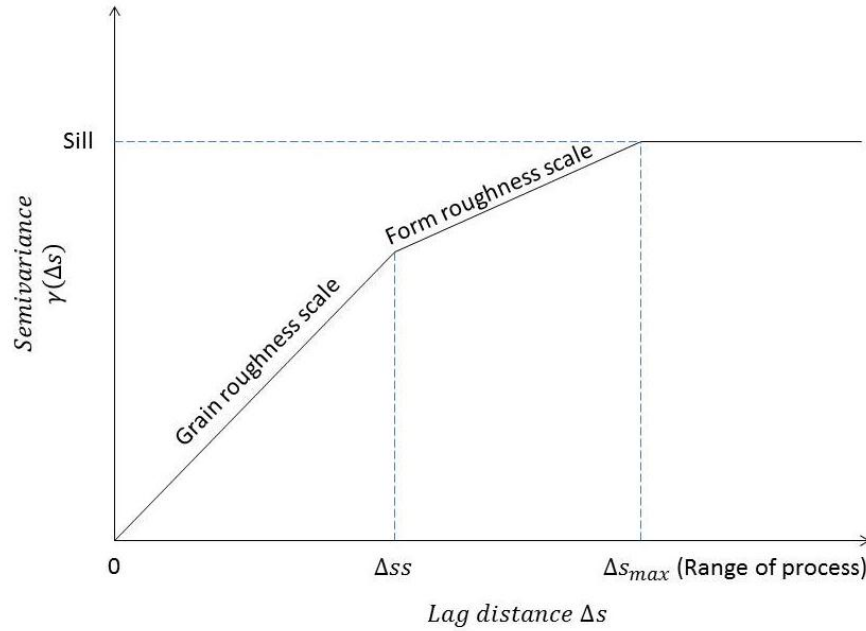
Figure 6.3.1 Schematic representation of fractal properties of sediment bed profiles.

Zero-crossing analysis provides a consistent measure of the amplitude and wavelength of both small scale oscillations and large scale bedforms. The bed elevation trend line is normally represented by a first-order polynomial, and individual LREs are defined between successive up-crossings of the trend line. Frequency distribution histograms of the amplitude and distance between zero-crossings are plotted to distinguish the contributions of smaller scale grain roughness created by very coarse fractions of the bed material and LREs, which correspond with low mode and the low frequency tails respectively (Clifford, et al., 1992).

The mean of maximum height differences associated with measured distances between successive up-crossings within the grain roughness scale ($0 < \Delta s < \Delta ss$), form

roughness scale ($\Delta ss < \Delta s < \Delta s_{max}$), and the total roughness scale ($0 < \Delta s < \Delta s_{max}$) are calculated for grain scale and cluster bedform scale effective roughness length K_g and K_f. The form resistance scale is considered a measure of the effective roughness height of the bed surface when the bed form is dominant on bed surface. Similarly, the mean of measured distances between successive up-crossing within each roughness scale ranges are considered as spacing for the corresponding roughness scales.

6.3.2   Bed Stability vs. Roughness length, Clusters Density, and Cluster Spacing

The flow resistance coefficient *ff* was proved to be only a function of Reynolds number *Re*, and relative roughness, usually expressed as K_s/R, where K_s is equivalent effective boundary roughness and *R* is the hydraulic radius (Moody, 1944). For highly turbulent flow with Re>25,000, the equation for flow resistance is often expressed as:

$$\frac{1}{\sqrt{ff}} = -K_1\log\left(\frac{K_s}{K_2R} + \frac{K_3}{4R\sqrt{ff}}\right) \text{ (Yen, 2002)} \qquad 6.3.1$$

where K_1, K_2, and K_3 are arbitrary coefficients to account for effects generated from channel geometry and other factors. An alternative equation to estimate flow resistance in both natural and flume channels is derived from the semilogarithmic equation describing turbulent flow over a rough, uniform boundary in a channel of finite width (Keulegan, 1938; Burkham and Dawdy, 1976, Hey, 1979):

$$ff = \frac{1}{\left(2.03\ln\left(\frac{aR}{K_s}\right)\right)^2} \qquad 6.3.2$$

Where *a* was defined as the ratio of hydraulic depth to maximum flow depth in order to incorporate the effect of channel shape. The effective roughness in mix-sized

sediment mixture is commonly represented by the larger particle in the bed, such as D_{84} and D_{90} multiplied by a multiplier factor. The particle size larger than median size was deployed to take into account the proportional influence of larger particles on flow resistance (Leopold et al., 1964). Eventually, researcher found the disparity between observed and predicted flow resistance as a result of underestimation of form roughness effects (Jaeggi and Smart, 1982; van Rijn, 1982; Church et al., 1990). The form drag associated with clusters affects significantly the flow resistance in gravel-bed rivers and because the cluster size and spacing are a function of the bed material size, it is reasonable to use multiplier factor of a characteristic grain size (e.g. $3.5D_{84}$) in the definition of effective roughness. According to Clifford et al. (1992), the component of grain resistance can be estimated from:

$$ff' = \frac{8}{\left(5.76\ln\left(\frac{12.27R}{K_g}\right)\right)^2} \qquad\qquad 6.3.3$$

where K_g is approximately equal to $0.4D_{50}$. The form resistance component can be estimated from:

$$ff'' = \frac{4C_d K_f}{\lambda_{cmedian}} \qquad\qquad 6.3.4$$

where C_d is the form drag coefficient. For gravel-bed rivers, the form drag coefficient C_d is the slope of correlation between shear velocity square and reference velocity square:

$$C_d = \left(\frac{u*}{U}\right)^2 \qquad\qquad 6.3.5$$

where u_* is shear velocity calculated from total shear stress, and U is the reference velocity in term of longitudinal double-averaged velocity.

Bed stability during segment 3 of each experiment, when the flow rate over the armored bed was increased, is a function of the flow rate, surface grain size distribution, bed surface roughness, and the spatial arrangement of bedforms including LREs and clusters. In total shear stress partitioning, bed stability is shown to be a function of not only cross-sectional double averaged flow velocity U, hydraulic radius R, but also the bulk sediment median particle size D_{50}, expressed in grain and form roughness (K_g, and K_f), shear velocity u_*, bed slope S, median cluster spacing $\lambda_{cmedian}$, cluster quantity n_c, mean cluster largest particle size d_{sm}, and standard deviation of cluster spacing data $\sigma_{\lambda c}$ (Refer to Chapter 1).

$$Bed\ stability = f\big(U, R, K_g, K_f, S, \lambda_{cmedian}, n_c, d_{sm}, \sigma_{\lambda c}, u_*\big)$$

One measure of bed surface stability is the non-dimensional reference shear stress for surface grain size fractions Ds_i. The critical or reference shear stress for the surface median grain size can be estimated from measured fractional bedload transport rates using the Surface-Based Transport Model developed by Wilcock and Crowe (2003) in its inverse application. Sediment fractional transport rates were directly measured during the armor breaking run segment (segment 3 of each experiment), q_{bi}. The armored bed surface size fractions F_i were measured through pebble counts of the bed surface and these were used for an iterative solution of bed stability through the equations below, where Wi^* is the non-dimensional transport rate of size fraction i:

$$W_i^* = \frac{(s-1)g q_{bi}}{F_i u_*^3} \qquad\qquad 6.3.6$$

$$W_i^* = \begin{cases} 0.002 \left(\dfrac{\tau_b}{\tau_{ri}}\right)^{7.5} & For \; \left(\dfrac{\tau}{\tau_{ri}}\right) < 1.35 \\[2em] 14 \left(1 - \dfrac{0.894}{\left(\dfrac{\tau_b}{\tau_{ri}}\right)^{0.5}}\right)^{4.5} & For \; \left(\dfrac{\tau}{\tau_{ri}}\right) \geq 1.35 \end{cases} \qquad 6.3.7$$

To simplify, the non-dimensional reference shear stresses for size D_{s50} is chosen as an indicator for overall bed stability.

Sediment transport rates q_{b50} for surface median size D_{s50} were roughly estimated from the collected and weighed sediment sample from segment 1 of each run when the bed was in a state of dynamic equilibrium and sediment was actively transported. Sediment size fractions were used to characterize the D_{s50} that were measured through the surface pebble count. For example, for Run 1, the sediment surface median grain size D_{s50} is determined as 21mm which falls in the range of size for green colored sediment, thus the transport rate for D_{s50} can be estimated from the mean around which the green colored sediment transport rate fluctuates.

To determine the relative influence of flow rate and sediment grain size distribution on bed stability, a regression model of the two variables was developed. Because the flume was a constant width, the unit flow rate q was used in place of total discharge. Unit flow rate is the product of cross-sectional double averaged velocity U and flow depth Z. Sediment grain size distributions are characterized by the median surface grain size D_{50}. The median surface grain-size D_{s50} is relatively coarse in the less sandy mixtures and much finer in the sandier mixtures (Figure 6.4.3).
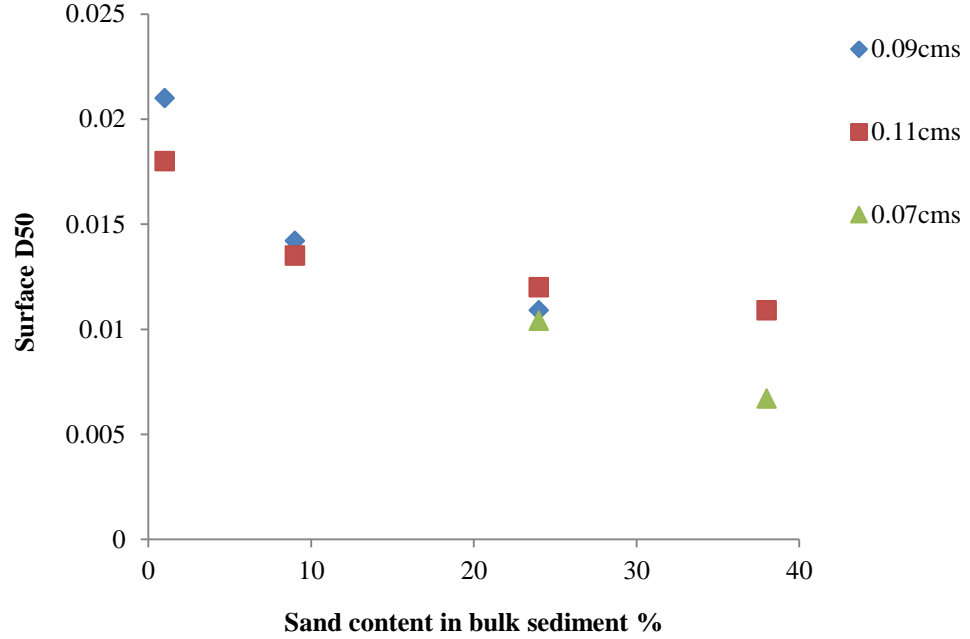
Figure 6.3.2 Surface grain size as a function of bulk sediment sand content under distinct flow rate

Cluster quantity and spacing were measured from the DEMs following the procedures described in Chapter 3. Clusters measured on bed surface for each run were categorized into isolated clusters, coupled clusters and grouped clusters following the threshold defined in Chapter 3 and Chapter 4. The total cluster density ρ_c was calculated as the total cluster quantity n_c divided by the entire bed area A_{bed}. The same procedure was taken for isolated clusters, coupled clusters, and grouped clusters to calculate the cluster densities of isolated clusters, ρ_{Ic} ; coupled clusters, ρ_{Cc} ; and grouped clusters, ρ_{Gc} .

Cluster spacing (λ) was computed manually by drawing lines between downstream neighboring clusters and averaging the distance between pairs of clusters (Strom and Papanicolaou, 2007). A median value of cluster spacing distribution $\lambda_{cmedian}$ was measured and compared for each run with different sand content and flow rate and

compared with the break of slope lag distance (Δss). The reason why we chose a median value for analysis instead of mean value is because the cluster spacing data was not symmetrically distributed. The standard deviation of cluster spacing values for each run was also calculated and compared to interpret the effects of cluster grouping and blank open bed areas. The bed roughness is dominated by bedforms including clusters and LREs. Therefore, the magnitudes of cluster spacing are hypothetically greater than the break of slope lag distance.

Strom and Papanicolaou (2007) found that the cluster spacing λ, which represents the downstream cluster-to-cluster spacing along diagonal lines, decreases with local slope S and increases with the size of the largest particle in the cluster d_{sm}. The grouping of $\lambda_{cmedian} S / d_{sm}$ was found to be consistent for all cluster spacing data. Therefore, the slope was dropped from this function.

The final linear model should describe the effects of grain and form roughness heights, cluster bedform spatial correlation, and the total bed shear stress on bed stability in term of reference shear stress required to mobilize the surface median sized particles.

The flow resistance contributed by grain roughness was discussed in preceding text and therefore, the bed stability in term of reference shear stress should be a function of grain roughness resistance component, $\left[ln\left(\frac{R}{K_g}\right)\right]^{-2}$ and form roughness resistance component; For cluster form resistance component, the cluster bedform spacing parameters should be taken into account including not only the median cluster spacing value listed in Equation 6.3.4, but also cluster density, mean largest grain size of clusters and standard deviation of the cluster spacing. A common sense provided form resistance

parameter, expressed in form of $\frac{n_c d_{cm}\left(\frac{u_*}{U}\right)^2 K_f}{\lambda_{median}\sigma_{\lambda c}}$ was employed to incorporate the effect of form roughness effective height as well as their spatial distribution characteristics. Hypothetically, the bed stability is positively correlated with cluster quantity, drag coefficient, form roughness effective height, and the cluster size in terms of an averaged largest grain size for all the identified clusters; and is inversely correlated with median value and variability of cluster spacing which is associated with the phenomenon of clusters grouping and open bed areas overrepresentation.

The bed resistance was also a function of non-dimensional total shear stress, in a simplified form as $\frac{u_*^2}{gD_{50}}$. That lead us to a hypothetical multi-linear function in form of:

$$\tau^*_{r50} = f\left(\left[ln\left(\frac{R}{K_g}\right)\right]^{-2}, \frac{n_c d_{sm}}{\sigma_{\lambda c}}\frac{\left(\frac{u_*}{U}\right)^2 K_f}{\lambda_{cmedian}}, \frac{u_*^2}{gD_{50}}\right)$$

A multiple linear regression is performed to validate this relationship.

6.3.3 Bed Stability Prediction Model using Two-way ANOVA

Two independent factors were taken into account to determine the optimum bed material composition and flow rate magnitude to create a stable, armored gravel bed channel: Factor 1: bulk sediment sand content; Factor 2: armoring flow rate.

In the course of this study, three responses were measured four levels of factor 1 which are sand content of 1%, 9%, 24% and 38%; and three levels of factor 2 which are flow rate of 0.07m³/s, 0.09m³/s and 0.11m³/s: X1 = relative grain roughness resistance $\left[ln\left(\frac{R}{K_g}\right)\right]^{-2}$; X2 = overall cluster effect term $\frac{n_c d_{sm}}{\sigma_{\lambda c}}\frac{\left(\frac{u_*}{U}\right)^2 K_f}{\lambda_{cmedian}}$; X3 =

dimensionless total shear stress $\frac{u*^2}{gD_{50}}$. Repeated measurements for each response were not feasible because of relative long time period required for each experimental run. The relationship between the responses and the factors were modeled using a two-way ANOVA statistical technique in the SAS program.

6.4   Results

6.4.1   The Bed Properties

A total of 9 runs under different hydraulic conditions were conducted to simulate armored gravel-bed rivers evolution and their DEMs are shown in Figure 6.4.1. For run 1 the laser scanning profiler was designed and made from a simple combination of a laser line emitter and a Basler Scout scA1390-17gc camera. For Runs 2 to Run 9, the DEM was generated using the Micro-Epsilon laser scanner. The topography of bed surface was reflected by the shape of the laser line for each step and the shape of the laser profile was transmitted to series of numerical data which were stacked together to create a DEM. The elevation of the weir at the downstream end of the flume was selected as a fixed arbitrary datum. Elevation data z for each point ranged from -120 to 120 pixels which were converted to -50 to 50 mm by a conversion factor. The conversion factor was determined by a scan test of a wood block attached on top of the weir with a known height which was reflected as pixels of surface elevation difference between the top of the weir and the top of the wood block. DEM resolution for Run 1 and Run 3 is 2mm/step. A total of 3246 profiles were recorded and stitched together to cover the entire bed surface with a length of 6.5m. For the rest of runs, the scanned length was shortened to 6m making a 1m long buffer zone in the upstream end to eliminate the impacts from sediment recirculation.
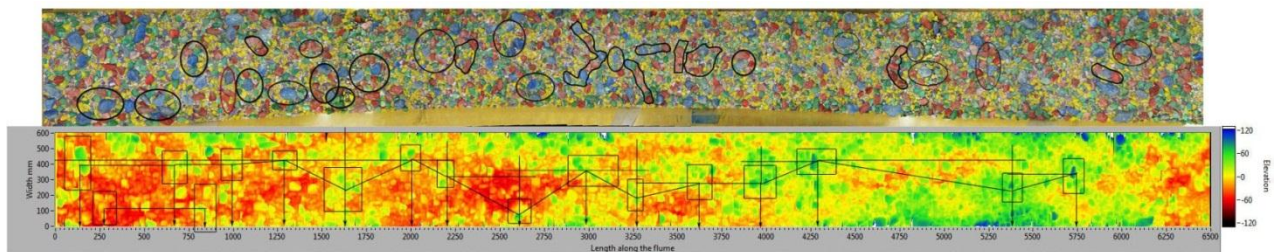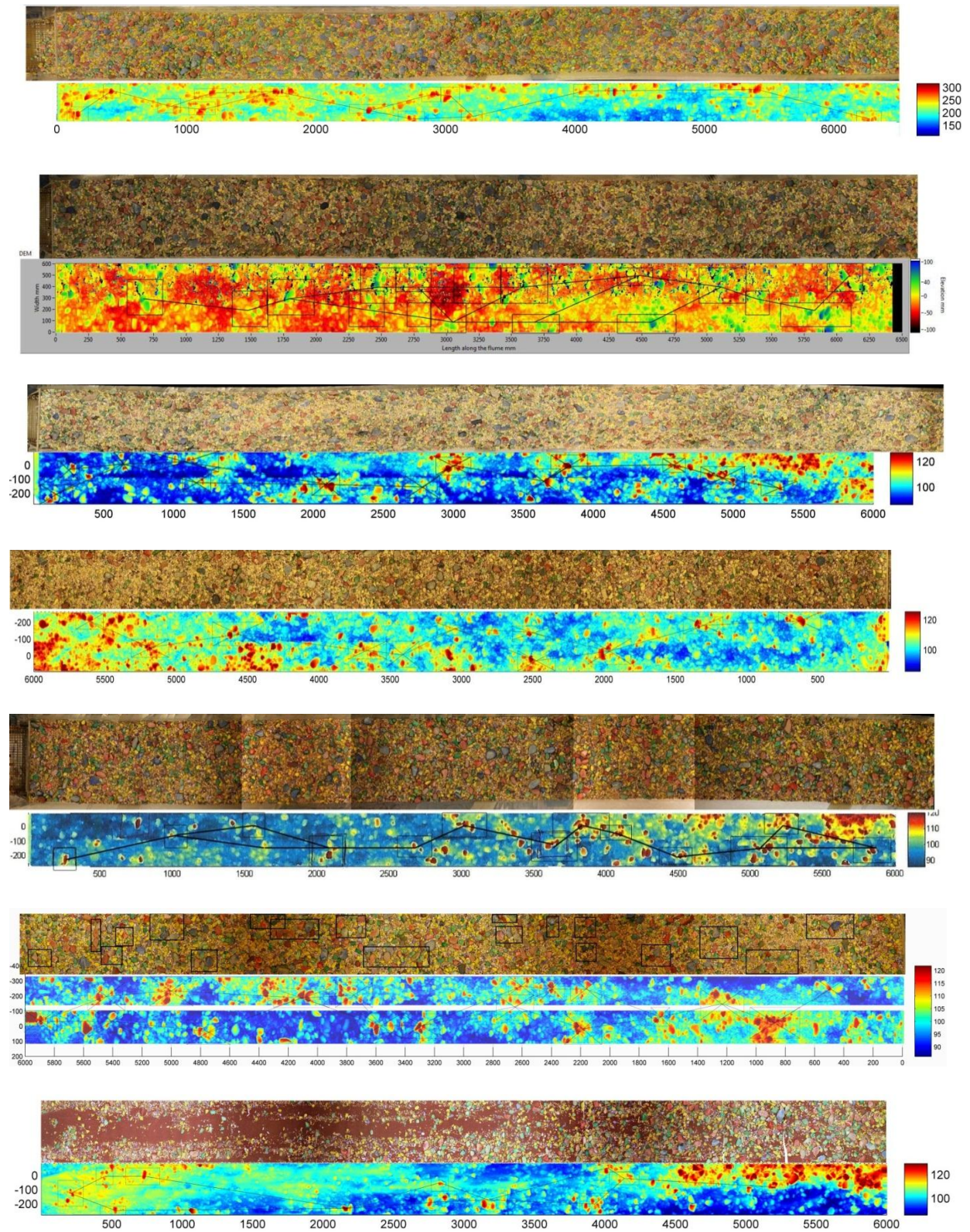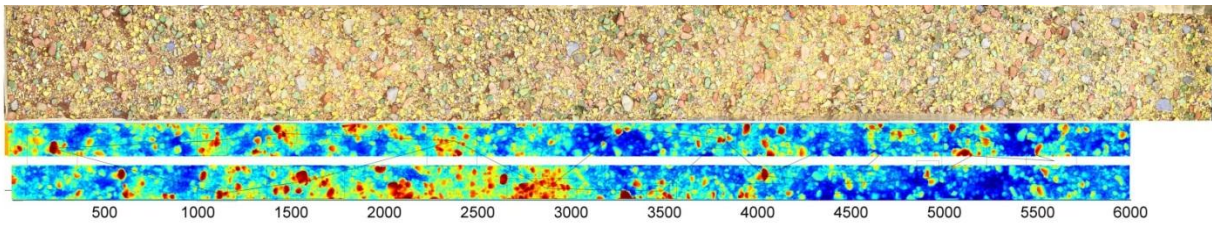
Figure 6.4.1 Surface profiles for Run 1 to Run 9 from top to bottom. Top figures are panoramic photographs of armored bed surfaces for each run. Lower images are DEMs with clusters marked in black boxes and the distances between each adjacent pair of clusters are indicated by the black lines.

A total of 8 Semivariograms are plotted and compared except Run 6, for which the elevation data is accidentally missing. For each semivariogram, the lag distance has a value ranging from 1mm to 1000mm (Figure 6.4.2). The maximum of 1m lag distance was chosen because it has the same magnitude as the entire armored bed length.

1% sand fraction

9% sand fraction

24% sand fraction

38% sand fraction
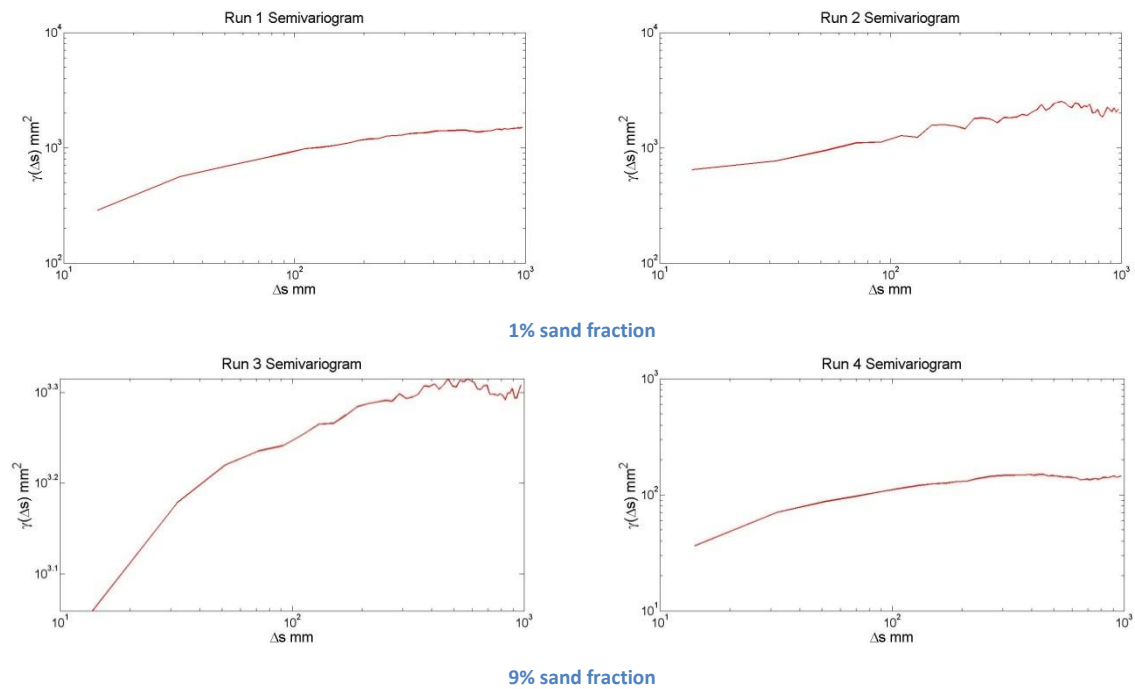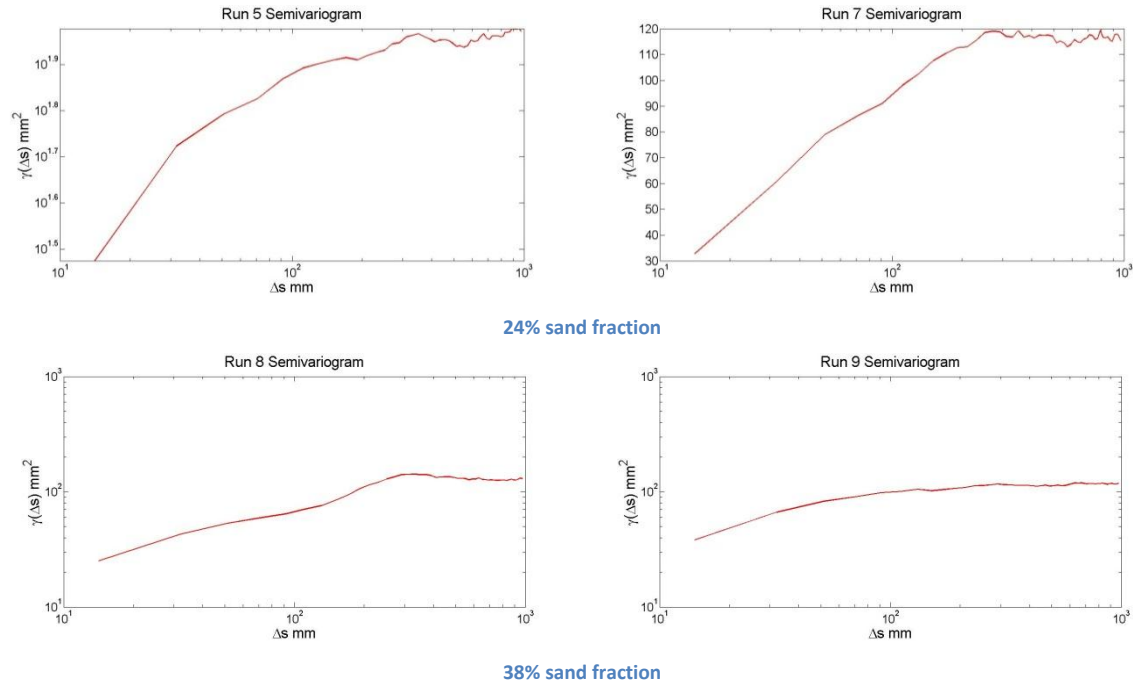
Figure 6.4.2 Semivariograms of armored bed surface profiles for sediment mixtures of different sand content

The break of slope identified in each semivariogram indicates a lag distance Δss, above which the effect of cluster bedforms on profile roughness becomes dominant. The results of Δss for each run are listed in Table 6.4.1. The semivariograms for each experiment excepting Runs 2 and 8 are composed of two fractal bands, which are considered to correspond respectively to a grain scale and to a scale at which cluster bedforms are effective. The semivariograms of Runs 2 and 8 have no identifiable break of slope to distinguish form roughness scale from grain scale. Compared with the actual armored bed surface documented by panoramic photographs, the semivariogram for Run 2 is confirmed to have only a form roughness scale for fractal regression and the semivariogram for Run 8 is dominated by grain roughness scale. The slope difference for the two fractal regressions of each semivariogram become more significant in runs with

sand fraction of 9% and 24% and diminishes for sediment with either higher or lower sand fractions.

Parameters of bed surface profile properties are listed in the Table 6.4.1. The armored ratio is defined as D_{s50}/D_{50} and provides a measure of the degree of armoring for each bed surface. For most of the runs, the armored ratio varies around 1.3 except the armored surface for Run 8, which was created with 38% sand fraction under the flow rate of 0.07m^3/s. When the armoring flow rate was equal to 0.035 m^3/s (Run 5 and 8), the armored bed slope decreased from 0.0099 to 0.007. When the armoring flow rate increased to 0.045m^3/s (Run 1, 3, and 6), the armored bed slope decreased from 0.0196 to 0.015 to 0.011; When the armoring flow rate was equal to 0.055m^3/s, the armored bed slope decreased slightly from 0.0134 to 0.012. The armored bed experienced degradation as a result of increasing sand content and reduction in sediment material size. The result verified the finding concluded by Galay (1983).

As the flow rate increases from 0.07 m^3/s to 0.11 m^3/s from Run 5 through Run 7, the break of slope and the maximum value of form roughness scale range increases from 31mm to 35mm, and 250mm to 300mm, respectively. Effective roughness lengths for grain scale and form scale (K_g, K_f) are found in the semivariograms. Effective roughness lengths (K_g, K_f) decrease as the sand fraction increases.

For coarser sediment mixtures (Runs 1, 2, 3, and 4), the quantity of clusters created under higher flow is fewer than that created under lower flow. For sediment mixtures with higher sand content (above 24%), the cluster quantity on armored surfaces created by higher flows is greater than for those created under low flows. Isolated clusters

dominate all bed surfaces compared to the other two cluster arrangements. The amount of isolated clusters follows the same trend as that of total clusters. The averaged isolated cluster quantity is a constant value around 12 regardless of the change in sand content. The amount of grouped clusters decreased from an averaged value of 2.5 for 1% sand sediment and 3 for 9% sand sediment to 1 for 24% sand sediment and 1.5 for 38% sand sediment. However, the numbers of grouped clusters increased from 0.5 for 1% sand to 1.5 for 38% sand.

The clusters spacing distances were measured using Photoshop software. The data of the spacing values are listed in appendix. Table 6.4.2 shows the statistics of cluster spatial distribution and Figure 6.4.3 is the boxplot for cluster spacing for all the flume runs. The mean cluster spacing λ_{cm} was generally reduced as the flow rate increased for each sediment mixture except Run 1 and Run 2. The median cluster spacing values λ_{median} as exhibited in Figure 6.4.3, represented two opposite trends: increase for coarse sediment armored bed (Run 1 through 4) and decrease for sandy sediment armored bed (Run 5 through 9). The standard deviations of the cluster spacing $\sigma_{\lambda c}$ were also listed and depicted in Table 6.4.2 and Figure 6.4.3, respectively. The variability of cluster spacing values for sediment with less sand content (1% and 9%) increased with flow rate. For 24% sand sediment armored bed, the cluster spacing standard deviation is almost constant without changing with flow rate. Although comparing the last two runs which have 38% sand content, the variability of cluster spacing on armored bed decreased when flow rate increased.

Run	1	2	3	4	5	6	7	8	9
Sand Fraction	1%		9%			24%		38%	
$Q_a\ m^3/s$	0.045	0.055	0.045	0.055	0.035	0.045	0.055	0.035	0.055
$D_{s50}\ mm$	14.8	15.1	14.2	13.5	10.4	10.9	14	4.4	11.6
$D_{50}\ mm$	11.5	11.5	14.6	14.6	8.4	8.4	8.4	6.4	6.4
armor ratio	1.29	1.31	1.26	1.19	1.24	1.30	1.67	0.46	1.22
S	0.0196	0.0134	0.015	0.0118	0.0099	0.0109	0.0119	0.007	0.0121
$R\ m$	0.136	0.136	0.136	0.104	0.075	0.104	0.086	0.075	0.104
$U\ m/s$	0.3000	0.3667	0.3000	0.6111	0.5833	0.4688	0.7639	0.5833	0.5729
$\Delta ss\ mm$	30	--	31	31	31	--	35	--	30
$K_g\ mm$	4.81	4.2	6.8	5.1	4.6	--	5.6	3.7	4.9
$K_f\ mm$	9.0	9.3	10.1	8.7	6.9	--	8	7.3	7.0
K_g/D_{50}	0.42	0.37	0.60	0.45	0.55		0.67	0.58	0.77
n_c	17	14	17	13	11	14	17	13	18
Measured Cluster quantity Nc	1	3	2	3	3	1	3	2	2
$\rho_{Ic}\ /m^2$	4.44	4.10	4.86	3.33	3.70	4.44	5.19	4.07	4.81
$\rho_{Cc}\ /m^2$	1.37	0.34	0.69	1.48	0.37	0.37	0.37	0.00	1.11
$\rho_{Gc}\ /m^2$	0.00	0.34	0.35	0.00	0.00	0.37	0.74	0.74	0.37
$\rho_c\ /m^2$	5.81	4.79	5.90	4.81	4.07	5.19	6.30	4.81	6.67

Table 6.4.1 Parameters of bed surface profile properties

Variable	Mean λ_{cm}	Median λ_{medain}	StDev $\sigma_{\lambda c}$	Minimum	Maximum	Qt1	Qt3
Run1	403.4	355.3	197.7	241.6	1080.3	299.9	442
Run2	580.1	484.2	333.5	132.6	1350.1	342.2	879.3
Run3	529.8	458.9	227.7	192.2	904.5	360	636.4
Run4	504.8	435.9	268.8	177.6	1015.3	269.4	707.4
Run5	568.2	554.6	170.4	252.8	917.8	460.7	672.5
Run6	522.4	549.3	184.1	219.2	797	374.6	635.5
Run7	485.2	493.4	176.7	220.9	891.4	323.5	612.8
Run8	615	378	464	142	1635	283	830
Run9	520.9	486.1	226.6	170.1	953.9	349.5	614.2

Table 6.4.2 Cluster spacing statistics for each flume test. *Qt1* and *Qt3* represent the upper and lower quartiles.
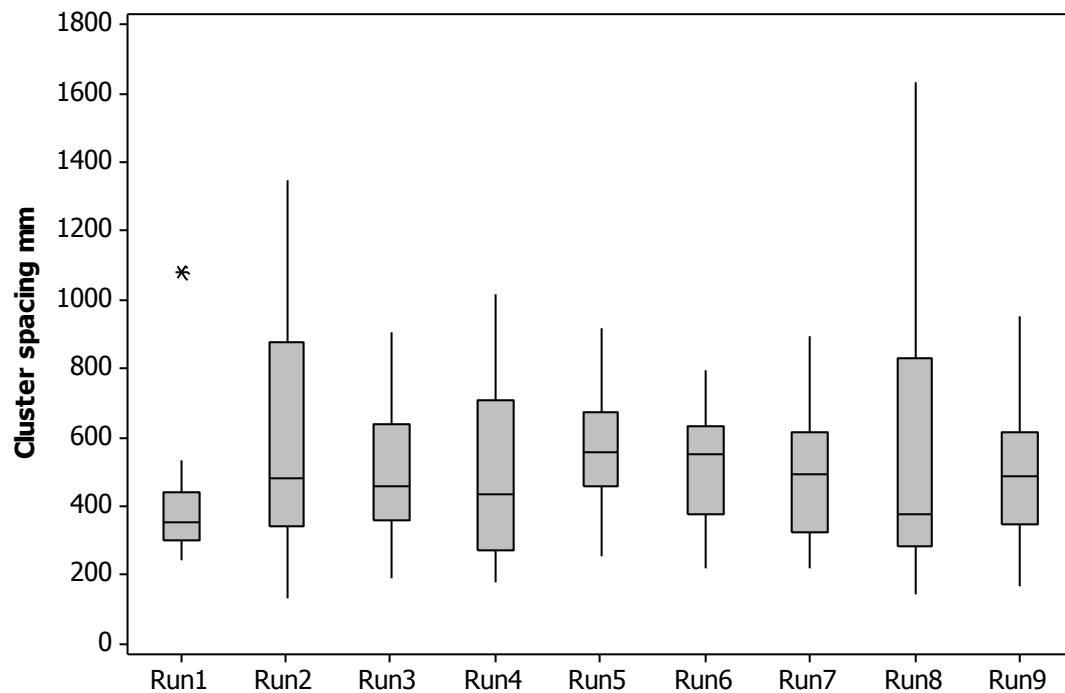
Figure 6.4.3 Boxplot of the cluster spacing data for each flume test

6.4.2 Bed Stability Evaluation

Armored bed stabilities are intuitively evaluated through the time required for the armored bed surface to become fully mobile under the flow rate that was used in Segment 1 that created an equilibrium transport condition of the same sediment. This was the third segment of each experiment. Sediment transport rates for D_{s50} size fraction are recorded and plotted against time at a time interval of 5 minutes (See Appendix I). Results of this comparison (Figure 6.4.4) illustrate that the time required to break the armored surface decreases with an increase of sand content in bulk sediment from 1% to 24%, regardless of the flow rate magnitude. However, the armored bed stability increases as the sand content increases from 24% to 38%, as indicated by slightly longer durations before armored bed breaks under the same discharge. For sediment with the same grain size distribution, the armored bed becomes more stable with higher flow rates and the time required for the previous equilibrium flow rate to destroy the armored bed surface decreases.

	1%	9%	24%	38%
■ 0.07cms			45	60
■ 0.09cms	155	60	22	
■ 0.11cms	80	55	25	45
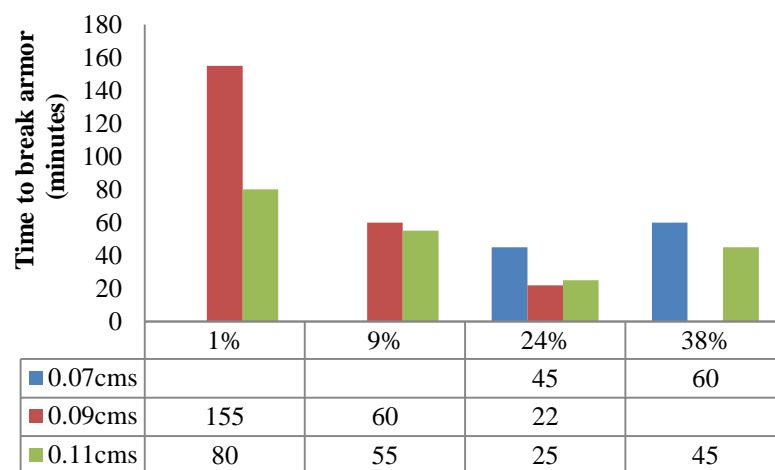
Figure 6.4.4 Comparison of time required for armored bed to break for sediment mixtures with 1% to 38% sand content under flow rate ranging from 0.07 to 0.11 m^3/s

This finding is further quantitatively confirmed and adjusted by results of use of non-dimensional reference shear stresses τ^*_{r50} for size D_{s50} as an indicator for overall bed stability. Measurements of the sediment transport rate q_{s50} for the median surface grain size D_{s50} and the calculated non-dimensional reference shear stress τ^*_{r50} are listed in Table 6.4.2. The fractions of particles of size D_{s50} on the bed surface are visually determined by the modified Wolman Pebble Count procedure (Wolman 1954). The non-dimensional reference shear stress for D_{s50} was calculated in two methods: from the sediment transport rate of size D_{s50} (identified here as $\tau^*_{r50}a$) and from the curve fitting equation (identified here as $\tau^*_{r50}b$):

$$\tau^*_{r50}a = \frac{\tau_{r50}}{(s-1)gD_{s50}}$$
6.4.1

$$\tau^*_{r50}b = 0.021 + 0.015\exp[-20F_s]$$
6.4.2

where D_{s50} is the fraction of particles of the median size on the bed surface and F_s is the sand fraction on bed surface, both determined through a modified Wolman Pebble Count (Wolman 1954). For low sand content sediments, the sand fraction on surface is as low as 0.5%. For bulk sediment with 38% sand content, the surface sand percentage is 34% for armored bed created under the flow rate of 0.07m³/s and 5% for armored bed created under the flow rate of 0.11m³/s.

Run	1	2	3	4	5	6	7	8	9
$Q\ (m^3/s)$	0.09	0.11	0.9	0.11	0.07	0.9	0.11	0.07	0.11
S	0.0196	0.0134	0.015	0.0118	0.0099	0.0109	0.0119	0.007	0.0121
$U\ m/s$	0.3000	0.3667	0.3000	0.6111	0.5833	0.4688	0.7639	0.5833	0.5729
$D_{s50}\ mm$	14.8	15.1	14.2	13.5	10.4	10.9	14	4.4	11.6
$q_{50}\ (g/m\text{-}s)$	0.21	0.74	0.35	0.45	0.37	1.2	1.55	0.6	1.5
$F_{50}\ \%$	0.22	0.18	16.1	18.3	17.5	17	22.2	6.1	16.3
$\tau*_{rs50}a$	0.236	0.227	0.263	0.123	0.039	0.072	0.054	0.072	0.070
$\tau*_{rs50}b$	0.035	0.035	0.035	0.035	0.034	0.035	0.035	0.021	0.027
n_c	17	14	17	13	11	14	17	13	18
d_{sm}	39.6	42	41.2	34.5	21.6	34.5	19.2	29.92	37.4
$\dfrac{\lambda_{median}S}{d_{sm}}$	0.20	0.19	0.19	0.17	0.26	0.17	0.15	0.14	0.17
$\left[ln\left(\dfrac{R}{K_g}\right)\right]^{-2}$	12.71	11.77	15.30	15.15	16.94		17.44	15.20	14.84
C_d*K_f/λ_{median}	0.0142	0.0045	0.0063	0.0009	0.0004	0.0000	0.0004	0.0004	0.0010
$n_c*d_{sm}/\sigma_{\lambda c}$	3.227	2.846	2.867	1.880	1.394	2.623	2.059	0.838	3.017
$\dfrac{(u^*)^2}{gD_{50}}\times 10^{-04}$	4.25	2.90	3.33	1.57	1.19	2.08	1.69	1.10	3.03
C_d	0.533	0.244	0.410	0.047	0.029	0.078	0.024	0.020	0.058

Table 6.4.3 Parameters for bed stability calculation and measured response variables for bed stability function

	1%	9%	24%	38%
■ 0.07cms			0.05	0.03
■ 0.09cms	0.24	0.16	0.07	
■ 0.11cms	0.12	0.07	0.04	0.08
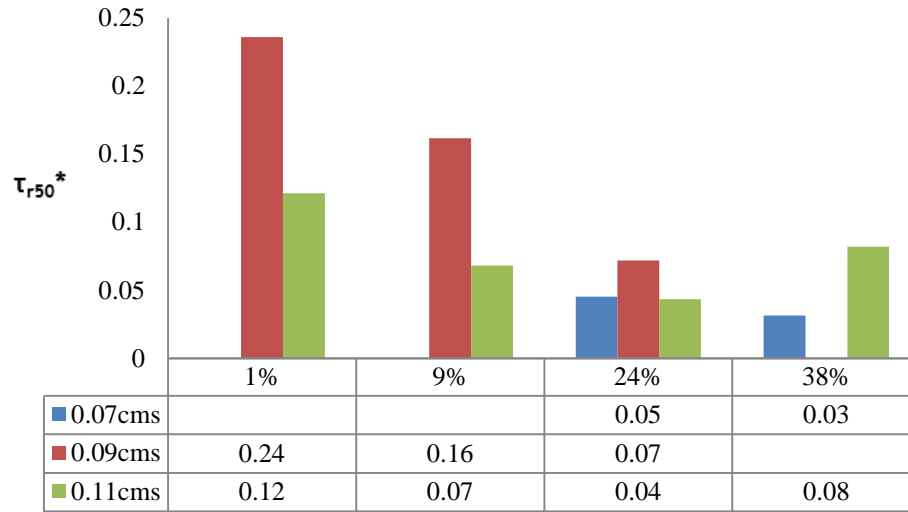
Figure 6.4.5 Bed stability in term of non-dimensional reference shear stress for D_{s50} for armored surface for sediment mixtures of different sand content under different flow rate

Figure 6.4.5 partially confirmed and further corrected the estimation of bed stability by comparing two calculations of the reference shear stress required for armored bed to break. Overall, the bed stability for coarse sediment is greater than the finer sediment. The reference shear stress for size D_{s50} decreases as the bulk sediment becomes sandier. For coarse sediment, the increase in bed stability can be assessed by the difference of $\tau^*_{r50}a$ and $\tau^*_{r50}b$. The reference shear stress of size D_{s50} yielded from inverse calculation is dramatically increased, reaching a higher value of 5-fold magnitude when compared to the value of 0.035 for minimal sand content.

To establish a multiple linear regression function for bed stability as a response to predictor variables, the fundamental simple one-predictor linear regression functions are first generated (Figure 6.4.6).
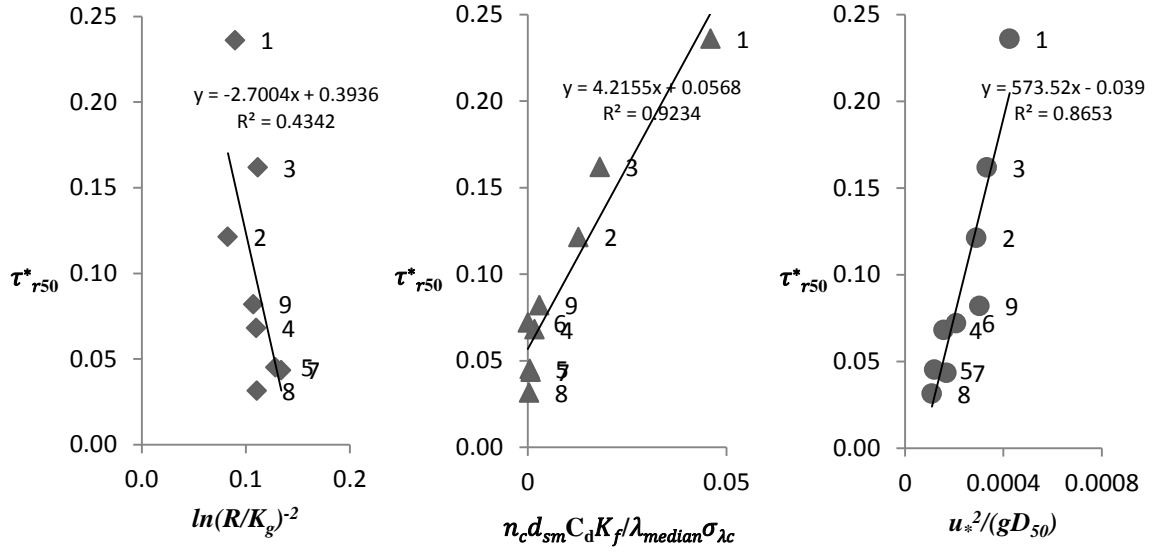
Figure 6.4.6 Linear regressions correlation of τ^*_{r50} with a) $ln(R/K_g)^{-2}$; b) $n_c d_{sm} C_d K_f / \lambda_{median} \sigma_{\lambda c}$; c) $u_*^2/(gD_{50})$;

Figure 6.4.6 shows the first order linear regression modeling for dimensionless reference shear stress and each of the three individual independent predictors. Data from measurements are well fitted into the linear regression models. Figure 6.4.6a shows a proportional linear correlation between τ^*_{r50} and grain resistance $\left[ln\left(\frac{R}{K_g}\right)\right]^{-2}$, form

roughness induced resistance $\frac{n_c d_{sm}\left(\frac{u_*}{U}\right)^2 K_f}{\lambda_{cmedian}\sigma_{\lambda c}}$ and bed boundary shear stress $\frac{u_*^2}{gD_{50}}$, which

means the bed stability increases with the non-dimensional relative grain roughness as well as the form roughness. The bed stability or resistance is also a function of cluster spatial distribution, whereby the bed stability is positively correlated with the number of clusters and size of clusters, whereas negatively correlated with median cluster spacing and variation of the cluster spacing data.

Recalling that the bed slope S is also a positive function of d_{sm}/λ_{median}, and bed stability is also potentially a linear proportional function with bed slope. The linear regression models for reference shear stress against grain resistance, form drag associated with cluster bedforms and total shear stress exhibit strong correlations, which imply a positive effect by flow conditions on armored bed stability. A further comparison is conducted in section 6.4.3 through two-way ANOVA modeling.

A first-order multiple regression model with three independent predictor variables is designed as:

$$Y = \beta_0 + \beta_1 X1 + \beta_2 X2 + \beta_3 X3$$

Where $Y = \tau^*_{r50}$; $X1 = \left[ln\left(\frac{R}{K_g}\right) \right]^{-2}$; $X2 = \frac{n_c d_{sm}\left(\frac{u_*}{U}\right)^2 K_f}{\lambda_{cmedian}\sigma_{\lambda c}}$; $X3 = \frac{u*^2}{g D_{50}}$.

This response function is a hyperplanes, which is in more than two dimensions. The parameter β_k indicates the change in the mean response of τ^*_{r50} with a unit increase in the corresponding predictor, when all other predictor variables in the regression model are held constant.

$Y=\tau^{*}{}_{r50}$	$X1=\left[ln\left(\dfrac{R}{K_g}\right)\right]^{-2}$	$X2=\dfrac{n_c d_{sm}\left(\frac{u_*}{U}\right)^2 K_f}{\lambda_{cmedian}\sigma_{\lambda c}}$	$X3=\dfrac{u_*^2}{gD_{50}}$
0.236	0.090	0.045976	0.00042513
0.1213	0.083	0.012745	0.000290396
0.1618	0.111	0.018171	0.000332549
0.0681	0.110	0.00171	0.000157181
0.0452	0.128	0.000521	0.000118938
0.072	.	0	0.000208254
0.0435	0.134	0.000777	0.000168972
0.0315	0.110	0.000323	0.000109725
0.082	0.107	0.002916	0.000303326

Analysis of Variance					
Source	**DF**	**Sum of Squares**	**Mean Square**	**F Value**	**Pr > F**
Model	3	0.034071	0.011357	49.77	0.001
Root MSE			0.0152	**R-Square**	0.974
Dependent Mean			0.09544	**Adj R-Sq**	0.954

Parameter Estimates					
Variable	**DF**	**Parameter Estimate**	**Standard Error**	**t Value**	**Pr > |t|**
Intercept	1	0.009	0.05	0.28	0.797
x1	1	0.043	0.8114	0.05	0.961
x2	1	2.79	0.6996	3.99	0.016
x3	1	242	99.23	2.44	0.071

Table 6.4.4 Data for Multi-linear regression model and modeling results from MINITAB linear regression

The final regression model fitted is:

$$\tau^{*}{}_{r50} = 0.009 + 0.043\left[ln\left(\frac{R}{K_g}\right)\right]^{-2} + 2.79\frac{n_c d_{sm} C_d K_f}{\lambda_{cmedian}\sigma_{\lambda c}} + 242\frac{u_*^2}{gD_{50}}$$

Overall the multi-linear model is valid with a P-value of 0.001 (Table 6.4.4), which means the probability of Type I error is 0.1% for linear prediction of bed stability

from linear combination of grain roughness resistance, form roughness resistance and total shear stress. In another word, the probability to accurately predict bed resistance using this linear model is 99.9%. However, when look at the P value for estimator of X1 (grain roughness resistance term) is above 0.95. That means the probability of Type I error for estimation bed stability is 95% when we only take grain roughness resistance into account. The result of higher P-value for coefficient of grain roughness resistance term implies for all the flume tests that were conducted in my research, the grain roughness resistance is negligible for the estimation of the total bed resistance. The most important component of bed resistance is contributed by the cluster form drag as well as the clusters spatial distribution characteristics. The bed stability is more sensitive to the effect from cluster form roughness geometry and spatial distribution than to the influence of total straight shear stress.

6.4.3 Bed Stability Prediction Model using ANOVA

The data for two-way ANOVA to establish the function of bed stability predictors with respect to factors of sediment sand content (Factor 1) and flow rate magnitude (Factor 2) are displayed in Table 6.4.5

$X1 = relative\ grain\ roughness\ resistance\ \left[ln\left(\frac{R}{K_g}\right)\right]^{-2};$				
$X2 = overall\ cluster\ form\ resistance\ \frac{n_c d_{sm}\left(\frac{u_*}{U}\right)^2 K_f}{\lambda_{cmedian}\sigma_{\lambda c}};\ X3 = dimensionless\ shear\ stress\ \frac{u_*^2}{gD_{50}};$				
Run	Factor 1	Factor 2	X1	X2	X3
1	1%	0.09	0.079	0.045976	0.000425
2	1%	0.11	0.085	0.012745	0.00029
3	9%	0.09	0.065	0.018171	0.000333
4	9%	0.11	0.066	0.00171	0.000157
5	24%	0.07	0.059	0.000521	0.000119
6	24%	0.09	.	0	0.000208
7	24%	0.11	0.057	0.000777	0.000169
8	38%	0.07	0.066	0.000323	0.00011
9	38%	0.11	0.067	0.002916	0.000303

Table 6.4.5 Data for ANOVA; the X1 data for run6 is missing and marked in dot.

$X1 = \left[ln\left(\frac{R}{K_g}\right)\right]^{-2}$					
Source	DF	Type III SS	Mean Square	F Value	Pr > F
factor1	3	0.00052675	0.00017558	41.31	0.0237
factor2	2	0.00001250	0.00000625	1.47	0.4048
$X2=\frac{n_c d_{sm}\left(\frac{u_*}{U}\right)^2 K_f}{\lambda_{cmedian}\sigma_{\lambda c}}$					
Source	DF	Type III SS	Mean Square	F Value	Pr > F
factor1	3	0.00084311	0.00028104	2.62	0.2247
factor2	2	0.00036987	0.00018493	1.73	0.3170
$X3=\frac{u_*^2}{gD_{50}}$					
Source	DF	Type III SS	Mean Square	F Value	Pr > F
factor1	3	2.7849423E-8	9.2831408E-9	2.00	0.2919
factor2	2	3.3272563E-8	1.6636281E-8	3.58	0.1603

Table 6.4.6 The data for Two-way ANOVA model, and modeling result from SAS programming

The two-way ANOVA model analyzed the individual correlation of each of the three independent measurements with respect to factors 1 and 2 (Table 6.4.6). The p-values are indicators of the influence for factor 1 and factor 2. For each response (X1, X2, and X3), the null hypothesis is that there is no correlation between each factor to the specific response value. The smaller the P value, the more strongly the test rejects the null hypothesis, that is, the non-correlation hypothesis. That is to say, for a certain preset confidence interval, the smaller P-value indicates a higher correlation. For our research, we set the confidence interval to 90%, which means if $P > 0.1$, the particular factor has barely any effects on the particular response parameter.

By comparing the p-values, it is found the factor 1, which is sediment sand content, has a more significant effect on $\left[ln\left(\frac{R}{K_g}\right)\right]^{-2}$ compared to effects on other two measurements. For form roughness resistance, both factor 1 and factor 2 have p-values larger than 0.1, which mean cluster roughness height as well as their spatial distribution pattern is not affected by either sediment sand content (factor 1) or flow rate (factor 2). Compared to sand content, the flow rate exhibits stronger correlation with bed stability by affecting the total shear stress exerting on bed surface. However, the fact of $P>0.1$ still cannot provide enough confidence to reject the null hypothesis. That is to say the flow rate has relatively stronger but still very limited influence on total shear stress compared to the effects from sand content variation.

6.5   Discussion

An increase in overall bed resistance has been documented as an increased time to entrainment of the grains comprising the cluster (De Jong 1991; Iseya and Ikeda 1987).

However, the empirical sediment sampling and data collection may be a potential source of error for bed stability assessment. Although the time record for armored bed breaking process provides a rough estimate of bed resistance, it can be considered only as qualitative evidence as it is difficult to accurately determine the breaking point of the armored bed or decide the moment of sediment incipient motion. Thus, the armored bed stability is also estimated through comparison of the time required for the fractional transport rate of the D_{50} sediment size to reach the corresponding equilibrium fractional transport rate measured before the surface was armored. The reference shear stress is then calculated to verify this estimate. The comparison of Figure 6.4.4 and Figure 6.4.5 indicates that the time method underestimates the bed stability for Run 3 and Run 4 and overestimates for Runs 1, 5 and 7.

The ability of a stream flow to mobilize sediment of a given size is quantified by the dimensionless critical or reference shear stress (also known as Shields number) exerted by the flow on the bed. While commonly estimated as $\tau_{cr}{}^{*} \approx 0.045$ for D_{s50}, for bed surface with minimal sand fraction the dimensionless reference shear stress can be as low as 0.035 (Wilcock and Crowe, 2003). These experiments showed that the reference shear stress for the D_{s50} particle of size from Runs 1 through 4, which had a low sand content in the bulk sediment, increased by 4~5 times the value computed from the $\tau^{*}{}_{r50} \sim F_s$ fitting curve equation. The increase in stability for Run 1 to Run 4 may be partly attributed to a coaction of high form roughness height, the hiding effect, and relatively large gravel sizes. The flow force exerted on large roughness element is greater

than that on fine sediment, but not necessarily high enough to entrain the intrinsically heavier large particles.

Clusters form within the structure of the bed surface when a gravel-bed river armors. The presence of large roughness elements such as cluster bedforms increase the bed resistance by enhancing the threshold shear stress that is required to mobilize particles within the armored surface structure (Brayshaw 1984; Canovaro et al. 2007). The three criteria, listed in order of priority, used to identify clusters for this study are:

1.   Mean elevation of the potential clusters must be above the mean elevation of the entire bed;

2.   A potential cluster must be composed by a key clast accompanied by two or more than two aggregates around it with the same or smaller grain size;

3.   A potential cluster must have a stoss and a wake component. The wake area of the potential cluster should be characterized by finer grains or small gravels, while in the stoss, the relatively large small gravels compared with that of wake side should lean against the key clast.

Similarly, to calculate the mean cluster spacing, there are also three rules in order of priority to connect the downstream neighboring clusters:

1. $\Delta x > \Delta y$, which means $\lambda cos\theta > \lambda sin\theta$ where θ is the angle formed by the line connecting the two clusters with respect to flow direction.

2.   Connect the target cluster to the closest downstream neighboring cluster. There should be no crossing for connecting lines.

3.   The cluster of interest must be connected to the closest upstream cluster. There should be at least two connecting lines start or end at each cluster, except the ones in upstream and downstream ends.

Clusters were identified and cluster spacing calculated for all the clusters formed on each of the experimental armored bed surfaces. The analysis in this chapter has focused on quantifying how much the bed stability is altered by the presence of an armor layer and clusters of different densities.

The statistics of the occurrences for each type of clusters of different densities assist to explain the reason why armored beds were divided into two types according to their bed stabilities and cluster densities. Figure 6.4.5 shows the difference of bed reference shear stress for these two groups of runs. The bed stability magnitude for coarse sediment armored bed is about 5-fold the scale higher than fine sediment armored bed. The boxplot showed in result section shows the opposite trends of cluster median spacing on coarse sediment armored bed and fine sediment armored bed. The standard deviation for coarse sediment increase with flow rate and reversed for fine sediment. Overall, the variability of cluster spacing distances tends to decrease when sand content increase from 1% to 24% and the variability increase when sand content increase from 24% to 38%. Coupled clusters were more effective on armored bed created in coarse sediment (1% and 9%), compared to sandier sediment.

The cluster spatial distribution on armored bed surfaces for coarse and fine sediment also behaved differently. The grouped cluster quantity on armored bed surface created in 38% sand sediment was highest. The standard deviation for clusters spacing

(variability) also reached its highest value of 464mm for Run8 with 38% sand content under a flow rate of 0.035m^3/s. Coincidently, armored bed created in Run 8 had the lowest reference shear stress and bed stability. This can be explained as a result of increased presentation of grouped clusters and large open bed areas without any types of clusters, even the median and mean cluster spacing was almost constant for each run. The reference shear stress decreases with an increasing sand content in bulk sediment as shown in Figure 6.5.1a. It complied with the fact that the amount of sand in bulk sediment directly impacts the overall transport rate (Wilcock and Crowe, 2003). This correlation is also verified in the Two-way ANOVA test. Figure 6.5.1b shows the inverse linear relationship between the bed resistance and total sediment transport rate. Increased sediment bedload transport rate fulfilled by incremental sand content, enhanced the probability of clusters to move downstream (Figure 6.4.1 Run 8) to form grouped cluster patches. With a constant overall cluster density non-correlated to sand contend change, the grouping of clusters would left long blank open bed areas without clusters for sandy armored bed. The local resistance for armored bed areas where the grouped clusters were effective was enhance by the presentation of reticulated grouped clusters, the form drag dominated the total shear stress whereby skin frictions were degraded. However, the overall armored bed stability was deteriorated by overrepresentations of large blank open bed areas without clusters where skin frictions were dominant and reference shear stress for sediment motion become lower.
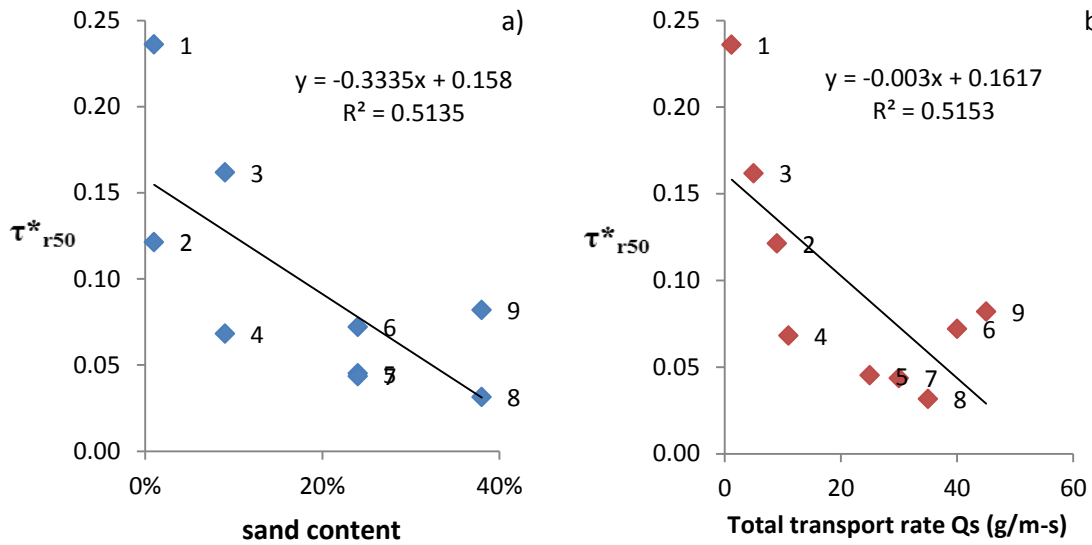
Figure 6.5.1 Linear regression of bed resistance vs. a) sand content, b) Total transport rate Qs. (Run indices are labeled)

The armored bed experienced degradation as a result of increasing sand content and reduction in both effective roughness and uniformity of cluster spatial distribution. Reduced bed stability as sand content increased can also be correlated to the decrease of momentum and energy resistance. The momentum and energy resistance slopes are positively correlated with total shear stress for which the turbulent shear stress (Reynolds stress) dominates (Yen, 2002). The increment of turbulence momentum and energy exchange associated with coupled clusters occurrence could possibly the cause of formation of a more stable armored bed created in coarse sediment where the coupled clusters were effective.

The median cluster spacing λ_{median} is larger than the maximum value of the form roughness scale range. This can be explained by the possibility of occurrence of other bed forms such as isolated coarse particles acting as LREs between the neighboring clusters. The value of grouping parameter $\lambda_{median}S/d_{sm}$ is fairly constant around a value of

0.15~0.2 for all armored bed surfaces, which confirms the findings of Strom and Papanicolaou (2007).

Semivariograms of those flume runs with bulk sand content of 9% and 24% are characterized by a sharp decrease in regression slope as the roughness scale transits from grain roughness to form roughness. The absence of a break in regression slope for the two fractal linear regression bands for Run 2 and Run 8 is a result of the dominance of effective roughness on those bed surfaces either by form scale or grain scale. Run 2 has lowest sand content and relatively high flow rate which rendered the absence of small grain roughness, and the same argument applies for Run 8 where coarse bedforms roughness is dominant for the entire bed surface. For all runs with two fractal features, the semivariograms exhibit a constant value of 30mm as the location of the break in slope or lag distance Δss. It corresponds roughly to $2\sim 3D_{s50}$ which confirms observations from previous research (Robert, 1988; Clifford et al., 1992).

By comparing the plot of relative roughness against sand content with the plot of bed stability against sand content, we find that the relative roughness height for grain scale roughness K_g/R exhibits coincidently the same trend as bed stability: it decreases with the sand content for armored bed created in coarse sediment mixture and the trend reversed for fine sediment mixture (Figure 6.5.2). The correlation between bed stability and relative grain roughness height can be possibly interpreted as that when sand content increased from 1% to 24%, the pores and openings in between the clusters and other large roughness elements became filled with more and more fine particles, the mean elevation of the bed surface elevated and the grain roughness became more significant which

lowered down the entire bed roughness factor; however, with a sand fraction increase from 24% to 38%, sand fraction on bed surface became over-represented and possible bedforms composed by finer sediment started to form, which turned out to increase the relative grain roughness factor.
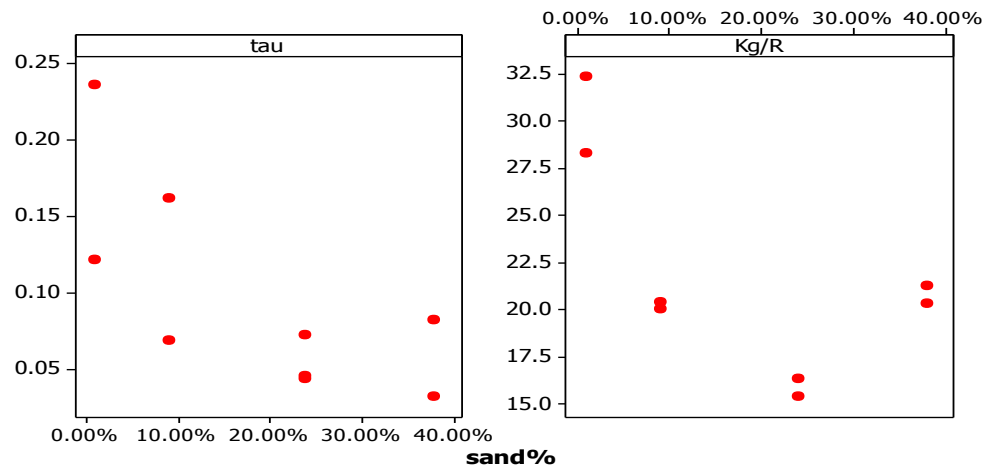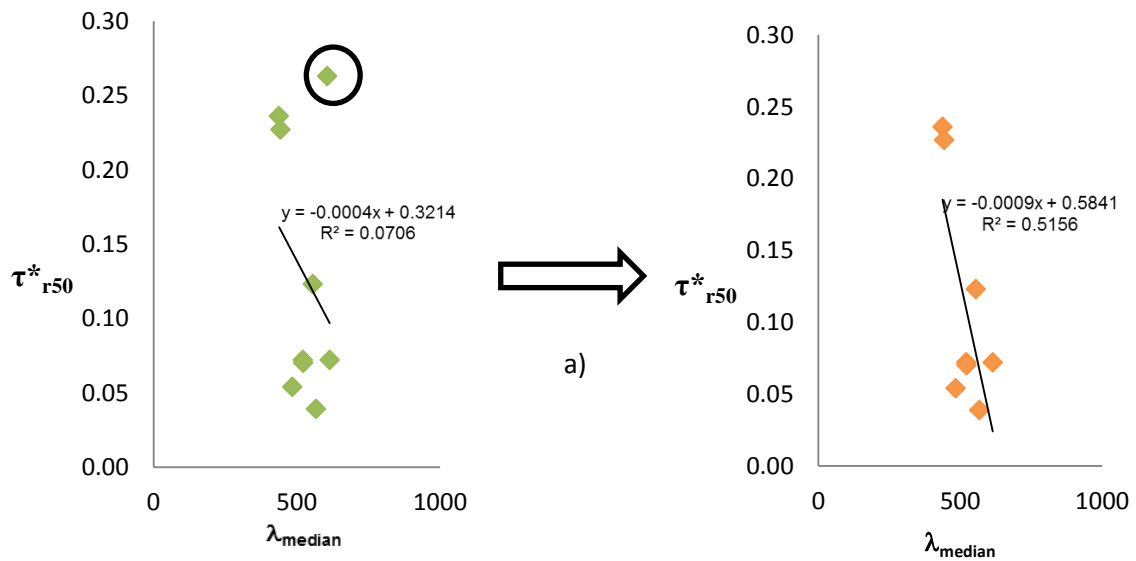

Figure 6.5.2 non-dimensional reference bed shear stress *tau* and relative grain roughness height *K$_g$* vs. sand content % (Created using MINITAB)

The correlation between reference shear stress and flow resistance associated with clusters and their spatial distribution characteristics is relatively strong (Figure 6.4.6b). The bed stability increased as the median cluster spacing reduced, which means clusters were more closely spaced and the entire cluster reticulation structure held the surface materials from being entrained. Bed stability for the armored bed is proportionally associated with the mean value of the maximum grain size for all clusters of each run and inversely associated with the variability of cluster spacing. In contrast, the grain roughness resistance was shown to be an ineffective parameter for bed stability prediction implied by an excessively large P-value in the multiple linear regression model.

The origin of error may stem from the scanning procedure. There was a gap between two individual DEMs that were stitched together to create the full bed DEM. Although small, this gap may have cause an underestimate of the cluster quantity and altered cluster spacing measurements.

By selectively eliminating outliers (data points in dark circles on the Figure 6.5.4) from the mean cluster spacing and cluster quantity data sets, the simple individual linear regression models are highly improved (Figure 6.5.3). However, the mean cluster spacing is around 500mm shown in Table 6.4.1 and the count for clusters is around 15 shown in Table 6.4.2. With or without considering outliers, the slopes of the regressions are so steep that even if cluster quantity and mean spacing were considered constant, a linear relationship might still be invalid.
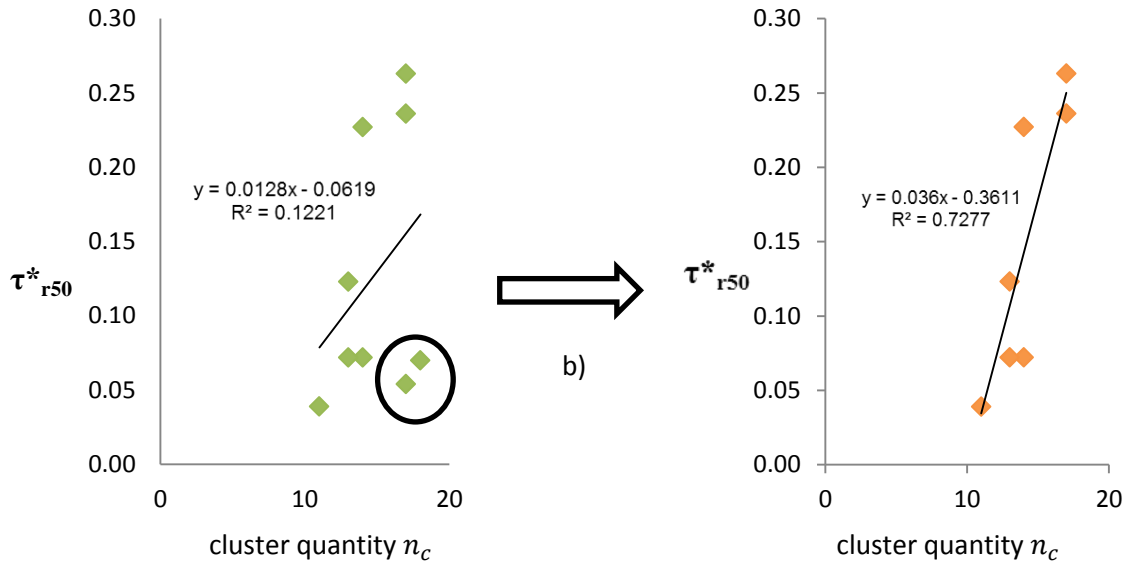
Figure 6.5.3 Linear regressions for filtered data of bed resistance vs. a) median cluster spacing λ_median, b) cluster quantity n_c

For sediment of 1% sand content, the non-dimensional reference shear stress is approximately 0.23 regardless of the increase of flow rate from $0.09\text{m}^3/\text{s}$ to $0.11\text{m}^3/\text{s}$, as the reference shear stress required to mobilize the armored surface cannot be met even under the highest flow rate ($0.11 \text{ m}^3/\text{s}$) in this research.

In order to calculate drag coefficient C_d, the shear velocity u_* is estimated from the total shear stress which is calculated by the depth-slope method. The depth-slope product method (aka the DuBoy's equation) was used for the reasons summarized by Hassan and Church (2000): (1) a description of mean hydraulic conditions is required to address the mean sediment transport rate (2) a mean rather than the local point values obtained from the velocity profiles is required from the entire bed aspect, and (3) making point estimates of u_* is difficult to establish and verify for flows with well-developed surface roughness where the velocity profiles deviate from logarithmic curves. The linear regression model shows that the drag coefficient is the most significant predictor for bed

resistance estimates. Drag coefficient is not as significant as grain friction for calculating the sediment transport rate in sand bed rivers. However, for armored gravel bed, the form drag plays the most important part of the shear stress exerted on bed surface. The high linear correlation of bed stability and drag coefficient or dimensionless total shear stress may be due to the fact that these two parameters are both expressed in terms of u_*^2, while the derivation of dimensionless reference shear stress τ^*_{r50} for sediment of size D_{s50} involves the term u_*^3.

6.6   Conclusion

The focus of this chapter is to investigate effects of flow rate and sand content within a bulk sediment mixture on bed resistance or bed stability for armored gravel-bed surfaces. To do this, a total of 8 armored beds were generated under a series of three discharge magnitudes ranging from 0.07 m^3/s to 0.09 m^3/s were analyzed against four sediment mixtures with increasing sand content from 1% to 38%. The cluster quantity and mean spacing of downstream neighboring clusters was measured using criteria for cluster and cluster spacing definition as well as a new procedure incorporating DEMs and panoramic photographs.

The armored bed stability was qualitatively evaluated in terms of time that required for post-armored bed sediment to reach a constant equilibrium transport rate. The time estimation by monitoring sediment transport rate is very empirical and hard to be consistent for each run. Therefore, the time evaluation for bed stability was verified and corrected through the non-dimensional reference shear stress which was calculated through inverse application of the Wilcock-Crowe Surface-based Transport Model

(WCSBTM) using the transport rate of sediment size D_{s50} from the armored bed surface. The difference between the reference shear stress calculated from WCSBTM and the value resulted from sand content fitting curve can be interpreted as the increase in bed stability due to armoring and cluster presence.

Semivariogram plots showed two fractal linear regressions bands with distinct slopes and they are defined as grain and form roughness scales, characterized by the thresholds of "break of slope" lag distance Δss and "the range of process" $\Delta smax$. K_g, the grain roughness length, and K_f, the form roughness length, were calculated by taking mean of the elevation differences for a certain value of lag distance Δs. Form roughness and K_f are normalized by median cluster spacing to account for the effect of not only the roughness effective height but the cluster spacing values. The bed resistance can be accordingly divided into two components: grain roughness resistance which is responsible for sediment transport and form roughness resistance which is associated with total form drag contributed by clusters geometry and spatial arrangement. Another important component for evaluating the bed stability is the total straight shear stress. Armored bed will rearrange the occurance of clusters distribution and effective roughness in response to high flow rate to maintain maximum resistance for sediment from entrainment.

Correlations between bed stability and the three predictor parameters were determined through simple linear regression. Flow resistance contributed by clusters height and distribution pattern had a best fit and the grain roughness resistance turned out to be an ineffective predictor for bed stability.

A first-order multiple regression model was designed to evaluate bed stability change in response to predictor variables. The dimensional analysis was performed to select independent predictor variables and a final model containing 3 independent non-dimensional variables was established:

$$\tau^*_{r50} = 0.009 + 0.043\left[ln\left(\frac{R}{K_g}\right)\right]^{-2} + 2.79\frac{n_c d_{sm} C_d K_f}{\lambda_{cmedian}\sigma_{\lambda c}} + 242\frac{u*^2}{gD_{50}}$$

The model has a p-value of 0.001 and a regression least square value of 0.974, indicating that the model itself is valid for the sediments and flows used in this study.

However, a two-way ANOVA analysis argued that the factor representing sediment sand content and flow rate turned out to have little significant effect on predictors (form roughness resistance and total shear stress) for bed resistance estimation, whereas sand content do have a relatively significant influence on grain roughness resistance compared to flow rate variation. In other word, varying flow rate magnitude and sand percentage will alternate the quantity and spatial distribution of cluster bedforms to a limited extend. However, they are strongly correlated with grain roughness resistance which is significant for sandier bed rivers. Flow associated shear stress plays an important role in both prediction of bed stability and in the correlation with flow rate. Increase in flow rate will positively increase the total shear stress and in turn increase the nondimensional reference shear stress for D_{s50} to be mobilized.

Chapter 7.

GENERAL DISCUSSION AND CONCLUSIONS

The goal of this research was to investigate the effects of hydraulic conditions on development of cluster bedforms during the armoring process and the subsequent implications for overall bed stability. A static bed armor developed under sustained low flows during which there is no upstream sediment input. During the process of bed surface armoring (finer material on surface being entrained downstream or penetrating into the substrate), there was an increased probability that the large sized particles would roll into contact with other larger particles and become key clasts in the formation of structured gravel bedforms, including streamwise stripes and transverse ribs. More complex bedforms such as linked gravel reticulates and clusters form as gravels develop into groups. Coarse sediments imbricate and provide shelter, or hiding, for fine sediments. Together with the armoring, imbrication and hiding increase the critical shear stress threshold and the resistance of the bed surface to mobilization. The cluster quantity and spatial grouping of downstream neighboring clusters was measured using innovate criterion for cluster and cluster spacing as well as a new procedure incorporating DEMs and panoramic photographs.

7.1 Hypotheses Tests and Interpretations

The hypotheses driving this research were based on previous studies of bed stability both in field and flume. The number and arrangement of clusters on the bed surface are hypothesized to be part of a feedback system with the flow rate in channel to

maintain a maximum flow resistance over the channel bed (Brayshaw, 1984; Hassan and Reid, 1990). The sand proportion in bulk sediment defined the grain size distributions used in these experiments and also the effective roughness height of the bed surface. Disparate studies have focused on defining the role of cluster bedform in bed stability and have indicated the dominant independent variables controlling cluster formation and topography were the flow rate during cluster formation and the sediment characteristic grain sizes. (Hassan, 1990; Wittenberg, 2007, Strom and Papanicolaou, 2009).

The armored bed stability was qualitatively evaluated in terms of the time that was required for an armored bed sediment to reach a constant equilibrium transport rate, and quantitatively determined through the normalized reference shear stress for surface sediment of size D_{s50}. Both approaches revealed that the sediment mixtures should be divided into two types when considering their armored bed stability: coarse sediment dominated sediment with 1% and 9% sand content and finer sediment where the sand content was 24-38%. The results of the research indicate that the sediment mixture could be divided into two types using 15% sand content as a threshold: coarse gravel sediment with 1% and 9% sand content (higher bed stability), and finer gravel sediment with 24% and 38% sand content (lower bed stability).

First Hypothesis: The density of clusters on the armored bed increases as the sand fraction in the bed sediment increases and the spacing between clusters decreases.

This hypothesis was directly tested by changing the sand fraction in the bulk sediment but armoring the bed at the same flow rate. Using four different sediments, the bed was armored at a series of flow rate ranging from 0.035 to 0.055m³/s and clusters

developed. The cluster density linearly increased with sand content except the case under $0.045m^3$/s (Figure 7.1.1a). With an increased sand portion in the bulk sediment, the overall bedload transport rate increased (refer to Figure 6.5.1b). This resulted in an increase of coarse sediment transport and the probability that large grains would roll into contact and form a cluster bedform. This may explain the measured increase in cluster density with bulk sediment sand content.

Cluster spatial distribution for Runs under the flow rate of 0.035 and $0.045m^3$/s shows an opposite trend. Under the flow rate of $0.045m^3$/s, the total clusters density linearly decreased with sand addition, and the grouped clusters density and median cluster spacing increased (Figure 7.1.1 marked in red). This indicated that clusters formed in the higher sand content sediment mixtures tended to locate with a high spatial density to induce skimming flow over the grouped clusters even though the overall cluster quantity decreased. Under the flow rate of $0.035m^3$/s, both of the total clusters density and grouped clusters density linearly increased with sand addition, and median cluster spacing decreased (Figure 7.1.1 marked in blue). Although the opposite behavior may stem from the diminished flow rate which was not adequate to generate momentum and energy associated shear to mobilize the grouped clusters into high cluster density regions, misestimate could be another possibility as there were only two data points for runs under this flow rate. This may not accurately represent the actual trend.
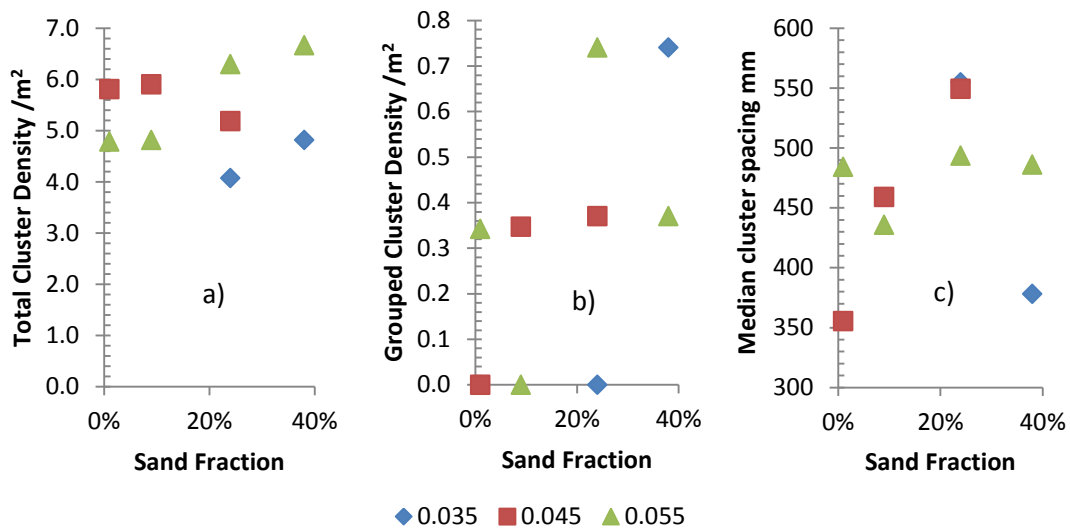
Figure 7.1.1 Correlation of sand content and cluster spatial distribution with an armoring flow rate of 0.035~0.055m^3/s: a) Cluster density linearly increased with sand content; b) Grouped cluster density increase with sand content; c) cluster spacing median value increase

Under the flow rate of 0.055m^3/s, the total clusters density and the grouped clusters density linearly increased with sand content, whereas the median cluster spacing increased (Figure 7.1.1 marked in green). This further verified the cluster spatial distribution trend showed for flow rate of 0.045m^3/s, that as overall cluster density increased, the possibility of clusters to form into high clusters density regions increased.

Generally, the first hypothesis validated in that an increased sand content in the bulk sediment would increase the grouped clusters density and median clusters spacing, regardless of the trend for total clusters density. The validation of this hypothesis could possibly be interpreted as a result of a combined effect of clusters on local turbulence and Shields stress at different locations on the bed surface.

The measured Reynolds stress decreased as clusters formed in groups. By comparing the flows around the clusters that formed isolated on the bed and in close

proximity to other clusters, we quantified the effect of increased cluster configuration on the turbulent flow field. As the number of closely spaced clusters increased to form coupled clusters, the flow Reynolds stress and TKE had magnitudes of 16% greater than over the isolated cluster. In contrast, as cluster density increased to that of grouped clusters, the overall turbulence statistics showed a weak energy (TKE) and momentum (Reynolds stress) flux. The flow pattern changed as clusters formed groups to that of a skimming flow, passing over the tops of the clusters.

The influence of sand on the armor layer that formed clusters was indicated by a reduction in turbulent parameters as the sand content of the bed increased and the armor ratio decreased. When sediment mixtures with low sand content are compared, the high sand content decreased the bed stability by increasing the grouped clusters density and occurrence of skimming flow over the grouped clusters. The higher sand content sediments developed more clusters during armoring and therefore, the density and potential for grouping of clusters was higher.

Second Hypothesis: The density and grouping of clusters on the armored bed increases as the flow rate during armor formation increases.

For all sediment mixtures, the flow rate was proportionally correlated with cluster density (Figure 7.1.2a), and inversely correlated with median cluster spacing (Figure 7.1.2b). This validated the second hypothesis.
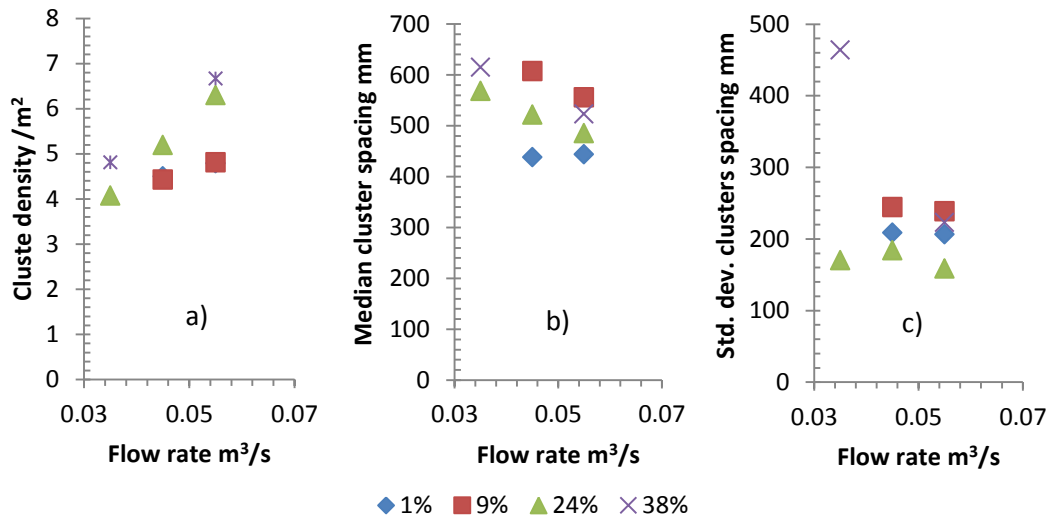
◆ 1% ■ 9% ▲ 24% ✕ 38%

Figure 7.1.2 Correlation of cluster spatial distribution and flow rate during armor formation for sediment with distinct sand content: a) cluster density linearly increase with flow rate; b) mean cluster spacing shows an overall decreasing trend with increasing flow rate.

Increasing the flow rate beyond what was tested in these experiments, would increase the turbulence in the flow field immediately around the clusters. For the same bulk sediment mixture composition, the cluster density will increase and median cluster spacing decrease, indicating a greater number of grouped clusters. (Figure 7.1.2 b and c). However, the strength of the observed correlation might be overestimated because of the limited number of samples using the same sand content but different levels of flow rate. From the two-way ANOVA modeling in Chapter 6, it was found the effect of flow rate during armor formation on the reference shear stress of the armored surface D_{s50} (bed stability) was not as important as the effect of sand content.

Third hypothesis: The stability of the bed surface increases with the density and the number of spatially coupled clusters on the bed.

The hypothesis was proved to be accepted for sediment with high sand content (the fine gravel sediment) but not valid for coarse sediment.

In those experiments with a constant armoring flow rate of $0.055m^3/s$, the armored bed stability in term of the nondimensional reference shear stress for surface particles of size D_{s50}, deceased for the coarse gravel dominated sediment (Run 2 with 1% sand to Run 4 with 9% sand) and increased for finer gravel dominated sediment (24% and 38%) as the cluster density increased (Figure 7.1.3a). Figure 7.1.3b shows that the two types of sediment categorized by sand content can be separated according to bed stability and cluster density. Reference shear stresses of fine gravel sediment (Run 1 through 4) were high while the cluster densities were low, for finer sediment mixtures (Run 5 through 9), the cluster densities were high while reference shear stress was low.
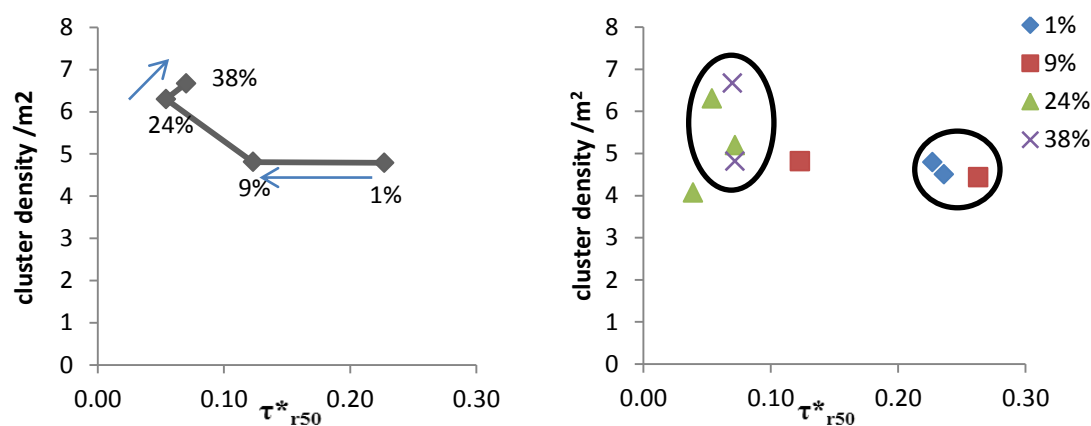

Figure 7.1.3 Cluster density vs. normalized reference shear stress for a) Run 2, 4, 7 and 9 (numbered in figure) under a flow rate of 0.055m³/s during armored bed formation; b) cluster densities and reference shear stresses grouped into two data clusters.

7.2   Recommendations and Possible Future Directions

Several recommendations can be made for future experimental work. In general, longer flumes may help in establishing flows with constant flow depth, while wider

flumes may diminish the sidewall effects. Repeated experiments for more measurements and verification procedure should have been conducted. The hydraulics analysis makes use of time-averaged turbulence parameters for data acquired through an ADV, which precluded direct analysis of the movement of coherent flow structures around clusters. Higher resolution velocimeter such as Particle image velocimetry (PIV) techniques could improve the quality of velocity measurements in turbulent flow around clusters and provide the time dependent variables necessary to define vortex movement.

Cluster definition and categorization can be modified based on the criteria and procedures proposed by this research. In order to identify clusters on armored bed surface more efficiently and more accurately, further information about clusters formation mechanism and characteristics need to be investigated thoroughly.

The bed stability model predictors such as total shear stress, cluster density were well documented, so that later comparisons with other studies are possible and unambiguous. The model should now be tested using some other factors that may cause armored bed stability to vary. Instead of the process used in this work where the flow rate was increased to the equilibrium flow rate to destroy the armored bed and evaluate bed stability, future comparison experiments could investigate the armor breaking process in response to increased sand input at upstream end.

7.3   Summary of Conclusions

The experiments verified two of three hypotheses raised by this research proposal, as the mean cluster spacing did not show a defined trend but instead an increase in variability. The cluster density increases with sediment sand fraction and flow rate magnitude. The median cluster spacing values were more difficult to interpret as they did not show a strong trend and were heavily influenced by cluster grouping. The two-way ANOVA results indicate that the factor of sand content has more effective influence on bed stability predictors than the facto of flow rate.

As local clusters density increased, coupled clusters formed, increased turbulence in the local flow field, mimicking the wake interference proposed by Morris (1955). As cluster density increased to form grouped clusters, the entire flow field showed dampened turbulent statistics, indicating that skimming flow was occurring for flow over grouped clusters. The turbulence parameters and the reference shear stress (bed stability) reduced as the sand content and cluster density increased.

The third hypothesis of this research is partially acceptable in cases for finer sediment mixtures. The armored bed stability can be evaluated either through the time required to break armored surface under equilibrium flow rate or the non-dimensional reference shear stress for surface grains of size D_{s50}. Results from both approaches indicate that armored bed stability was enhanced with clusters formation. The extent of stability increase varied when compared to the reference shear stress calculated from the equation that involved the surface sand fraction. By partitioning the total bed resistance into components of grain roughness resistance, cluster form resistance and total shear

resistance, and fitting into a multi-linear regression model, we found that the armored bed stability has a combined positive response to variables of total shear stress, clusters form roughness (length and distribution), and weakly correlated with the grain roughness contributed resistance. However, the grain form roughness is much more sensitive than the other two terms in response to the varying hydraulic conditions of sand content and flow rate. Sand content within the bulk sediment played a more important and effective role for bed stability assessment.

References

Andrews, E. D., and Parker, G. (1987). "Formation of a coarse surface layer as the response to gravel mobility." *Sediment Transport in Gravel-bed Rivers*, John Wiley & Sons, 269–300.

Aberle, J., and Nikora, V. (2006). "Statistical Properties of Armored Gravel Bed Surfaces." *Water Resour. Res.*, 42(11), W11414.

Agelinchaab, M., Paul, S. S., Tachie, M. F. (2009). "Velocity characteristics of flow and finite square and circular cylinders." *Proc., 33rd IAHR Congress: Water Engineering for a Sustainable Environment, International Association of Hydraulic Engineering and Research (IAHR)*, Vancouver, BC, 480-487.

Afzalimehr, H., and Anctil, F. (2000). "Accelerating shear velocity in gravel-bed channels." *J. Hydrol. Sci.*, 7, 37–44.

Baik, J-J., and Kim, J-J. (1999). "A numerical study of flow and pollutant dispersion characteristics in urban street canyons." *J. Appl. Meteor.*, 38, 1576–1589.

Bartley, R., and Rutherfurd, I. (2005). "Re-Evaluation of the Wave Model as a Tool for Quantifying the Geomorphic Recovery Potential of Streams Disturbed by Sediment Slugs." *Geomorphology*, 64(3–4), 221-242.

Bathurst, R. G. C. (1982). "Genesis of Stromatactis Cavities between Submarine Crusts in Palaeozoic Carbonate Mud Buildups." *J of the Geological Society*, 139(2), 165-181.

Best, J. L. (1996). "The fluid dynamics of small-scale alluvial bed forms." *Advances in Fluvial Dynamics and Stratigraphy*, John Wiley & Sons, 67–125.

Biron, P. M., Lane, S. N., Roy, A. G., Bradbrook, K. F., Richards, K. S. (1998). "Sensitivity of bed shear stress estimated from vertical velocity profiles: The problem of sampling resolution." *Earth Surf. Process. Landforms*, 23, 133–9.

Bomminayuni, S., and Stoesser, T. (2011). "Turbulence Statistics in an Open-Channel Flow Over a Rough Bed." *J. Hydraul. Eng.*, 137(11), 1347-1358.

Brandt, S. A. (2000). "Classification of Geomorphological Effects Downstream of Dams." *Catena*, 40(4), 375-401.

Bray, D. I., (1979), "Estimating average velocity in gravel-bed rivers." *Proc ASCE, J of Hydraulic Division*, 105(9), 1103-1122

Bray, D. I., (1985). "Flow resistance in gravel-bed rivers." *Gravel-Bed Rivers*, John Wiley, 109-132.

Brayshaw, A. C. (1984). "Characteristics and Origin of Cluster Bedforms in Coarse-Grained Alluvial Channels." *Sedimentology of Gravels and Conglomerates*, *Candaian Soc. of Petrol. Geol.*, 77-85.

Brayshaw, A. C., Frostick, L. E., Reid, I. (1983). "The Hydrodynamics of Particle Clusters and Sediment Entrainment in Coarse Alluvial Channels." *Sedimentology*, 30(1), 137-143.

Brown, S., Nickling, W. G., Gillies, J. A. (2008). "A Wind Tunnel Examination of Shear Stress Partitioning for an Assortment of Surface Roughness Distributions." *J. Geophys. Res.*, 113(F02S06).

Buffin-Bélanger, T., and Roy, A. G. (2005). "1 Min in the Life of a River: Selecting the Optimal Record Length for the Measurement of Turbulence in Fluvial Boundary Layers." *Geomorphology*, 68(1-2), 77-94.

Buffin-Bélanger, T., Roy, A. G., Kirkbride, A. D. (2000). "On Large-Scale Flow Structures in a Gravel-Bed River." *Geomorphology*, 32(3-4), 417-435.

Buffin-Bélanger, T., and Roy, A. G. (1998). "Effects of a Pebble Cluster on the Turbulent Structure of a Deth-Limited Flow in a Gravel-Bed River." *Geomorphology*, 25, 254-267.

Buffington, J. M. (1999). "The legend of A. F. Shields." *J. Hydraul. Eng.*, 125(4), 376-387.

Buffington, J. M., and Montgomery, D. R. (1999). "Effects of Hydraulic Roughness on Surface Textures of Gravel-Bed Rivers." *Water Resour. Res.*, 35(11), 3507-3521.

Canovaro, F., Paris, E., Solari, L. (2007). "Effects of Macro-Scale Bed Roughness Geometry on Flow Resistance." *Water Resour. Res.*, 43(10), W10414.

Canovaro, F., and Solari, L. (2007). "Dissipative Analogies between a Schematic Macro-Roughness Arrangement and Step-Pool Morphology." *Earth Surf. Process. Landforms*, 32(11), 1628-1640.

Cardinale, B. J., Palmer, M. A., Collins, S. L. (2002). "Species Diversity Enhances Ecosystem Functioning through Interspecific Facilitation." *Nature*, 415(6870), 426-429.

Carling, P. A., Kelsey, A., Glaister, M. S. (1992). "Effect of bed roughness, particle shape and orientation on initial motion criteria." *Dynamics of Gravel-Bed Rivers*, John Wiley & Sons, 23-38.

Carling, P. A., and Reader, N.A. (1982), "Structure, composition and bulk properties of upland stream gravels." *Earth Surf. Processes Landforms*, 7, 349–365.

Carr, J. R. (1995). "Numerical analysis for the geological sciences" Englewood Cliffs, New Jersey, Prentice Hall.

Chow, V. T., (1959). *Open-Channel Hydraulics*, McGraw-Hill, New York.

Church, M., Hassan, M. A., Wolcott, J. F. (1998). "Stabilizing Self-Organized Structures in Gravel-Bed Stream Channels: Field and Experimental Observations." *Water Resour. Res.*, 34(11), 3169-3179.

Clayton, J. A., and Pitlick, J. (2008). "Persistence of the Surface Texture of a Gravel-Bed River during a Large Flood." *Earth Surf. Process. Landforms*, 33(5), 661-673.

Clifford, N. J., Robert, A., Richards, K. S. (1992). "Estimation of flow resistance in gravel-bedded rivers: A physical explanation of the multiplier of roughness length." *Earth Surf. Processes Landforms*, 17(2), 111-126.

Clifford, N.J. (1996). "Morphology and stage-dependent flow structure in a gravel-bed river." *Coherent Flow Structures in Open Channels*. 545-566, Wiley, Chichester.

Curran, J. C., and Wilcock, P. R. (2005). "The Effect of Sand Supply on Transport Rates in a Gravel-Bed Channel." *J. Hydraul. Eng.*, 131(11), 961-968.

Curran, J. C., and Tan, L. (2010). "An investigation of bed armoring process and the formation of microclusters." *Proc., Proceedings of the Joint Federal Interagency Conference 2010: Hydrology and Sedimentation for a Changing Future: Existing and Emerging Issues*, JFIC, Las Vegas, NV, 1-12.

Darboux F., Huang C. (2003). "An instantaneous-profile laser scanner to measure soil surface microtopography." *Soil Science Society of America Journal*, 67, 92–99.

Davies, T. R. H. (1980). "Bedform Spacing and Flow Resistance." *ASCE, J of Hydraulic Division*, 106, 423-433.

Day, T. J., and Egginton, P. (1983). "Particle-size distribution of the surface of alluvial channel beds." *Geological Survey Canada Paper*, 83-lB, 229-302.

De Jong, C. (1991). "A Reappraisal of the Significance of Obstacle Clasts in Cluster Bedform Dispersal." *Earth Surf. Proces. Landforms*, 16, 737-744.

Dietrich, W. E., Kirchner, J. W., Ikeda, H., Iseya, F. (1989). "Sediment Supply and the Development of the Coarse Surface Layer in Gravel-Bedded Rivers." *Nature*, 340(6230), 215-217.

Frey, P., and Church, M. (2011). "Bedload: A Granular Phenomenon." *Earth Surf. Process. Landforms*, 36(1), 58-69.

Frey, P., and Church, M. (2009). "How River Beds Move." *Science*, 325(5947), 1509-1510.

Frostick, L.E., Lucas, P.M. and Reid, I. (1984). "The infiltration of fines into coarse grained alluvial sediments and its implications for stratigraphical interpretation." *Journal of the Geological Society of London*, 141, 955-965.

Galay, V. J. (1983). "Causes of River Bed Degradation." *Water Resour. Res.*, 19(5), 1057-1090.

Gomez, B. (1993). "Roughness of Stable, Armored Gravel Beds." *Water Resour. Res.*, 29(11), 3631-3642.

Gran, K. B., Montgomery, D. R., Sutherland, D. G. (2006). "Channel Bed Evolution and Sediment Transport Under Declining Sand Inputs." *Water Resour. Res.*, 42(10), W10407.

Grant, G. E. (2001). "Dam Removal: Panacea Or Pandora for Rivers?" *Hydrol. Process*, 15, 1531-1532.

Grass, A. (1971). "Structural Features of Turbulent Flow Over Smooth and Rough Boundaries." *J. Fluid Mech.*, 50, 233-255.

Hardy, R. J., Best, J. L., Lane, S. N., Carbonneau, P. E. (2009). "Coherent Flow Structures in a Depth-Limited Flow Over a Gravel Surface: The Role of Near-Bed Turbulence and Influence of Reynolds Number." *J. Geophys. Res.*, 114(F01003).

Hardy, R. J., Best, J. L., Lane, S. N., Carbonneau, P. E. (2010). "Coherent Flow Structures in a Depth-Limited Flow Over a Gravel Surface: The Influence of Surface Roughness." *J. Geophys. Res.*, 115(F03006), 22.

Hardy, R. J., Best, J. L., Parsons, D. R., Keevil, G. M. (2011). "On Determining the Geometric and Kinematic Characteristics of Coherent Flow Structures Over a Gravel Bed: A New Approach using Combined PLIF-PIV." *Earth Surf. Process. Landforms*, 36(2), 279-284.

Hassan, M. A., and Church, M. (2000). "Experiments on Surface Structure and Partial Sediment Transport on Gravel Bed." *Water Resour. Res.*, 36(7), 1885-1895.

Hassan, M. A., and Reid, I. (1990). "The Influence of Microform Bed Roughness Elements on Flow and Sediment Transport in Gravel Bed Rivers." *Earth Surf. Process. Landforms*, 15, 739-750.

Hey, R. D., (1979)," Flow resistance in gravel bed rivers." *Proc ASCE, J of Hydraulic Division*, 105(4), 365-379

Hey, R. D., and C. R. Thorne, (1983), "Accuracy of surface samples from gravel bed material.", *J. Hydraul. Eng.*, 109, 842-851.

Hey, R. D., and Thorne, C. R. (1986). "Stable channels with mobile gravel beds." *J. Hydraul. Eng.*, 112(8), 671–689.

Imamoto, H., and Ishigaki, T. (1986). "Visualization of longitudinal eddies in an open channel flow." *Proc., Flow Visualization IV: Proceedings of the Fourth International Symposium on Flow Visualization*, Hemisphere, Ecole Nationale Superieure de Techniques Avancees, Paris, France, 333-337.

Iseya, F., and Ikeda, H. (1987). "Pulsations in Bedload Transport Rates Induced by a Longitudinal Sediment Sorting: A Flume Study using Sand and Gravel Mixtures." *Geografiska Annaler*, 69, 15-27.

Jaeggi, M. and Smart, G. (1982). "Discussion of Channel bars in gravel-bed rivers." *Gravel-Bed Rivers*, Wiley and Sons, 325.

Jain, S. C. (1990). "Armor Or Pavement." *J. Hydraul. Eng.*, 116(3), 436-440.

Jimenez, J. (2004). "Turbulent Flows Over Rough Walls." *Annu. Rev. Fluid Mech.*, 36, 173-196.

Johnson, P.A., Gleason, G.L., and Hey, R.D. (1999). "Rapid Assessment of Channel Stability in Vicinity of Road Crossing." *J. Hydraul. Eng.*, 125(6), 645-651.

Judd, H. E., and Peterson, D. F. (1969). "Hydraulics of large bed element channels." *Rep. PRWG 17-6*, Utah Water Res. Lab., Utah. State Univ., Logan.

Kaufmann, P. R., Faustini, J. M., Larsen, D. P., Shirazi, M. A. (2008). "A Roughness-Corrected Index of Relative Bed Stability for Regional Stream Surveys." *Geomorphology*, 99(1–4), 150-170.

Kaufmann, P.R., P. Levine, E.G. Robison, C. Seeliger, and D.V. Peck. (1999), "Quantifying Physical Habitat in Wadeable Streams." *EPA 620/R-99/003*. Environmental Monitoring and Assessment Program, U.S. Environmental Protection Agency, Corvallis, OR.

King, J., Nickling, W. G., Gillies, J. A. (2008). "Investigations of the Law-of-the-Wall Over Sparse Roughness Elements." *J. Geophys. Res.*, 113(F02S07).

Kirchner, J. W., Dietrich, W. E., Iseya, F., and Ikeda, H. (1990). "The variability of critical shear stress, friction angle, and grain protrusion in water- worked sediments.", *Sedimentology*, 37, 647-672.

Kondolf, G. M. (1997). "Hungry Water: Effects of Dams and Gravel Mining on River Channels." *Environ. Manage.*, 21, 4.

Lacey, R. W. J., Legendre, P., Roy, A. G. (2007). "Spatial-Scale Partitioning of in Situ Turbulent Flow Data Over a Pebble Cluster in a Gravel-Bed River." *Water Resour. Res.*, 43(W03416).

Lacey, R. W. J., and Roy, A. G. (2007). "A Comparative Study of the Turbulent Flow Field with and without a Pebble Cluster in a Gravel Bed River." *Water Resour. Res.*, 43(W05502).

Lacey, R. W. J., and Roy, A. G. (2008a). "The Spatial Characterization of Turbulence Around Large Roughness Elements in a Gravel-Bed River." *Geomorphology*, 102(3-4), 542-553.

Lacey, R. W. J., and Roy, A. G. (2008b). "Fine-Scale Characterization of the Turbulent Shear Layer of an Instream Pebble Cluster." *J. Hydraul. Eng.*, 134(7), 925-936.

Lamarre, H., and Roy, A. G. (2005). "Reach Scale Variability of Turbulent Flow Characteristics in a Gravel-Bed River." *Geomorphology*, 68(1-2), 95-113.

Lamberti, A., and Paris, E. (1992). "Analysis of Armouring Processes through Laboratory Experiments." *Dynamics of Gravel-Bed Rivers*, John Wiley & Sons, 227-250.

Lane, S. N. (2005). "Roughness - Time for a Re-Evaluation?" *Earth Surf. Process. Landforms*, 30(2), 251-253.

Lawless, M., and Robert, A. (2001a). "Three-Dimensional Flow Structure Around Small-Scale Bedforms in a Simulated Gravel-Bed Environment." *Earth Surf. Process. Landforms*, 26(5), 507-522.

Lawless, M., and Robert, A. (2001b). "Scales of Boundary Resistance in Coarse-Grained Channels: Turbulent Velocity Profiles and Implications." *Geomorphology*, 39(3–4), 221-238.

Lawless, M. R., Lane, S. N., Best, J. L. (2004). "The Junction Vortex System: Time-Mean and Instantaneous Flow Fields." *Shallow Flows*, Taylor and Francis, London, 117-124.

Leopold, L. B. (1992). "Sediment size that determines channel morphology." *Dynamics of Gravel Bed Rivers*, John Wiley & Sons, 287-311.

Little,W.C., Mayer, P.G. (1976). "Stability of channel beds by armoring." *ASCE, J of Hydraulic Division*, 192(HY11), 1647-1661.

Lu, S. S., and Willmarth, W. W. (1973), "Measurements of structure of Reynolds stress in a turbulent boundary layer." *J. Fluid Mech.*, 60, 481–511.

Lyn, D. A. (1993). "Turbulence Measurements in Open-Channel Flows Over Artificial Bed Forms." *J. Hydraul. Eng.*, 119(3), 306-326.

Maddux, T. B., McLean, S. R., Nelson, J. M. (2003a). "Turbulent Flow Over Three-Dimensional Dunes: 2. Fluid and Bed Stresses." *J. Geophys. Res.*, 108(F1), 6010.

Maddux, T. B., Nelson, J. M., McLean, S. R. (2003b). "Turbulent Flow Over Three-Dimensional Dunes: 1. Free Surface and Flow Response." *J. Geophys. Res.*, 108(F1), 6009.

Madej, M. A. (2001). "Development of Channel Organization and Roughness Following Sediment Pulses in Single-Thread, Gravel Bed Rivers." *Water Resour. Res.*, 37(8), 2259-2272.

Measures, R., and Tait, S. (2008). "Quantifying the Role of Bed Surface Topography in Controlling Sediment Stability in Water-Worked Gravel Deposits." *Water Resour. Res.*, 44(4), W04413.

Martin, V., Fisher, T., Millar, R., Quick, M. (2002). "ADV data analysis for turbulent flows: Low correlation problem." *Proc., Proceedings of the EWRI and IAHR Int. Conf. on Hydraulic Measurements and ExperimentalMethods*, ASCE, Estes Park, CO, 101.

Marion, A., Tait, S. J. and McEwan I. K. (1997). "On the competitive effects of particle rearrangement and vertical sorting." *Proceedings of the 27th IAHR Congress, International Association for Hydraulic Research*. Madrid. Spain. 2; 1493–1498.

Marion, A., Tait, S.J. and McEwan, I.K. (2003). "Analysis of small-scale gravel bed topography during armouring." *Water Resour. Res.*, 39, 1334-1345.

Mao L., Cooper, J.R. and Frostick L.E. (2009). "Armour layer development during sediment starvation and recirculation flume experiments." 3*3rd IAHR Congress: Water Engineering for a Sustainable Environment.* Vancouver; Canada.

Matheron, G. (1971). "The Theory of Regionalized Variables and its Applications." Centre de Geostatistique, Fontainebleau, France, 212

Michael, F., and Gerhard, G. (2006). "Description of a Flume Channel Profilometry Tool using Laser Line Scans." *Aquatic Ecology*, 40, 493-501.

Morris, H. M. (1955). "Flow in Rough Conduits." *Transactions of ASCE*, 120, 373-398.

Nakagawa, H. and Nezu, I. (1977). "Prediction of the contributions to the Reynolds stress from bursting events in open-channel flows." *J. Fluid Mech.*, 80(01), 99-128.

Nezu, I. and Nakagawa, H.(1993a). "Turbulence in Open-Channel Flows." *IAHR-monograph*, Balkema, Netherlands.

Nezu, I. and Nakagawa, H.(1993b). "Basic structure of turbulence in unsteady open-channel flows." *Proc. 9th Symp. on Turbulent Shear Flows*, vol.1, Kyoto, pp.7.1.1-7.1.6.

Nikora, V. I., Goring, D. G., Biggs, B. J. F. (1998). "On Gravel-Bed Roughness Characterization." *Water Resour. Res.*, 34(3), 517-527.

Nikora, V. I., Goring, D. G., (2000). "Eddy Convection Velocity and Taylor's Hypothesis of 'Frozen' Turbulence in a Rough-Bed Open Channel Flow." *Journal of Hydroscience and Hydraulic Engineering*, 18(2), 75-91.

Ockelford, A., Haynes, H., Hodge, R. and Haynes, R. (2010). "Using high resolution laser scanning to indicate mechanisms of stabilisation under varying sub threshold flow exposures." *17th Congress of the Asia and Pacific Division of the International Association of Hydro-Environment Engineering and Research*. Auckland; New Zealand

Ojha, S. P., and Mazumder, B. S. (2010). "Turbulence Characteristics of Flow Over a Series of 2-D Bed Forms in the Presence of Surface Waves." *J. Geophys. Res.*, 115(F04016), 1-15.

Oldmeadow, D. F., and Church, M. (2006). "A Field Experiment on Streambed Stabilization by Gravel Structures." *Geomorphology*, 78, 335-350.

Oliver, M. A. and Webster, R. (1986). "Semivariograms for modeling the spatial pattern of landform and soil properties." *Earth Surf. Process. Landforms,* 11, 491-504.

Parker, G., Klingeman, P.C., McLean, D. G. (1982). "Bedload and Size Distribution in Paved Gravel-Bed Streams." *ASCE, J of Hydraulic Division*, 108(HY4), 544-571.

Papanicolaou, A.N., Diplas, P., Dancey, C. L., Balakrishnan, M. (2001). "Surface Roughness Effects in Near-Bed Turbulence: Implications to Sediment Entrainment." *Journal of Engineering Mechanics*, 127(3), 211-218.

Parker, G. and Toro-Escobar, C.M. (2002). "Equal mobility of gravel in streams: The remains of the day." *Water Resour. Res.*, 38 (1264)

Parker, G., and Sutherland, A. J. (1990). "Fluvial Armor." *J. Hydraul. Eng.*, 28(5), 529-544.

Parker, G., and Wilcock, P.,R. (1993). "Sediment Feed and Recirculating Flumes: Fundamental Difference." *J. Hydraul. Eng.*, 119(11), 1192.

Parker, G., and Klingeman, P.C. (1982). "On why gravel bed streams are paved." *Water Resour. Res.*, 18 (5), 1409-1423.

Peakall, J., Ashworth, P. J., Best, J. L. (1996). "Physcal modelling in fluvial geomorphology: Principles, applications, and unresolved issues." *Proc., The Scientific Nature of Geomorphology: Proceedings of the 27th Binghamton Symposium in Geomorphology*, John Wiley & Sons, 221-253.

Pender, G., Hoey, T.B., Fuller, C., and Mcewan, I.K. (2001). "Selective bedload transport during the degradation of a well sorted graded sediment bed." *J. Hydraul. Res*. 39; 269-277

PIEDRA, M. M., HAYNES, H., HOEY, T. B. (2012). "The Spatial Distribution of Coarse Surface Grains and the Stability of Gravel River Beds." *Sedimentology*, 59(3), 1014-1029.

Proffitt, G. T. (1980). "Selective Transport and Armouring of Non-Uniform Alluvial Sediments."

Reidenbach, M. A., Limm, M., Hondzo, M., Stacey, M. T. (2010). "Effects of Bed Roughness on Boundary Layer Mixing and Mass Flux Across the Sediment-Water Interface." *Water Resour. Res.*, 46(15), W07530,.

Rice, S., and Church, M. (1996). "Sampling Surficial Fluvial Gravels: The Precision of Size Distribution Percentile Estimates." *Journal of Sedimentary Res*., 66(3), 654-665.

Richards, K., and Clifford, N. J. (1991). "Fluvial Geomorphology: Structured Beds in Gravelly Rivers." *Prog. Phys. Geogr.*, 15(4), 407-422.

Richards, K. S. (1982). "Rivers, Form and Process in Alluvial Channels." Methuen.

Robert, A. (2011). "Flow Resistance in Alluvial Channels." *Prog. Phys. Geogr.*, 35(6), 765-781.

Robert, A. (1990). "Boundary roughness in coarse-grained channels." *Prog. Phys. Geogr.*, 14(1), 42-70.

Robert, A., (1988). "Statistical properties of sediment bed profiles in alluvial channels." *Mathematical Geology*, 20(3), 205-225.

Roussinova, V., Balachandar, R., Biswas, N. (2009). "Reynolds Stress Anisotropy in Open-Channel Flow." *J. Hydraul. Eng.*, 135(10), 812-824.

Roy, A. G., Biron, P. M., Buffin-Bélanger, T., Levasseur, M. (1999). "Combined Visual and Quantitative Techniques in the Study of Natural Turbulent Flows." *Water Resour. Res.*, 35(3), 871-877.

Roy, A. G., and Buffin- Bélanger, T. (2001). "Advances in the Study of Turbulent Flow Structures in Gravel-Bed Rivers." *Gravel-Bed Rivers V*, New Zealand Hydrological Society, Wellington, New Zealand, 375-404.

Roy, A.G, Buffin- Bélanger, T., Lamarre, H., Kirkbride, A. D. (2004). "Size, Shape and Dynamics of Large-Scale Turbulent Flow Structures in a Gravel-Bed River." *J. Fluid Mech.*, 500(1), 27.

Schvidchenko, A. B., and Pender, G. (2001). "Macroturbulent Structure of Open-Channel Flow Over Gravel Beds." *Water Resour. Res.*, 37(3), 709-719.

Shao, Y., and Yang, Y. (2008). "A Theory for Drag Partition Over Rough Surfaces." *J. Geophys. Res.*, 113(F02S05).

Sharp, J. J. (1981). "Hydraulic Modeling." Butterworths, London.

Shen, H. W., and Lu, J. (1983). "Development and Prediction of Bed Armoring." *J. Hydraul. Eng.*, 109(4), 611-629.

Sirovich, L., and Karlsson, S. (1997). "Turbulent Drag Reduction by Passive Mechanisms." *Nature*, 388, 753-755.

Strom, K. B., and Papanicolaou, A. N. (2009). "Occurrence of Cluster Microforms in Mountain Rivers." *Earth Surf. Process. Landforms*, 34(1), 88-98.

Strom, K. B., and Papanicolaou, A. N. (2008). "Morphological Characterization of Cluster Microforms." *Sedimentology*, 55(1), 137-153.

Strom, K. B., and Papanicolaou, A. N. (2007). "ADV Measurements Around a Cluster Microform in a Shallow Mountain Stream." *J. Hydraul. Eng.*, 133(12), 1379-1389.

Strom, K., Papanicolaou, A. N., Evangelopoulos, N., Odeh, M. (2004). "Microforms in Gravel Bed Rivers: Formation, Disintegration, and Effects on Bedload Transport." *J. Hydraul. Eng.*, 130(6), 554-567.

Sutherland, A.J. (1987). "Static Armour Layers by Selective Erosion." *Sediment Transport in Gravel-Bed Rivers.* John Wiley & Sons, 243-267.

Sutherland, A.J. (1992) Hiding functions to predict self armouring, Vol. 117, *Proc. Int. Grain Sorting Seminar, Mitt. der Versuchanstaldt fur Wasserbau, Hydrologie und Glaziologie (English translation)*, ETH, Zurich, Switzerland, 273–298.

Tait S.J., Willetts B.B, and Maizels, J. (1992). "Laboratory observations of bed armouring and changes in bedload composition." *Dynamics of Gravel Bed Rivers,* John Wiley & Sons, 205-225.

Tennekes, H., and Lumley, J. L. (1972). *A First Course in Turbulence.* MIT Press, Cambridge, MA.

Thoroddsen, S. T., Etoh, T. G., Takehara, K. (2008). "High-Speed Imaging of Drops and Bubbles." *Annu. Rev. Fluid Mech.*, 40, 257-285.

Van Rijn, L. C., (1982), "Equivalent Roughness of Alluvial Bed.", *J. Hydraul. Eng.*, 108(HY10), 1215-1219.

Venditti, J. G. (2007). "Turbulent Flow and Drag Over Fixed Two- and Three-Dimensional Dunes." *J. Geophys. Res.*, 112(F04008).

Venditti, J. G., and Bennett, S. J. (2000). "Spectral Analysis of Turbulent Flow and Suspended Sediment Transport Over Fixed Dunes." *J. Geophys. Res.*, 105(C9), 22035-22047.

Vanoni, V. A., and Brooks, N. H. (1957). "Laboratory studies of the roughness and suspended load of alluvial streams." Sedimentation Laboratory, California Institute of Technology, Pasadena, California, U. S. A.

Vericat, D., Batalla, R. J., Garcia, C. (2006). "Breakup and Reestablishment of the Armour Layer in a Large Gravel-Bed River Below Dams: The Lower Ebro." *Geomorphology*, 76, 122-136.

Voulgaris, G., and Trowbridge, J. (1998). "Evaluation of the Acoustic Doppler Velocimeter (ADV) for turbulence measurements." *J. Atmos. Ocean. Technol.*, 15(1), 272–288.

Wang, X. y., Yang, Q. Y., Lu, W. Z., Wang, X. K. (2012). "Experimental Study of Near-Wall Turbulent Characteristics in an Open-Channel with Gravel Bed using an Acoustic Doppler Velocimeter." *Exp. Fluids*, 52, 85-94.

Wiberg, P. L., and J. D. Smith, (1991), "Velocity distribution and bed roughness in high-gradient streams.", *Water Resour. Res.*, 27(5), 825-838.

Wilcock, P. R., and DeTemple, B. T. (2005). "Persistence of Armor Layers in Gravel-Bed Streams." *Geophys. Res. Lett.*, 32(8), L08402.

Wilcock, P.R., and McArdell, B.W. (1997), "Partial transport of a sand-gravel sediment." *Water Resour. Res.*, 33(1), 233-245.

Wilcock, P.R. (2001). "The flow, the bed, and the transport: interaction in flume and field." *Gravel-bed Rivers V*, New Zealand Hydrological Society, 183-220.

Wilcock, P. R., Kenworthy, S. T., Crowe, J. C. (2001). "Experimental Study of the Transport of Mixed Sand and Gravel." *Water Resour. Res.*, 37(12), 3349-3358.

Wilcock, P. R., and Crowe, J. C. (2003). "Surface-Based Transport Model for Mixed-Size Sediment." *J. Hydraul. Eng.,* 129(2), 120-128.

Wilcock, P.R.; Pitlick, J., Cui, Y., (2009). "Sediment transport primer: estimating bed-material transport in gravel-bed rivers." *Gen. Tech. Rep. RMRS-GTR-226*. Fort Collins, CO: U.S. Department of Agriculture, Forest Service, Rocky Mountain Research Station. 78 p.

Wilcock, P. R., and Southard, J. B. (1989). "Bed Load Transport of Mixed Size Sediment: Fractional Transport Rates, Bed Forms, and the Development of a Coarse Bed Surface Layer." *Water Resour. Res.*, 25(7), 1629-1641.

Williams, G. P., and Wolman, M. G. (1984). Downstream Effects of Dams on Alluvial Rivers, United States Geological Survey, Washington, D.C.

Wittenberg, L., Laronne, J. B., Newson, M. D. (2007). "Bed Clusters in Humid Perennial and Mediterranean Ephemeral Gravel-Bed Streams: The Effect of Clast Size and Bed Material Sorting." *Journal of Hydrology*, 334(3–4), 312-318.

Wittenberg, L., and Newson, M. D. (2005). "Particle Clusters in Gravel-Bed Rivers: An Experimental Morphological Approach to Bed Material Transport and Stability Concepts." *Earth Surf. Process. Landforms*, 30(11), 1351-1368.

Wolman, M. G. (1954). "A Method of Sampling Coarse River-Bed Material." *Transactions of the American Geophysical Union*, 35(6), 951-956.

Wong, M., and Parker, G. (2006). "Reanalysis and Correction of Bed-Load Relation of Meyer-Peter and Müller using their Own Database." *J. Hydraul. Eng.*, 132(11), 1159-1168.

Yalin, M.S. (1977). *Mechanics of Sediment Transport. (2nd edition)*. Pergamon Press, Oxford.

Yalin M.S. (1992). *River Mechanics*. Pergamon Press: Oxford.

Yang, S. -., and Tan, S. -. (2008). "Flow Resistance Over Mobile Bed in an Open-Channel Flow." *J. Hydraul. Eng.*, 134(7), 937-948.
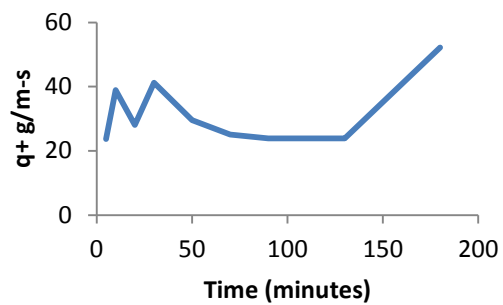
Yen, B. (2002). "Open Channel Flow Resistance." *J. Hydraul. Eng.*, 128(1), 20-39.

Zimmermann, A.E. (2009). "Experimental investigations of step-pool channel formation and stability."
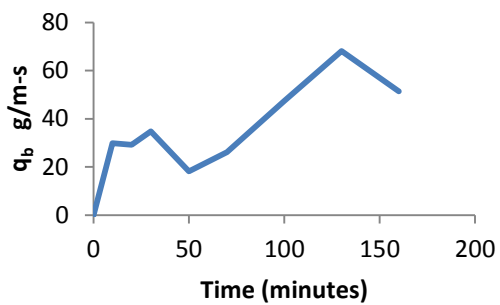
APPENDIX I

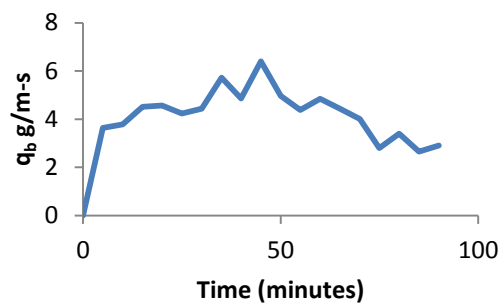Total unit sediment transport rate q_b vs. time in segment 3:
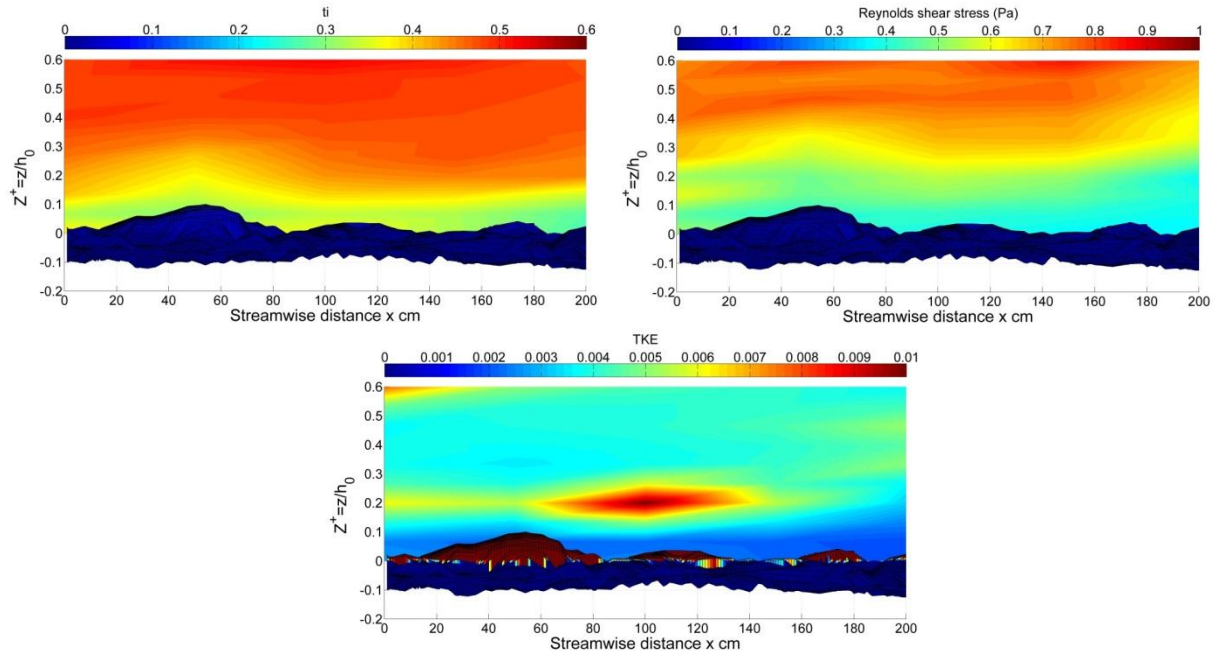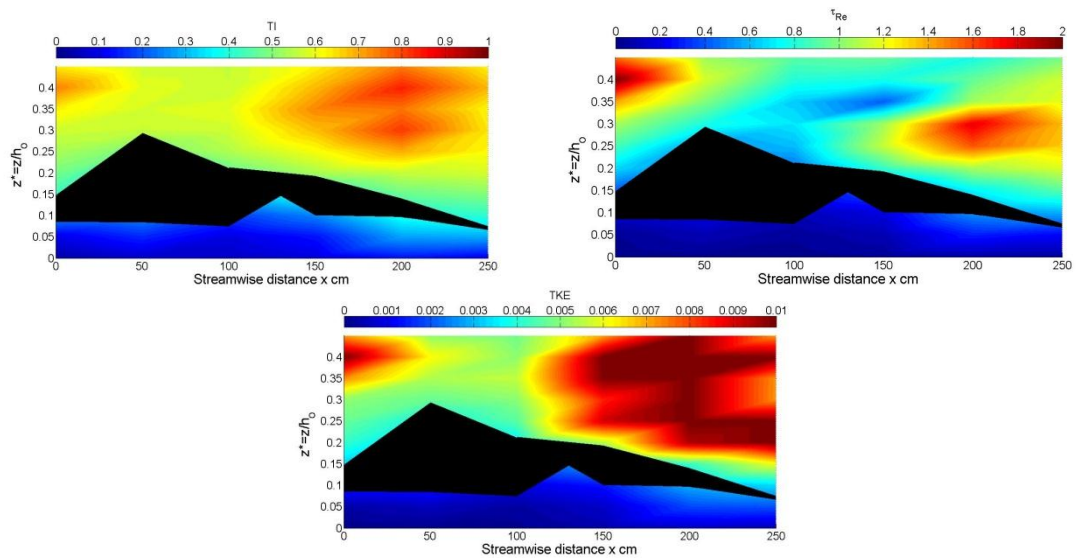

Run 1

Run2

Run 3

Run 4

Run 5

Run 6
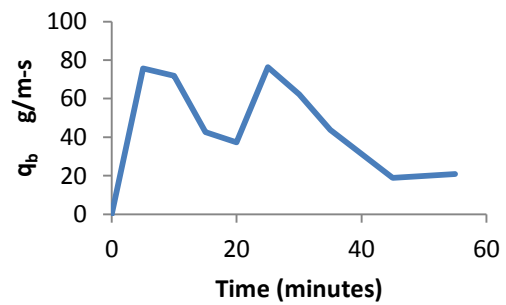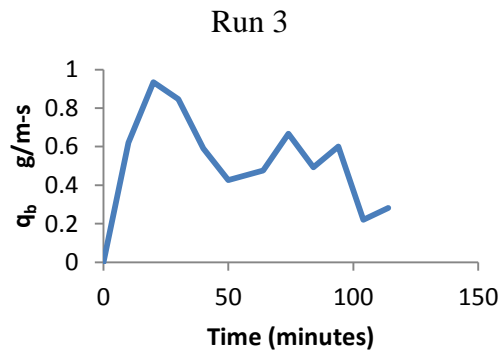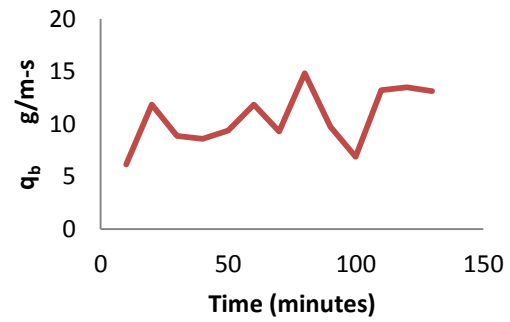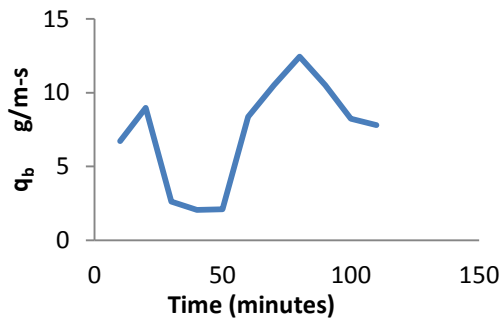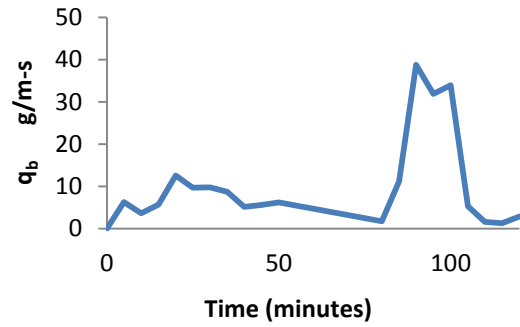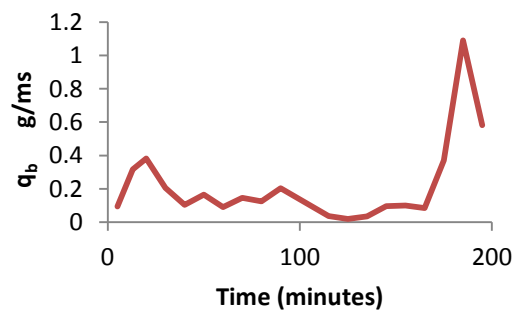
Run 7

Run 8

Run 9

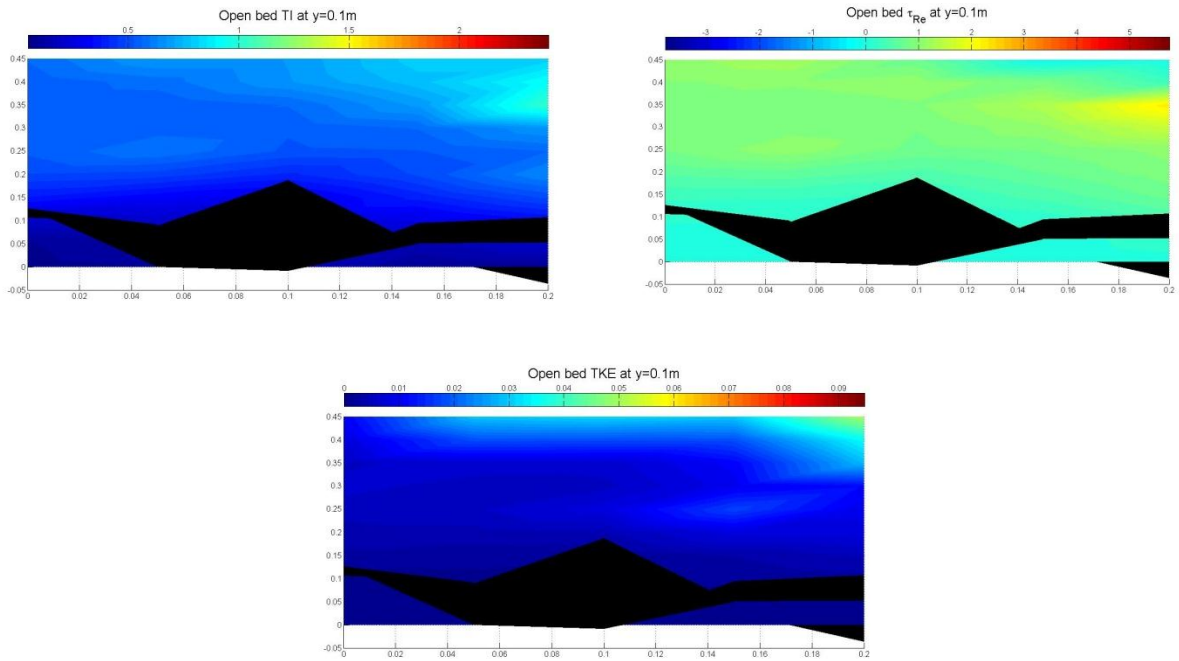# APPENDIX II

Isolated cluster "0724G" Run5
Q=0.07cms 24% sand

Isolated cluster "0724H" Run5
Q=0.07cms 24% sand

206

openbed "0724open" Run5
Q=0.07cms 24%sand

Open bed TI at y=0.1m

Open bed τ_{Re} at y=0.1m

Open bed TKE at y=0.1m

Isolated cluster "0738I" Run8
Q=0.07cms 38%sand

Ti

Re

TKE
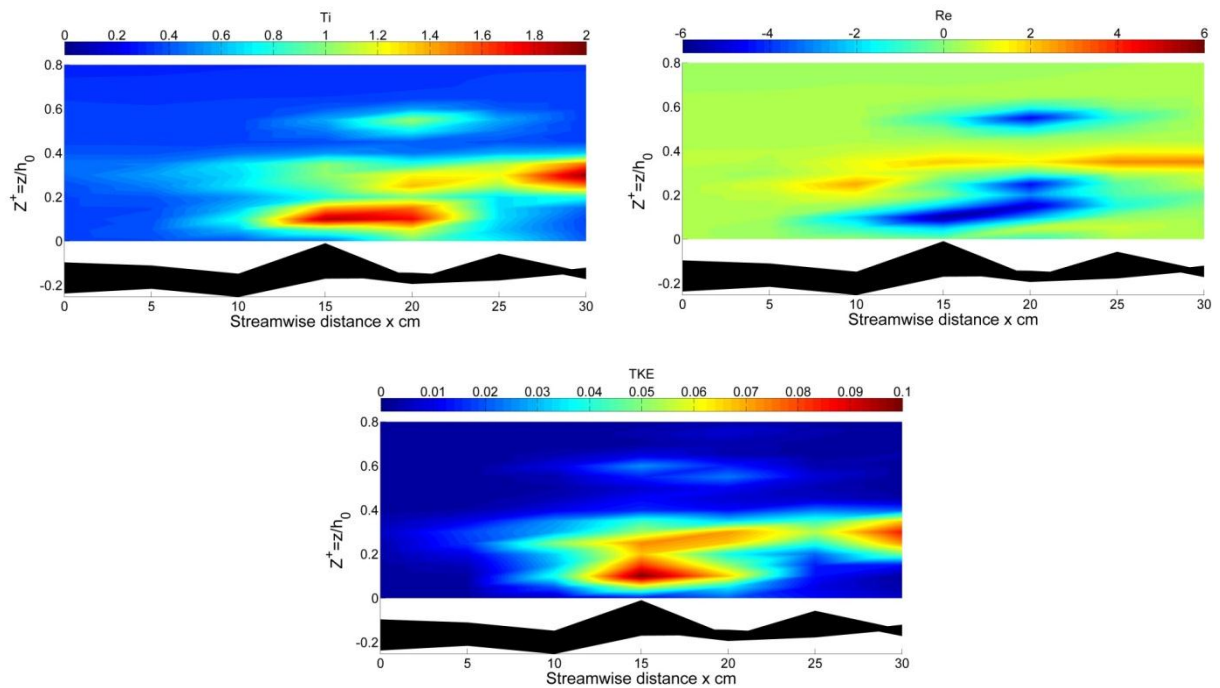
Isolated cluster "0901J" Run1

Q-0.09cms, 1% sand
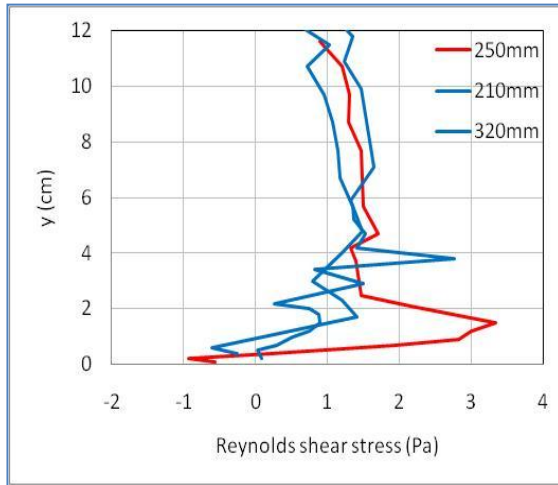
"0909open" Run3
Q=0.09cms 9% sand

Single cluster "0909K" Run3
Q=0.09cms 9% sand

Open bed "1138open" Run9
Q=0.11cms 38% sand

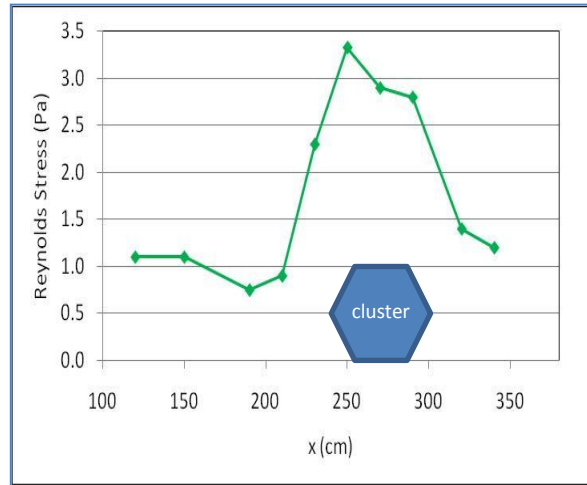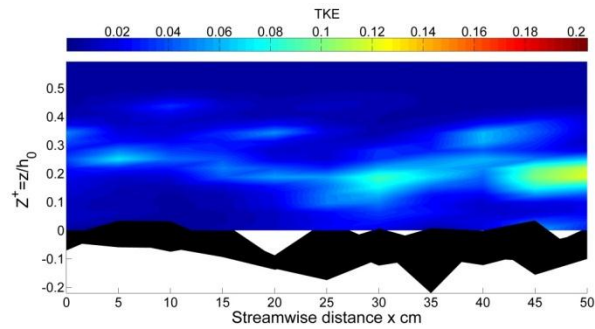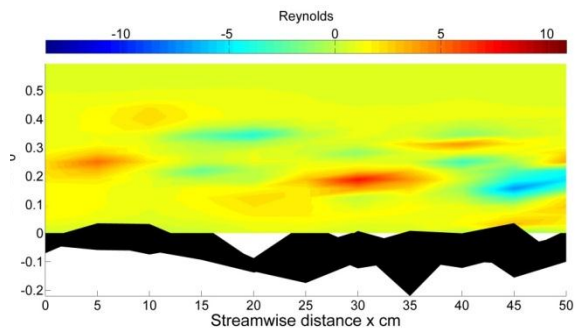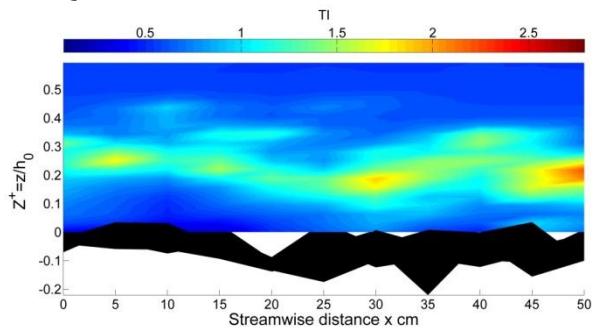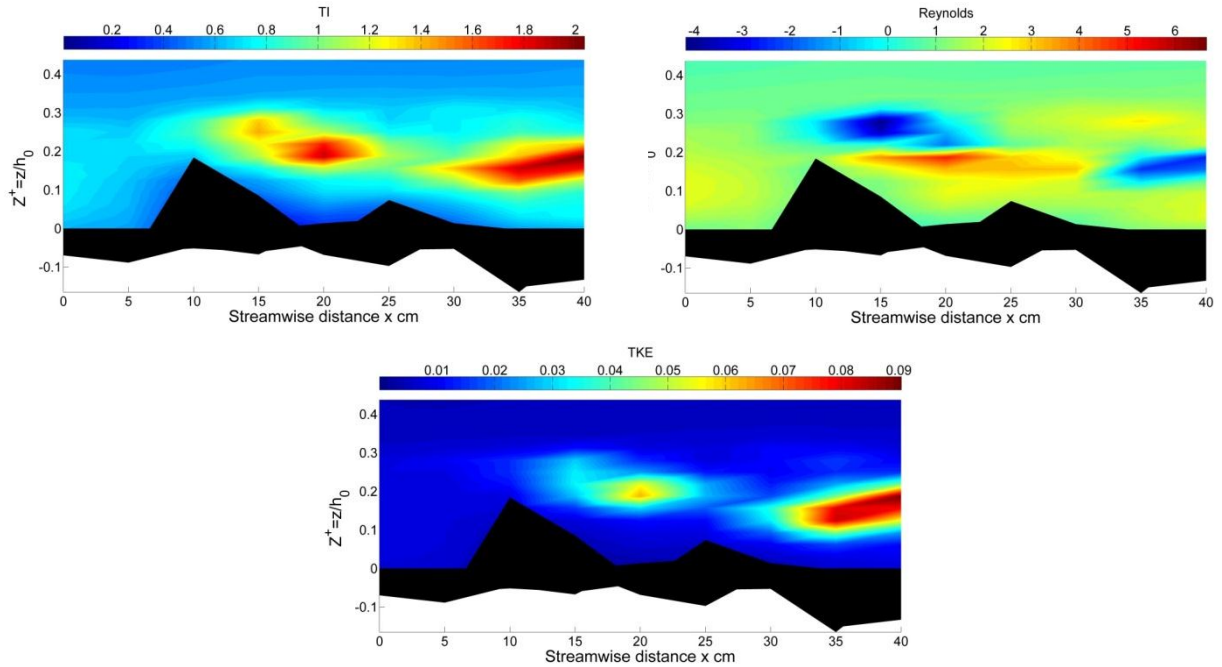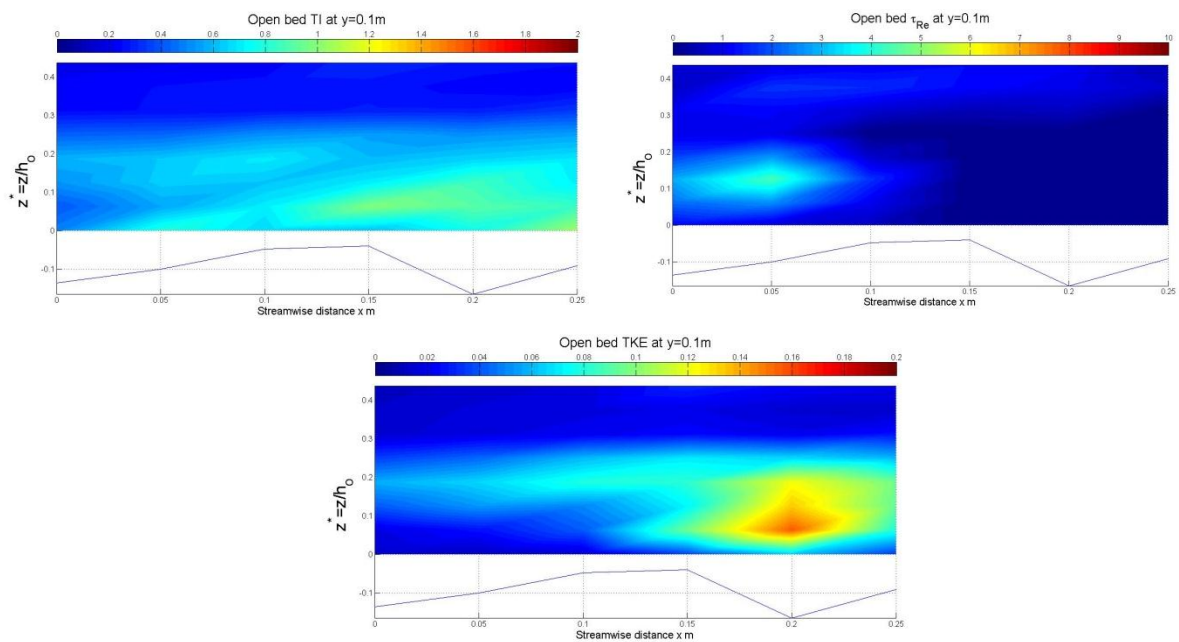| ID	Time and Space Averaged (m/s)			TKE at z*=0.3	τ_{Re} at z*=0.3	TKE at z*=0.5	τ_{Re} at z*=0.5
	$\bar{U}$	$\bar{V}$	$\bar{W}$	Max	Max	Max	Max
				Average	Average	Average	Average
				Min	Min	Min	Min
0724open	0.1671	0.006	-0.0039	0.0136	1.6458	0.0947	5.75
				0.0065	0.9361	0.0392	1.1911
				0.0042	0.6116	0.0106	-3.7896
0724G	0.2032	0.0094	0.0003	0.0163	0.7134	0.0235	0.9988
				0.0055	0.6021	0.0056	0.7376
				0.0034	0.4664	0.0027	0.6039
0724H	0.187	0.0041	-0.0013	0.0139	1.8068	0.0169	2.4396
				0.0065	0.9777	0.0071	1.1142
				0.0047	-0.5264	0.0047	0.4673
0738I	0.2381	0.0018	-0.0032	0.1317	4.4451	0.0111	0.5213
				0.0511	0.6194	0.003	0.2345
				0.0052	-4.3894	0.002	-1.6336
0901J	0.4	0.009	0.0037	0.0295	2.755	0.018	3.289
				0.0103	1.4572	0.01	1.264
				0.0068	1.127	0.0052	0.627
0909open	0.3424	0.0142	-0.0032	0.0699	1.3536	0.0093	4.8783
				0.0272	1.0302	0.0058	1.2484
				0.0102	0.4654	0.005	-1.588
0909K	0.3462	0.0022	-0.002	0.0264	3.5978	0.0079	2.0265
				0.0104	1.4188	0.0058	1.2189
				0.006	-2.1976	0.0038	0.6078
1138open	0.3205	0.00077	-0.001	0.0948	4.3068	0.0357	2.2638
				0.0273	1.19	0.0186	0.818
				0.0125	-0.8646	0.0093	-0.2912

APPENDIX III

Cluster spacing data (mm) for each flume experiment. Data highlighted in red has a magnitude smaller than 7ds , indicating formation of coupled clusters; Data highlighted in dark blue has a magnitude smaller than 7ds, whereas there are more than two elements within the 7ds radius, indicating the formation of grouped clusters. Quantity of each category can be determined through counting red data points for coupled clusters and counting paired or grouped dark blue data clusters.

Run1	Run 2	Run3	Run4	Run5	Run6	Run7	Run8	Run9
242	372	815	201	686	797	444	268	881
536	481	636	381	672	548	383	337	954
335	428	371	533	519	549	508	285	387
335	249	192	449	542	620	536	319	486
268	488	306	178	555	375	535	1635	841
361	593	363	1015	605	450	230	1443	922
420	778	459	932	413	625	493	647	560
242	332	274	690	253	636	221	390	633
449	516	360	287	918	254	286	684	539
465	133	604	647	627	256	653	365	539
288	387	630	216	461	439	732	751	438
375	286	904	759		625	270	277	312
335	1052	886	358		775	283	142	456
350	925	900	423		669	361	1067	400
1080	1350	636			219	572		280
375	913	604				684		596
		285				891		264
		459				654		455
		382				472		170
						481		291
						500		235
403	580	530	505	568	522	485	615	521
1080	1350	904	1015	918	797	891	1635	954
205	333	244	269	170	184	159	464	223

The last three rows of the table are calculated cluster spacing mean, maximum and standard deviation, respectively.

APPENDIX IV

Recirculating Flume:									
Parameters to pre-set									
Flowtube diameter r (m)=	0.2032	**B =**	0.6	**g =**	9.8	**τ^*_c =**		0.045	
		D_{50} =	0.0088	**ρ =**	1000	**Z =**		0.1	
Pump ft/s	*Pump m/s*	*Pump flow rate m^3/s*	Q	$f\!f$	U	S	τ_b	q_b	Q_b
1	0.305	0.0099	0.0099	0.0749	0.165	0.0003	0.25	#NUM!	#NUM!
2	0.610	0.0198	0.0198	0.0749	0.329	0.0010	1.02	#NUM!	#NUM!
4	1.219	0.0395	0.0395	0.0749	0.659	0.0041	4.06	#NUM!	#NUM!
5	1.524	0.0494	0.0494	0.0749	0.824	0.0065	6.35	#NUM!	#NUM!
6	1.829	0.0593	0.0593	0.0749	0.988	0.0093	9.14	0.0001	0.00004
7	2.134	0.0692	0.0692	0.0749	1.153	0.0127	12.44	0.0002	0.00014
8	2.438	0.0791	0.0791	0.0749	1.318	0.0166	16.25	0.0005	0.00029
9	2.743	0.0890	0.0890	0.0749	1.483	0.0210	20.57	0.0008	0.00050
10	3.048	0.0988	0.0988	0.0749	1.647	0.0259	25.39	0.0013	0.00078
11	3.353	0.1087	0.1087	0.0749	1.812	0.0313	30.73	0.0019	0.00112

The recirculating flume calculation use Darcy-Weisbach flow resistance equations to iterate result of sediment transport rate under different flow rate and pre-settings. Above spreadsheet is an example of how to convert pump reading from ft/s to Q in m³/s, and further calculate the unit and total bedload transport rate under different flow rates. Aside from sediment transport rate estimate, this spreadsheet also provides a reference for setting the initial flume slope to minimize time to reach equilibrium transport status.